

INFORMATION TO USERS

This manuscript has been reproduced from the microfilm master. UMI films the text directly from the original or copy submitted. Thus, some thesis and dissertation copies are in typewriter face, while others may be from any type of computer printer.

The quality of this reproduction is dependent upon the quality of the copy submitted. Broken or indistinct print, colored or poor quality illustrations and photographs, print bleedthrough, substandard margins, and improper alignment can adversely affect reproduction.

In the unlikely event that the author did not send UMI a complete manuscript and there are missing pages, these will be noted. Also, if unauthorized copyright material had to be removed, a note will indicate the deletion.

Oversize materials (e.g., maps, drawings, charts) are reproduced by sectioning the original, beginning at the upper left-hand corner and continuing from left to right in equal sections with small overlaps. Each original is also photographed in one exposure and is included in reduced form at the back of the book.

Photographs included in the original manuscript have been reproduced xerographically in this copy. Higher quality 6" x 9" black and white photographic prints are available for any photographs or illustrations appearing in this copy for an additional charge. Contact UMI directly to order.

UMI

**A Bell & Howell Information Company
300 North Zeeb Road, Ann Arbor MI 48106-1346 USA
313/761-4700 800/521-0600**

UNIVERSITY OF ALBERTA

**DYNAMIC MODELLING AND SIMULATION
OF AN
INDUSTRIAL BOILER SYSTEM**

BY
ALBERT CHIU



A THESIS
SUBMITTED TO THE
FACULTY OF GRADUATE STUDIES AND RESEARCH
IN PARTIAL FULFILLMENT OF THE REQUIREMENTS FOR THE DEGREE
OF

MASTER OF SCIENCE
IN
PROCESS CONTROL

DEPARTMENT OF CHEMICAL AND MATERIALS ENGINEERING

EDMONTON, ALBERTA

SPRING, 1997



**National Library
of Canada**

**Acquisitions and
Bibliographic Services**

**395 Wellington Street
Ottawa ON K1A 0N4
Canada**

**Bibliothèque nationale
du Canada**

**Acquisitions et
services bibliographiques**

**395, rue Wellington
Ottawa ON K1A 0N4
Canada**

Your file Votre référence

Our file Notre référence

The author has granted a non-exclusive licence allowing the National Library of Canada to reproduce, loan, distribute or sell copies of his/her thesis by any means and in any form or format, making this thesis available to interested persons.

The author retains ownership of the copyright in his/her thesis. Neither the thesis nor substantial extracts from it may be printed or otherwise reproduced with the author's permission.

L'auteur a accordé une licence non exclusive permettant à la Bibliothèque nationale du Canada de reproduire, prêter, distribuer ou vendre des copies de sa thèse de quelque manière et sous quelque forme que ce soit pour mettre des exemplaires de cette thèse à la disposition des personnes intéressées.

L'auteur conserve la propriété du droit d'auteur qui protège sa thèse. Ni la thèse ni des extraits substantiels de celle-ci ne doivent être imprimés ou autrement reproduits sans son autorisation.

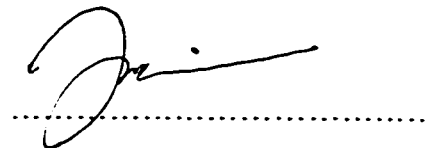
0-612-21158-4

UNIVERSITY OF ALBERTA
LIBRARY RELEASE FORM

NAME OF AUTHOR: Albert Chiu
TITLE OF THESIS: Dynamic Modelling and Simulation of an
Industrial Boiler System
DEGREE: Master of Science
YEAR THIS DEGREE GRANTED: 1997

Permission is hereby granted to the University of Alberta Library to reproduce single copies of this thesis and to lend or sell such copies for private, scholarly or scientific purposes only.

The author reserves all other publication and other rights in association with the copyright in the thesis, and except as hereinbefore provided neither the thesis nor any substantial portion thereof may be printed or otherwise reproduced in any material form whatever without the author's prior written permission.

A handwritten signature in black ink, appearing to be 'Albert Chiu', is written over a horizontal dotted line.


ADDRESS:

5825-185 Street
Edmonton, Alberta
Canada T6M 1Y

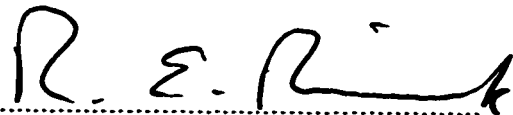
Date: January 12, 1997

UNIVERSITY OF ALBERTA
FACULTY OF GRADUATE STUDIES AND RESEARCH

The undersigned certify that they have read, and recommend to the Faculty of Graduate Studies and Research for acceptance, a thesis entitled **DYNAMIC MODELLING AND SIMULATION OF AN INDUSTRIAL BOILER SYSTEM** submitted by **ALBERT CHIU** in partial fulfillment of the requirements for the degree of **MASTER OF SCIENCE in PROCESS CONTROL**.



Prof. S. L. Shah (Supervisor)



Prof. R. E. Rink (Elect. Eng., U. of A.)



Prof. R. K. Wood

Date: *January 15, 1997*

Abstract

The main objective of this thesis is to develop a first-principles dynamic model for an industrial boiler system. The purpose of the model was to provide — a means of investigating the dynamic behaviour, in particular the stability, of an industrial steam and power cogeneration system; a basis for the development of a simulator for operator training; and estimates of transient variations of metal wall temperatures at various boiler sections for use in studying boiler life expectancy.

A dynamic state space model for the boiler system including the utility boilers, the common steam header, and their controls has been developed. The dynamic model was based on the methods presented by Dieck-Assad [6], Rackette [20], and Kakaç [13]. A detailed description of the model development is provided in this thesis.

This model has been evaluated under both dynamical and in steady state conditions via closed-loop simulations. The overall energy balance of the model is correct — the fuel flow rates were within 2.28 % and the flue gas exit temperatures were within 13.2 % of those provided in a Syncrude report on the boiler system — for steam loads of 94.5 *kg/s*, 100.8 *kg/s*, and 108.9 *kg/s*. The transient characteristics of the dynamic model were correct qualitatively. The responses of all the variables reached steady state within 1500 *s* using the actual PI controller parameters from the Syncrude boiler system implemented. The behaviour of important variables such as the steam drum and common header pressures, the fuel and air flow, and the temperatures of the flue gas and steam/water, in the various boiler sections also matched that observed in the real process.

Contents

| | | |
|----------|---|----------|
| 1 | Introduction | 1 |
| 1.1 | Background | 1 |
| 1.2 | Scope and Objective of Study | 3 |
| 1.3 | Thesis Organization | 4 |
| 2 | Boiler System | 6 |
| 2.1 | Introduction | 6 |
| 2.2 | Description of an Industrial Boiler System | 9 |
| 2.3 | Boiler Sectioning | 13 |
| 2.3.1 | Boiler Sections on the Steam-water Side | 13 |
| 2.3.2 | Boiler Sections on the Flue Gas Side | 14 |
| 2.4 | Assumptions and Simplifications | 15 |
| 2.5 | Development of the State Space Boiler Model | 18 |
| 2.5.1 | Furnace | 19 |
| 2.5.2 | Generator | 26 |
| 2.5.3 | Steam Drum | 35 |

| | | |
|----------|---|-----------|
| 2.5.4 | Superheaters and Economizer | 43 |
| 2.5.5 | Attemperator | 44 |
| 2.5.6 | Common Steam Header | 46 |
| 2.5.7 | Swelling and Shrinking in the Steam Drum | 49 |
| 2.6 | Summary | 55 |
| 3 | Evaluation of Methods for Simulating Heat Transfer in an Industrial Boiler | 56 |
| 3.1 | Introduction | 56 |
| 3.2 | Methods for Modelling Heat Exchangers | 57 |
| 3.2.1 | Direct Feedback Method | 58 |
| 3.2.2 | Energy Balance Method | 60 |
| 3.2.3 | Differential Energy Balance (DEB) Method | 62 |
| 3.3 | Evaluation of the Three Methods | 71 |
| 3.3.1 | Simulation Setup | 71 |
| 3.3.2 | Results and Discussions | 75 |
| 3.4 | Summary | 83 |
| 4 | Control and Validation of the State Space Model of the Boiler System | 84 |
| 4.1 | Introduction | 84 |
| 4.2 | Boiler Control | 85 |
| 4.2.1 | Feedwater Control | 86 |

| | | |
|----------|---|------------|
| 4.2.2 | Main Steam and Attenuator Temperature Control | 89 |
| 4.2.3 | Firing Rate Demand | 92 |
| 4.2.4 | Combustion Control | 92 |
| 4.3 | Model Validation | 95 |
| 4.3.1 | Simulation Setup | 96 |
| 4.3.2 | Simulation Results | 97 |
| 4.3.3 | Discussions on the Simulation Results | 110 |
| 4.4 | Summary | 114 |
| 5 | Conclusions | 117 |
| 5.1 | Conclusions | 118 |
| 5.2 | Recommendations for Future Work | 119 |
| A | Parameters for the Dynamic Model | 124 |
| A.1 | Different Parameters for the Various Boiler Sections | 125 |
| A.2 | Tuning Parameters for the PI controllers in the Dynamic Model . | 126 |
| B | Simulink Block Diagrams of the Dynamic Model | 127 |
| C | MATLAB Script Files | 145 |
| D | Physical Properties Correlations | 170 |

List of Figures

| | | |
|-----|--|----|
| 2.1 | Process and Instrument Diagram for the Syncrude Letdown System | 11 |
| 2.2 | Schematic Diagram of the Utility Boiler | 12 |
| 2.3 | Drum liquid-water control volume | 36 |
| 2.4 | Drum vapour control volume | 38 |
| 2.5 | Control volumes of the steam generation section | 50 |
| 3.1 | Schematic diagram showing a counter flow heat transfer component in a boiler | 58 |
| 3.2 | Flow chart showing the direct feedback method. | 61 |
| 3.3 | Flow chart showing the energy balance method. | 63 |
| 3.4 | Temperature profile of the flue gas and steam/water sides along the length of heat exchanger. | 66 |
| 3.5 | Flow chart showing the DEB method. | 72 |
| 3.6 | A schematic diagram showing an arrangement for connecting coun- terflow heat exchangers in series. | 73 |
| 3.7 | A schematic diagram showing another arrangement for connecting counterflow heat exchangers in series. | 74 |

| | | |
|------|---|-----|
| 3.8 | Flue gas and steam exit temperatures and wall temperature of the heat exchanger in simulation s1 <i>ii</i> using the Direct Feedback Method. | 77 |
| 3.9 | Flue gas and steam exit temperatures and wall temperature of the heat exchanger in simulation s1 <i>ii</i> using the Energy Balance Method. | 79 |
| 3.10 | Flue gas and steam exit temperatures and wall temperature of the heat exchanger in simulation s1 <i>ii</i> using the DEB Method. | 80 |
| 3.11 | Flue gas and steam exit temperatures and wall temperature of the heat exchanger in simulation s2 <i>ii</i> using the Energy Balance Method. | 81 |
| 3.12 | Flue gas and steam exit temperatures and wall temperature of the heat exchanger in simulation s2 <i>ii</i> using the DEB Method. | 82 |
| 4.1 | Feedwater Control | 87 |
| 4.2 | Main Steam and Attemperator Temperature Control | 91 |
| 4.3 | Firing Rate Demand (Plant Master) | 93 |
| 4.4 | Combustion Control | 94 |
| 4.5 | Steam demand from the boiler system | 101 |
| 4.6 | Pressure variation of the common steam header | 101 |
| 4.7 | Temperature variation of the common steam header | 102 |
| 4.8 | Transient response of feedwater flow | 102 |
| 4.9 | Transient response of attemperator water flow | 103 |
| 4.10 | Transient response of steam drum pressure | 103 |
| 4.11 | Transient response of steam drum liquid level | 104 |
| 4.12 | Transient response of fuel flow | 104 |

| | | |
|------|--|-----|
| 4.13 | Transient response of air flow | 105 |
| 4.14 | Transient response of flue gas temperature at various boiler sections | 105 |
| 4.15 | Transient response of water temperature at the economizer exit . | 106 |
| 4.16 | Transient response of steam temperature at the secondary super- heater exit | 106 |
| 4.17 | Transient response of circulation rate | 107 |
| 4.18 | Transient response of the average steam quality at the exit of risers | 107 |
| 4.19 | Transient response of the economizer metal wall temperature . . . | 108 |
| 4.20 | Transient response of the generator metal wall temperature | 108 |
| 4.21 | Transient response of the primary superheater metal wall temperature | 109 |
| 4.22 | Transient response of the secondary superheater metal wall tem- perature | 109 |
| B.1 | First level of the model | 128 |
| B.2 | Second level of the model including the utility boiler, the common steam header and the control schemes | 129 |
| B.3 | This level contains the various boiler sections of the utility boiler . | 130 |
| B.4 | This level contains the economizer section in the utility boiler . . | 131 |
| B.5 | This block diagram shows the furnace section in the utility boiler | 132 |
| B.6 | This block calculates the steam flow from the steam drum to the common steam header using the steam drum and header pressures | 133 |
| B.7 | This block diagram contains the slag screen and the generator sec- tions in the utility boiler | 134 |

| | |
|---|-----|
| B.8 This block diagram shows the screen section in the utility boiler . | 135 |
| B.9 This block diagram shows the generator section in the utility boiler | 136 |
| B.10 This block diagram contains the superheaters and the attemperator in the utility boiler | 137 |
| B.11 This block diagram shows the primary superheater in the utility boiler | 138 |
| B.12 This block diagram shows the secondary superheater in the utility boiler | 139 |
| B.13 This block diagram shows the common steam header in the dynamic model | 140 |
| B.14 This block diagram shows the plant master (firing rate demand) control scheme | 141 |
| B.15 This block diagram shows the combustion and oxygen trim control schemes | 142 |
| B.16 This block diagram shows the feedwater control scheme | 143 |
| B.17 This block diagram shows the final steam temperature and attem- perator control schemes | 144 |

List of Tables

| | | |
|-----|---|-----|
| 3.1 | Excitations to the series of heat exchangers | 75 |
| 3.2 | Number of floating point operations performed to simulate the series of heat exchangers for 5000 s. | 76 |
| 4.1 | Mean temperatures of metal walls at various boiler sections | 98 |
| 4.2 | Comparison of fuel composition of the simulation and the Syncrude report | 98 |
| 4.3 | Comparison of the reported and simulated variables of the boiler system at steam loads of 94.5 kg/s, 100.8 kg/s, and 108.9 kg/s . . | 99 |
| 4.4 | Flue gas temperatures ($^{\circ}C$) at the exits of the various boiler sections at three steam loads | 99 |
| A.1 | Various parameters used in the simulation | 125 |
| A.2 | PI tuning parameters | 126 |

Chapter 1

Introduction

1.1 Background

This project has arisen out of discussions between members of the Faculty of Engineering, University of Alberta, and personnel from Utilities Engineering, Syncrude Canada Ltd. (SCL), Fort McMurray, Alberta. The question under discussion concerned the stability status of the SCL steam / electrical system. While this question relates to a very specific operational system, it was recognized that it may be an example of an important general class of questions that arise whenever large industrial cogeneration systems are designed and operated.

The specific system under study is the SCL steam generation / turbo-generator / electrical / load / intertie system. The major concern is with the transient stability of the local system when intertie power is interrupted. The SCL steam generation system consists of five boilers connected in parallel to a common header which supplies steam for bitumen extraction and other plant processes, and for electric power generation by four turbogenerators, also connected

in parallel. Three boilers are pressure-controlled, two are flow-controlled. Under conditions of large transient excursions away from previous operating point, the numerous single-loop controllers can interact strongly and poor stability of the transient recovery has been observed. There exists the possibility of automatic boiler trip and cascading outage, leading to complete plant shutdown.

The transient excursions referred to above are, in most cases, triggered by a loss of the intertie power that normally is taken from the Alberta grid. Plant electrical load at SCL is highly variable, due mainly to the use of large draglines that can each draw several megawatts, but only during the loading phase. This in itself causes detectable voltage transients on the grid. Draglines are quickly shed when the intertie is lost. The electrical load seen by SCL generators may suddenly increase by as much as 10% or more during the loading phase. This is a very large transient change, compared with the typical case of utility-company powerplants, and can cause rapid decay of electrical frequency, limit governor and/or exciter response, large steam-pressure transient, and limit pressure / flow regulator and feedwater regulator responses. All of these phenomena interact, and the standard single-loop PID-type controllers, which are typically tuned on the basis of linearized models to deal with small excursions away from a stable operating point, can fail to provide adequate stability for the overall system.

1.2 Scope and Objective of Study

A valid dynamic simulation model is required to efficiently and effectively investigate the stability and interaction of a steam and power generation system under changing conditions, such as jumps in steam and power demands.

Although many general boiler models have previously been published (see references [6], [4], [17]), none satisfactorily met the requirements of this project in terms of level of detail, configuration of the boiler system, and parameters. Hence the decision to develop specific models for the Syncrude boilers, using an intermediate level, physical-principles approach as suggested by the work of Dieck-Assad [6], was made.

Due to the complexity of the system, the development of the dynamic model of the overall system is divided into three parts: the steam system, the electrical system, and the letdown system. The steam system includes the boilers, their control, and the common steam header; the electrical side includes all of the turbines and generators, and their control; and the letdown system includes all the different steam headers.

This thesis will focus on the development of the simulation model for the steam system. MATLAB / Simulink are used as software tools. MATLAB is a technical computing environment for numeric computation, whereas Simulink is an object oriented tool for modeling, analyzing, and simulating physical and mathematical systems as an extension of MATLAB. The dynamic model of the steam system will be connected with the other models upon completion to facili-

tate studies of the entire Syncrude power generation system.

The main contributions of this study are:

- It provides a means of investigating the dynamic behaviour of a complex, large-scale steam and power generation system.
- It provides a basis for the development of a simulator for operator training.
- It provides estimates of transient variations of metal wall temperatures at various boiler sections for use in studying boiler life expectancy.

1.3 Thesis Organization

Chapter 2 presents the development of the simulation model for the utility boilers and the common steam header. The assumptions imposed and the equations for use in the simulation are included in this chapter.

Chapter 3 is a study of three different algorithms for use in simulating a heat exchanger unit in the industrial boiler model. The algorithms presented are evaluated in terms of their efficiency.

Chapter 4 is divided into two parts. Discussion and implementation of the existing control scheme for the boiler system are provided in the first part of this chapter. The second half of the chapter is dedicated to validation of the developed model and discussions on the simulation results.

Chapter 5 provides a few concluding remarks and suggestions for future work.

All MATLAB/Simulink script files and block diagrams are included in the appendix to this thesis for completeness.

Chapter 2

Boiler System

2.1 Introduction

A steam boiler is one of the most important components in industrial plants such as conventional power generation plants or chemical plants. Its operation has great impact on other parts of the plant. Failure of a boiler may lead to complete plant shutdown. Therefore, a means that would facilitate its study without disturbing the plant and could also provide proper operator training can prove to be beneficial.

One way to achieve the above is through simulation. In order to perform simulations of existing processes, dynamic mathematical models which describe the processes accurately are required. There are two main categories as far as obtaining a mathematical model is concerned. One could treat the process as a black box and determine the model statistically by perturbing the process with known excitations, and identifying coefficients of an ad hoc set of mathematical input/output relationships to fit the observed data. The other method is to obtain

a mechanistic model from first principles that govern the process, such as energy and material balances, heat transfer, and mass transfer.

The two methods each have their own advantages. By treating the process as a black box, a fairly accurate model for a limited range of operating conditions can be obtained quite conveniently via time series analyses. This requires large sets of data for each of the variables of interest. This is often difficult to obtain since the introduction of test excitations to the plant is generally undesirable and measurements of variables are sometimes unavailable.

One advantage of the time series approach is that it does not require *a priori* knowledge of the processes to be modelled such as physical laws governing the processes. However, since it often assumes linear structures for the process model, and most real processes are inherently nonlinear, this limits the range of accuracy of the model to only around a certain nominal operating region in which data are collected. As the operating conditions drift away from this small neighbourhood of the original operating point, the accuracy of the model deteriorates, especially if the processes exhibit strong nonlinearities.

The first principles approach, on the other hand, does not require large sets of transient process data under artificial excitations. Nonetheless, knowledge about the involved physical phenomena in the form of theoretical equations has to be incorporated into the modelling procedure. The theoretical aspect of the processes, which is then part of the model, allows one to obtain prediction of the behaviour of the processes irrespective of the operating conditions. Nonlinearities

are also included explicitly into the model. Further, a model like this can be used to estimate variables of interest which are not measured. There is, however, one drawback to this approach: this type of model is only practical for processes governed by physical laws that are well understood. For highly complex processes, such as social or biological systems, it is virtually impossible to derive this type of model.

In general, the former type of model is often best or most accurate for processes that have smooth and weak nonlinearities and always operate within a small neighbourhood of some known operating point. The latter type is often better for predicting process behaviour when state variables undergo large transient excursions and/or when strong nonlinearities, such as saturation, are present.

The mechanistic approach to arriving at a model for the boiler is employed in this project since many of the variables of interest, such as the metal wall temperatures at the different boiler sections, and the flue gas and steam temperatures at the various locations in the utility boiler, are unavailable through measurements. The wall temperatures play important roles in the prediction of boiler life expectancy, and the gas and steam temperatures facilitates the study of heat transfer in each of the boiler sections.

Although many general boiler models have previously been published (see references [6], [4], [17]), none satisfactorily met the requirements of this project in terms of level of detail, configuration of the boiler system, and parameters. Hence the decision to develop specific models for the Syncrude boilers, using an

intermediate level, physical-principles approach as suggested by the work of Dieck-Assad [6], was made.

A detailed process description of the Syncrude boiler system, including the utility boiler and the common steam header, is provided in this chapter. Assumptions are used to simplify the development of the simulation model since the underlying principles used in the development of this simulation model, such as material and energy balances, heat transfer mechanism, and combustion, are extremely complicated. These assumptions are listed in the second part of this chapter. The utility boiler is divided into different sections on the flue gas side and the steam/water side to facilitate its modelling. The sectioning for both sides is supplied in the third part of the chapter. Finally, the development of the state space dynamic model for the boiler system is presented.

2.2 Description of an Industrial Boiler System

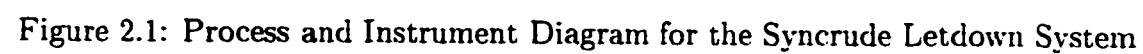
The existing Syncrude boiler system consists of three identical utility boilers (UB) and two identical carbon monoxide (CO) boilers. The utility boilers are pressure-controlled and the CO boilers are flow-controlled. Only the utility boiler model will be presented since the basic idea and underlying principles behind the development of the utility boiler and CO boiler models are the same.

The five boilers, each producing a nominal 94.5 kg/s of steam, are connected in parallel to a nominal 6.6 MPa (absolute) common steam header which supplies steam for bitumen extraction and other plant processes, and for electric

power generation by four turbogenerators, also connected in parallel. Figure 2.1 shows the process and instrument diagram of the Syncrude letdown system. A schematic diagram of the utility boiler is shown in Figure 2.2.

Feedwater at a pressure of 6.6 *MPa* (absolute) and a rate of 94.5 *kg/s* is fed to the utility boiler. It is preheated in the economizer section from 141 °C to approximately 184 °C before it enters the steam drum. Subcooled water at 184 °C, upon entering the steam drum, flows through the downcomers into the mud drum. The mud drum serves to distribute water to the waterwalls, the slag screen, and the riser tubes, where liquid water is heated to saturation conditions. The waterwalls, the slag screen, and the riser tubes will be known collectively as the riser section hereafter. The circulation of the steam-water mixture in the downcomers and the riser section is induced by the density difference between subcooled water and saturated steam-water mixture in the downcomers and the riser section respectively. The saturated steam-water stream re-enters the steam drum where the saturated steam is separated from the liquid and exits the steam drum into the superheaters. Steam is superheated to 510 °C in the two superheaters, the primary and secondary superheaters, and is fed into the common steam header. An attemperator is present between the superheaters. It regulates the temperature of steam leaving the secondary superheater by mixing subcooled water with the steam exiting the primary superheater.

The fuel used by the utility boilers is refinery gas which contains mainly methane, ethane and hydrogen. Fuel at 101.3 *kPa* (absolute) and 25 °C is fed at



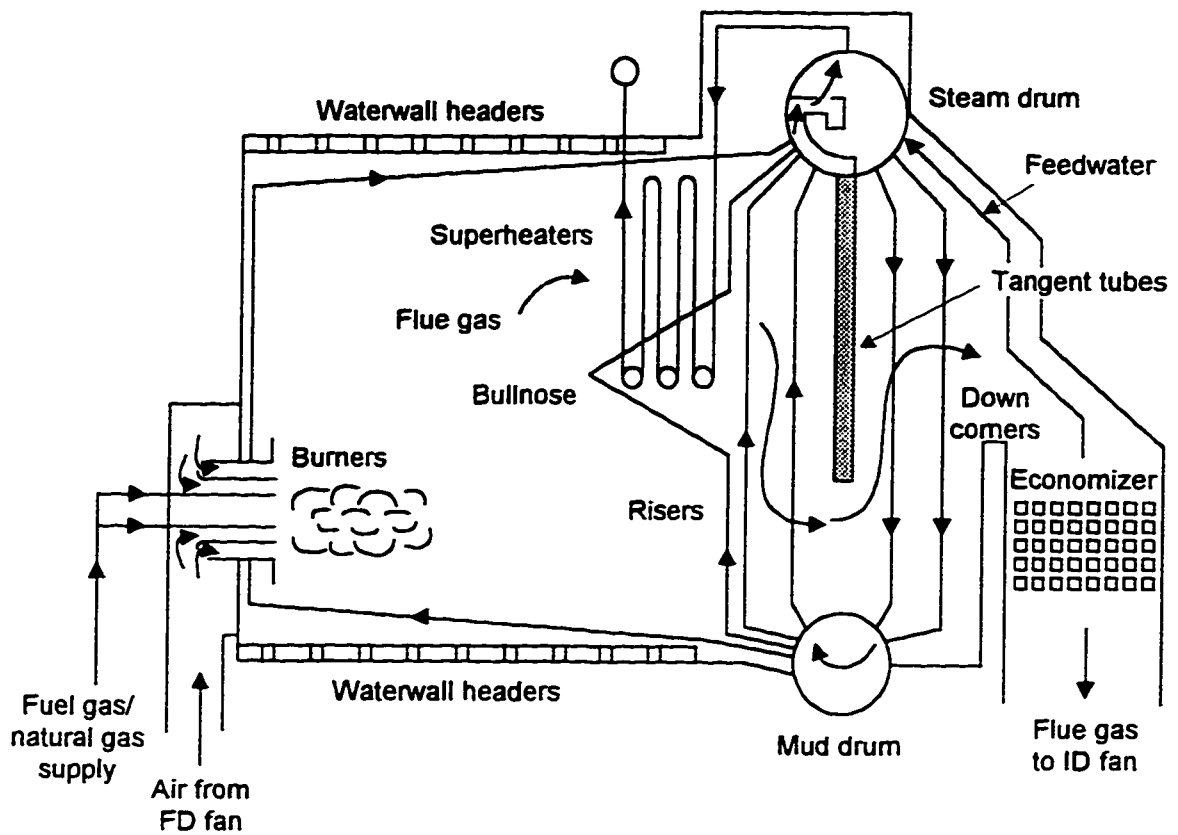


Figure 2.2: Schematic Diagram of the Utility Boiler

a rate of approximately 5.5 kg/s to the furnace section of the boiler where it is combusted with air. Air is fed at a rate such that the excess oxygen level in the flue gas leaving the stack is 1.5 mole percent. The hot flue gas then passes through the slag screen, the superheaters, the generator section (risers and downcomers), and finally through the economizer into the stack.

2.3 Boiler Sectioning

The dynamic model for the Syncrude boiler system is developed based on Dieck-Assad [6], Rackette [20] and Kakaç [13]. The utility boiler is divided into several boiler sections on both the flue gas side and the steam-water side to facilitate its modelling. Figure 2.2 shows the locations of the various boiler sections within the utility boiler. The following describes the functions and certain assumptions concerning each of the boiler sections on the steam-water and the flue gas sides.

2.3.1 Boiler Sections on the Steam-water Side

1. Economizer — Feedwater enters the boiler and is preheated in this section.

The mode of heat transfer inside the tubes is convection.

2. Generator — This section consists of all the elements of the boiler in which water can vaporize into a water-steam mixture. This includes the waterwalls, the slag screen, the riser tubes, and the downcomers. Heat transfer from the metal walls to the water-steam side is by convection and/or radiation

depending on the location of the various components.

3. **Steam Drum** — Saturated water and steam are separated in the steam drum. Accumulation of water and steam is important.
4. **Primary superheater** — Saturated steam from the steam drum is superheated in this section. Heat transfer inside the tubes is by convection only.
5. **Attenuator** — Subcooled liquid at the economizer exit conditions is mixed with superheated steam exiting the primary superheater. The attenuator is assumed to be adiabatic, thus no heat transfer takes place.
6. **Secondary superheater** — The exit stream from the attenuator is again superheated in this section. Convection heat transfer is important from the metal wall to the superheated steam.
7. **Common steam header** — Steam from the secondary superheater enters the steam header. Steam is distributed to other parts of the plant from this header. There is no heat transfer in this section.

2.3.2 Boiler Sections on the Flue Gas Side

1. **Furnace** — This is the chamber where air and fuel are mixed and combusted to provide energy to produce steam. Radiation is the primary mode of heat transfer from the furnace to the surrounding waterwalls.

2. Primary and secondary superheaters — Flue gas leaves the furnace and enters the primary and secondary superheater sections. Both radiation and convection are important heat transfer mechanisms from the flue gas.
3. Generator — This includes the waterwalls and the slag screen upstream of the superheaters and the risers and downcomers downstream of the superheaters. Radiation is important for the components upstream of the superheaters and convection in the risers and downcomers.
4. Economizer — Flue gas exits the boiler through the economizer section. Convection is the only mechanism of heat transfer.

2.4 Assumptions and Simplifications

The heat transfer, combustion, fluid flow, and thermodynamics phenomena in the boiler are extremely complicated; therefore, it is virtually impossible to incorporate all the details into the model. Thus, further assumptions are made to simplify the model development. A list of these assumptions is provided below:

1. Pressure losses due to elevation changes, pipe friction, and exit and entrance effects within a section of the boiler are ignored. For example, the outlet pressure of water leaving the economizer is assumed to be the same as that at the inlet.
2. The steam drum is assumed to be in saturated equilibrium and is adiabatic.

3. The steam drum is a right cylinder.
4. The metal walls in each boiler section are assumed to be thin so that no radial temperature gradient is present in the metal wall.
5. The metal walls in each heat exchange section in the boiler are represented as a lumped element characterized by an average metal temperature.
6. The flue gas stream in each boiler section is assumed to be well mixed: that is, the flue gas exit temperature in a boiler section is the same as that inside the section. The same assumption is made on the steam-water side.
7. Radiative heat transfer is only important in the furnace/waterwalls, the superheaters, and the slag screen. Convective heat transfer is present in all the boiler sections except at the waterwalls.
8. The steam drum, the attemperator, and the common steam header are assumed to be adiabatic.
9. Mass and energy accumulations of water and steam in the boiler are neglected except at the steam drum and the steam header.
10. Mass accumulation of flue gas in each boiler section is neglected.
11. Transport delay is assumed to be negligible compared with the time constants of the boiler system as the boiler is operating at such high rates of water and fuel.

12. Heat transfer between the various streams and the metal walls is assumed to be at steady state; that is, the dynamics of heat transfer, apart from energy accumulation with temperature change in lumped heat capacities, is ignored.
13. Pressure loss on the flue gas side is ignored.
14. Complete combustion of fuel is assumed in the furnace section of the boiler.
15. Fuel composition is assumed to be constant and the fuel is assumed to contain only hydrogen, methane, ethane, ethylene and propane.
16. Feedwater entering the steam drum is assumed to go directly through the downcomers, and then returns through the risers at the drum liquid conditions.
17. Steam quality at the exit of the steam drum is assumed to be 100 %.
18. Swelling and shrinking phenomena of water level in the steam drum are ignored in the first part of this chapter. This assumption is later removed and the dynamic model is modified. A section discussing the swelling and shrinking effects is provided in the last part of this chapter. This also removes Assumption 9, as mass and energy accumulated in the generator tubes is involved in these phenomena.
19. The presence of the mud drum is ignored; except as it defines a common pressure node for the circulation model. Implicit in this is the assumption

that no boiling occurs in the downcomers, so that the water there and in the mud drum remains in liquid phase.

20. Superheated steam is assumed to be an ideal gas in the modelling of the steam header.

2.5 Development of the State Space Boiler Model

The boiler sections defined previously in Section 2.3 can further be grouped into three groups of components:

1. Heat exchangers — the economizer, primary and secondary superheaters, the waterwalls, the screen tubes and the risers;
2. Furnace; and
3. Steam drum and steam header.

Material and energy balances on these components are facilitated by the principles of heat transfer and combustion. Heat transfer is important in the development of the model of the heat exchangers, and combustion is essential for the furnace model, whereas the steam drum and steam header models are determined exclusively from material and energy balances.

The process equations are lumped parameter expressions: for instance, the mean or effective water temperature in the economizer is assumed to be the same as that at its outlet, and a uniform superheater wall temperature is assumed

throughout the length of the tubes. This simplifies the dynamic equations from partial differential equations to first order ordinary differential equations. This approximation reduces the computation requirements of the model. The state variables involved in the boiler models are the metal wall temperatures of the various boiler sections, the flue gas exit temperature at each boiler section, the steam drum liquid level and pressure, and the common steam header temperature and pressure. A total of nineteen state variables are required to represent these primary variables of interest in the boiler.

The development of each of the boiler sections are discussed in the following sections.

2.5.1 Furnace

The furnace is where air and fuel are mixed and combusted. It is modelled after Blokh [1] and Kakaç [13]. These methods are derived primarily to determine the temperature of gas leaving the furnace based on the type of fuel, the furnace geometry, and the heat transfer from the fire ball to the waterwalls and screen tubes. This part of the model calculates the flue gas temperature at the exit of the furnace and the radiative heat transfer to the slag screen, the superheaters and the waterwalls. These calculations will be described in the following sections.

Flue Gas Temperature at Furnace Exit

The method for calculating the flue gas exit temperature in the furnace is based on the semi-empirical formula given in Kakaç [13]:

$$\frac{T_{gFe}}{T_a} = \frac{Bo^{0.6}}{Bo^{0.6} + Ma_F^{0.6}} \quad (2.1)$$

where T_{gFe} is the gas temperature at the furnace outlet, T_a is the adiabatic flame temperature of combustion, M is a coefficient relating to the pattern of the temperature field in the furnace, a_F is the coefficient of thermal radiation of the furnace, and Bo is the Boltzmann number.

The coefficient of thermal radiation of the furnace, a_F , and the Boltzmann number, Bo , can be calculated respectively as

$$a_F = \frac{1}{1 + (\frac{1}{a_{fl}} - 1)\psi_{ef}} \quad (2.2)$$

$$Bo = \frac{\phi m_f \overline{VC}}{\sigma_0 \psi_{ef} A_w T_a} \quad (2.3)$$

where ψ_{ef} is the waterwall thermal efficiency for the utility boiler. ϕ is the heat retention coefficient, m_f is the fuel mass flow rate, \overline{VC} is the heating value of the fuel, A_w is the waterwalls area, and σ_0 is the Stephan-Boltzmann constant.

The coefficient M is calculated according to the type of fuel consumed in the furnace. For fuel gas,

$$M = 0.54 - 0.2X \quad (2.4)$$

where the constant coefficients are determined empirically and X is the relative position of the highest temperature zone in the furnace.

The flame emissivity, a_{fl} , in Equation 2.2 is calculated from

$$a_{fl} = ma_{lum} + (1 - m)a_g \quad (2.5)$$

The emissivity of the luminous portion of the flame, a_{lum} , is defined as

$$a_{lum} = 1 - e^{-k_{lum}pS} \quad (2.6)$$

p is the furnace pressure, and S and k_{lum} are defined respectively as follows

$$S = 3.6 \frac{V_f}{A_w} \quad (2.7)$$

$$k_{lum} = k_g r + k_s \quad (2.8)$$

k_g , k_s , and a_g are in turn defined in the following equations

$$k_g = 10 \left[\frac{0.78 + 1.6r_{H_2O}}{(10pSr)^{0.5}} - 0.1 \right] \left(1 - 0.37 \frac{T_{gFc}}{1000} \right) \quad (2.9)$$

$$k_s = 0.3(2 - \alpha_{Fe})(1.6 \frac{T_{gFe}}{1000} - 0.5) \frac{C^w}{H^w} \quad (2.10)$$

$$a_g = 1 - e^{-k_g r p S} \quad (2.11)$$

where r_{H_2O} and r are the volume concentration of H_2O and the total volume concentration of CO_2 and H_2O respectively, C^w and H^w are the carbon and hydrogen mass content of fuel on a moist basis respectively, and α_{Fe} is the excess air ratio at the furnace exit.

Rearranging Equation 2.1, the following is obtained

$$T_{gFe} = \frac{T_a}{M(\frac{5.67 \times 10^{-11} \psi_{ef} A_w a_F T_a^3}{\phi m_f V C})^{0.6} + 1} \quad (2.12)$$

The adiabatic flame temperature, T_a , can be solved iteratively by performing a simple energy balance

$$n_{flue} \bar{H}_{flue}(T_a) = -n_f \Delta H_c + n_f \bar{H}_{fuel}(T_f) \quad (2.13)$$

where $\bar{H}_{flue}(T_a)$ is the average specific enthalpies of the flue and fuel gas as a function of temperature T_a , \bar{H}_{fuel} is the average specific heat capacity of fuel at the inlet conditions, n_{flue} denotes the molar flow rate of the flue gas. n_f is the total molar flow rate of the fuel gas, T_f is the feed temperature of fuel. and ΔH_c is the heat of combustion of the fuel.

However, iteration at each time step during the simulation is undesirable for dynamic modelling; hence, an approximation for the adiabatic flame temperature is calculated at each time step to spare computational effort. By approximating the average specific heat capacity of flue gas as a third order polynomial in T_a ,

$$\bar{H} = \bar{C}_{p,0}T_a + \bar{C}_{p,1}T_a^2 + \bar{C}_{p,2}T_a^3 + \bar{C}_{p,3}T_a^4 \quad (2.14)$$

where \bar{H} is the average enthalpy, and $\bar{C}_{p,i}$ for $i = 0, 1, 2, 3$ are the coefficients for the polynomial as given by Felder and Rousseau [8], the specific enthalpy of flue gas with a reference temperature of 25 °C can be written as:

$$\bar{H}_{flue} = \bar{C}_{p,0}(T_a - 25) + \frac{1}{2}\bar{C}_{p,1}(T_a^2 - 25^2) + \frac{1}{3}\bar{C}_{p,2}(T_a^3 - 25^3) + \frac{1}{4}\bar{C}_{p,3}(T_a^4 - 25^4) \quad (2.15)$$

Substituting Equation 2.15 into Equation 2.13 and replacing the third and fourth order temperature terms by the adiabatic flame temperature at the previous time step, the adiabatic flame temperature can be solved directly from the resulting quadratic equation:

$$AT_a^2 + BT_a + C = 0 \quad (2.16)$$

where

$$A = \frac{1}{2}\bar{C}_{p,1}$$

$$B = \bar{C}_{p,0}$$

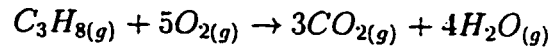
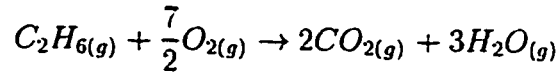
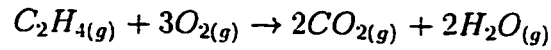
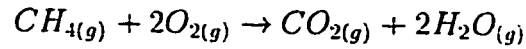
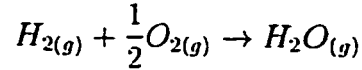
and

$$C = n_f \Delta H_c - n_f \bar{H}_{fuel} - 25 \bar{C}_{p,0} - \frac{25^2}{2} \bar{C}_{p,1} + \frac{1}{3} (T_{a,p}^3 - 25^3) \bar{C}_{p,2} + \frac{1}{4} (T_{a,p}^4 - 25^4) \bar{C}_{p,3}$$

and $T_{a,p}$ is the adiabatic flame temperature calculated at the previous time step. Note that only the positive root of Equation 2.16 is taken since the adiabatic flame temperature cannot physically be negative. That is

$$T_a = \frac{-B + \sqrt{B^2 - 4AC}}{2A} \quad (2.17)$$

The heat of combustion of the fuel, ΔH_c , is calculated assuming complete combustion of fuel according to the fuel composition and the following reactions:



Since pressure on the flue gas side is approximately 101.3 kPa, and the temper-

ature of flue gas inside the boiler is high, the products of combustion are at the gaseous state. Fuel for the utility boilers is assumed to contain only five components — hydrogen, methane, ethylene, ethane and propane; and air is assumed to contain 79 mole percent nitrogen and 21 mole percent oxygen. The excess oxygen level is set to zero if it is less than the required amount for complete combustion. This would not affect the fidelity of the combustion model since an excess supply of oxygen or air is always guaranteed in reality by all the safety features that are present in the boiler control system.

Radiative Heat Transfer from the Furnace

The total heat released per unit mass flow of fuel gas in the furnace by the combustion, H_r , is obtained from the heat balance equation of the gas side

$$H_r = \phi \left(\frac{m_f \Delta H_{c,mb} - m_{flue} H_{Fe}}{m_f} \right) = \phi \overline{VC} (T_a - T_{gFe}) \quad (2.18)$$

where H_{Fe} is the specific enthalpy of the flue gas exiting the furnace, $\Delta H_{c,mb}$ is the heat of combustion per unit mass of fuel, and m_f and m_{flue} are the mass flow rates of fuel and flue gas respectively.

The average heat flux, q_{rF} , of the furnace heating surfaces is given by

$$q_{rF} = \frac{m_f H_r}{A} \quad (2.19)$$

where A is the radiant heating surface area of the furnace. This calculated heat

flux and the area of the slag screen determine the amount of radiant heat transferred to the slag screen, the superheaters and the waterwalls.

The radiant heat transferred from the flue gas to the slag screen tubes and the superheaters, H_{rF} , is given by

$$H_{rF} = \frac{\eta_h q_{rF} A_{Fe}}{m_f} \quad (2.20)$$

A_{Fe} is the furnace exit area and η_h is 1.2 for gas furnaces. A fraction x_s of H_{rF} is assumed to be transferred to the slag screen, and the remaining energy is evenly distributed to the primary and secondary superheaters. x_s is determined based on the ratio of the heat transfer areas of the slag screen and the superheaters.

The radiant heat transfer to the waterwalls, H_{ww} , from the fire side is therefore

$$H_{ww} = H_r - H_{rF} \quad (2.21)$$

Radiant heat released by the flue gas to the waterwalls is assumed to transfer directly to the steam-water stream. The accumulation of heat in the metal walls is ignored.

2.5.2 Generator

The generator includes all the components involved in the transformation of liquid water into steam, namely the riser section and the steam drum.

The energy and continuity equations describing this system are coupled. The flow inside the riser and the downcomer sections is driven by the density difference between the water and the steam-water streams in the downcomers and the riser section respectively. This density difference is dependent on the amount of steam in the two-phase mixture which in turn depends on the heat transfer in the generator. The amount of heat transfer affects the steam generation rate which ultimately affects the density of the two-phase mixture at the riser outlet, and hence the density difference driving the flow.

Modelling of this section of the boiler can be divided into four parts:

1. Natural circulation in the downcomer and riser circuit:
2. Heat transfer from the metal walls in the riser section to the two-phase steam-water stream:
3. Heat transfer from the flue gas to the riser metal walls: and
4. Energy balance on the generator metal walls.

Transient Natural Circulation Flow Model

The natural circulation rate in a boiler can be determined by balancing the pressure drops in the downcomers and the riser section [16]. By lumping the downcomers into one downcomer section, and leaving the risers as a collection of its individual components — the slag screen, the waterwalls (including front and rear and side walls), and the riser section — the momentum equations describing the

fluid flow in the downcomers and riser section are respectively

$$-\rho_d h_d \frac{dv_d}{dt} = P_{md} - P_{sd} - \bar{\rho}_d h_d g + \Delta P_d \quad (2.22)$$

$$\rho_i h_i \frac{dv_i}{dt} = P_{md} - P_{sd} - \sum_i \bar{\rho}_i h_i g - \sum_i \Delta P_{r,i} \quad (2.23)$$

where the subscripts i and d denote the individual components in the riser section and the downcomers respectively, P_{md} and P_{sd} are the mud drum and steam drum pressures respectively, h is the height of the various sections. v is the velocity of fluid flow inside the sections, ΔP is the pressure loss across the sections, and g is the acceleration due to gravity.

Combining Equations 2.22 and 2.23 and expressing the velocities of the streams in terms of mass flow rates, the derivatives of the local mass flows with respect to time can be obtained as

$$\frac{dW_i}{dt} = \frac{A_i}{h_i} [\rho_d h_d g - \sum_i \bar{\rho}_i h_i g - \Delta P_d - \sum \Delta P_{r,i} - \frac{h_d}{A_d} \frac{dW_d}{dt}] \quad (2.24)$$

where A_i and A_d are the cross sectional areas of the risers and downcomers respectively, and $\frac{dW_i}{dt}$ and $\frac{dW_d}{dt}$ are respectively the derivatives of the local mass flow in the riser section and the total mass flow in the downcomers with respect to time.

The model for this two-phase flow calculation on the steam side developed by Leung [16] is incorporated into the overall boiler model. From this model, the total flow rate of the two-phase mixture in riser section, W_r , and the amount of

steam generation, $W_{s,gen}$, can be obtained. From these values, the steam quality, x , exiting the riser section can be obtained. W_r and x are employed to evaluate the steam drum level and the steam drum pressure in Section 2.5.3.

Notice the heat transfer enters implicitly into the calculation since the steam-water density, which is a function of the amount of heat transfer, affects the pressure drop in the riser section.

Heat Transfer to the Water Stream in the Downcomers

Once the flow rates inside the riser and downcomer sections are established, the rate of heat transfer from the metal walls to the water stream in the downcomers can be calculated.

Assuming feedwater to the steam drum enters directly into the downcomer, the water temperature at the downcomer inlet, T_{dc} , can be calculated as

$$T_{dc} = \frac{W_f}{W_d} T_f + \left(1 - \frac{W_f}{W_d}\right) T_{sat} \quad (2.25)$$

and equivalently, assuming a constant specific heat capacity for the water stream, the specific enthalpy of water at the downcomer inlet is

$$h_{dc} = \frac{W_f}{W_d} h_f + \left(1 - \frac{W_f}{W_d}\right) h_{l,sat} \quad (2.26)$$

where W_f and W_d are the feedwater flow rate and the total water flow in the downcomer, T_f is the exit temperature of the water stream at the economizer

outlet, T_{sat} is the saturation temperature of the steam drum liquid, h_f is the specific enthalpy of the water stream at the economizer outlet, and $h_{l,sat}$ is the specific enthalpy of saturated water at the steam drum pressure.

The single-phase heat transfer coefficient, h_s , for the subcooled water stream in the downcomers is determined from the modified Dittus-Boelter correlation

$$\frac{h_s D}{k} = 0.0279 \left(\frac{GD}{\mu} \right)^{0.8} \left(\frac{\mu C_p}{k} \right)^{0.4} \left(\frac{T_{bs}}{T_{fs}} \right)^{0.8} \quad (2.27)$$

where k is the thermal conductivity of the fluid, G is the mass flux of fluid inside the tubes, D is the diameter of the metal tubes, μ is the viscosity of the fluid. C_p is the specific heat capacity, T_{bs} is the bulk temperature of the water stream calculated as the average of its inlet and outlet temperatures, and T_{fs} is the film temperature which is average of the bulk temperature and the mean metal wall temperature. The physical properties of the water stream are evaluated at the film temperature.

The heat transfer rate, Q_s , from the metal walls to the subcooled water stream in the downcomers is then

$$Q_s = h_s A (T_w - T_b) \quad (2.28)$$

where A is the heat transfer area and T_w is the mean metal wall temperature.

The temperature of the water stream at the exit of the downcomers, $T_{dc,o}$,

can be calculated from

$$T_{dc,o} = T_{dc} + \frac{Q_s}{W_d C_p} \quad (2.29)$$

Since the mud drum is assumed to be adiabatic, the water temperature into the mud drum, $T_{dc,o}$, is thus equal to that at the inlet of the riser section.

Heat Transfer to the Steam-water Stream in the Riser Section

Since water is subcooled at the exit of the mud drum into the riser section, the riser section can be divided into two distinct parts: the bottom part, in which a single liquid water phase is present; and the top part, which contains a two-phase mixture of steam and water. The heat transfer coefficients are different for the two parts; and therefore, the heat transfer calculations must be separated. Heat transfer in the subcooled region, Q_{rb} , can be evaluated in the same fashion as provided in the previous section using Equations 2.27 and 2.28, and the heat transfer in the two-phase part of the risers can be determined from

$$Q_{TP} = h_{TP} A (T_w - T_{sat}) \quad (2.30)$$

where Q_{TP} is the rate of heat transfer from the metal wall to the two-phase part of the steam-water stream, h_{TP} is the two-phase heat transfer coefficient. A is the area available for heat transfer, and T_w is the average metal wall temperature.

The two-phase heat transfer coefficient, h_{TP} , can be determined from the

Pujol and Stenning correlation [19] as suggested by Butterworth and Hewitt [2]

$$\frac{h_{TP}}{h_i} = 4.0 \left(\frac{1}{\chi_{tt}} \right)^{0.37} \quad (2.31)$$

where h_i is the heat transfer coefficient for the single phase turbulent flow inside a tube calculated from Equation 2.27, and χ_{tt} is the Lockhart-Martinelli parameter defined as

$$\chi_{tt} = \left(\frac{1-x}{x} \right)^{0.9} \left(\frac{\rho_g}{\rho_l} \right)^{0.5} \left(\frac{\mu_l}{\mu_g} \right)^{0.1} \quad (2.32)$$

with x being the average steam quality in the riser section. ρ and μ denoting the density and viscosity respectively of the two-phase stream, and the subscripts l and g referring to the liquid and vapour phases respectively.

The quality of steam at the exit of the riser, x_e , can be calculated from

$$x_e = \frac{h_e - h_{l,sat}}{h_{lg}} \quad (2.33)$$

where h_e refers to the specific enthalpy of the steam-water stream at the riser exit and is determined from

$$h_e = h_{l,sat} + \frac{Q_{TP}}{W_d} \quad (2.34)$$

$h_{l,sat}$ is the saturation liquid enthalpy, and h_{lg} is the heat of vaporization.

The average quality x is then calculated as

$$x = \frac{x_c}{2} \quad (2.35)$$

The total rate of heat transfer, Q_{sww} , from the metal walls to the steam-water stream in the riser section is therefore

$$Q_{sww} = Q_s + Q_{rb} + Q_{TP} \quad (2.36)$$

Heat Transfer from Flue gas

The high flow rate of flue gas justifies the assumption of negligible mass accumulation on the flue gas side. Energy accumulation, however, is not ignored. It is used to calculate the flue gas temperatures at the exits of the various boiler sections to avoid solving for the exit temperatures via algebraic iterations, thereby improving the numerical properties of the simulation.

Since mass accumulation is neglected, the steady state material balance can be used.

$$m_{in} = m_{out} = m \quad (2.37)$$

where m represents the mass flow rate of flue gas, and the subscripts *in* and *out* refer to the inlet and outlet of each boiler section respectively. Thus the mass flow rate or the velocity of the flue gas within each boiler section can be regarded as constant. Assuming the flue gas inside a boiler section is well-mixed, the exit

temperature of flue gas at the exit of a boiler section can be calculated as:

$$\frac{dT_{out}}{dt} = \frac{1}{M_g C_{p,g}} [m C_{p,g} (T_{in} - T_{out}) - Q_g] \quad (2.38)$$

where T is the flue gas temperature, $C_{p,g}$ is the average specific heat capacity of the flue gas, M_g is the flue gas mass storage in the boiler section, and Q_g is the heat transfer from the flue gas to the metal wall.

This approach of calculating the flue gas exit temperature is also used for the other boiler sections.

The flue gas side heat transfer is given by an equation similar to Equation 2.28,

$$Q_g = h_o A (T_g - T_w) \quad (2.39)$$

Here, T_g is the temperature of the flue gas flowing over the bank of tubes which is assumed to be equal to T_{out} by the well-mixed assumption, T_w is the metal wall temperature, Q_g is the heat transfer from the flue gas to the metal wall. and A is the heat transfer area. According to Stultz and Kitto [21], the outside heat transfer coefficient, h_o , for turbulent flow over a bank of tubes is given by

$$h_o = 0.287 \left(\frac{G^{0.61}}{D^{0.39}} \right) \left(\frac{C_p^{0.33} k^{0.67}}{\mu^{0.28}} \right) F_a \quad (2.40)$$

where F_a is an arrangement factor to account for the tube configuration.

Energy Balance on the Generator Metal Wall

To complete the calculation for the generator section, the generator metal wall temperature has to be evaluated. This can be accomplished by performing a simple energy balance on the metal wall,

$$\frac{dT_w}{dt} = \frac{Q_g - Q_{sww}}{MC} \quad (2.41)$$

where M is the mass of the metal wall and C is the specific heat capacity of the metal. From this state equation, T_w can be obtained by directly integrating Equation 2.41 and be used in Equations 2.28, 2.30, and 2.39 for the determination of the heat transfer to and from the metal walls.

2.5.3 Steam Drum

Material Balance of the Steam Drum

Using the liquid control volume illustrated in Figure 2.3, the mass balance equation for the saturated liquid in the drum is

$$\frac{d\rho_l V_l}{dt} = W_f + (1 - x)W_r - W_d = W_f - xW_r \quad (2.42)$$

Note here, the mass flow in the downcomers is assumed to be the same as that in the riser section, that is, the flow rate is uniform through a complete circulation path. With this assumption, swelling and shrinking effects are ignored. This assumption will later be removed to account for the accumulation of steam in the

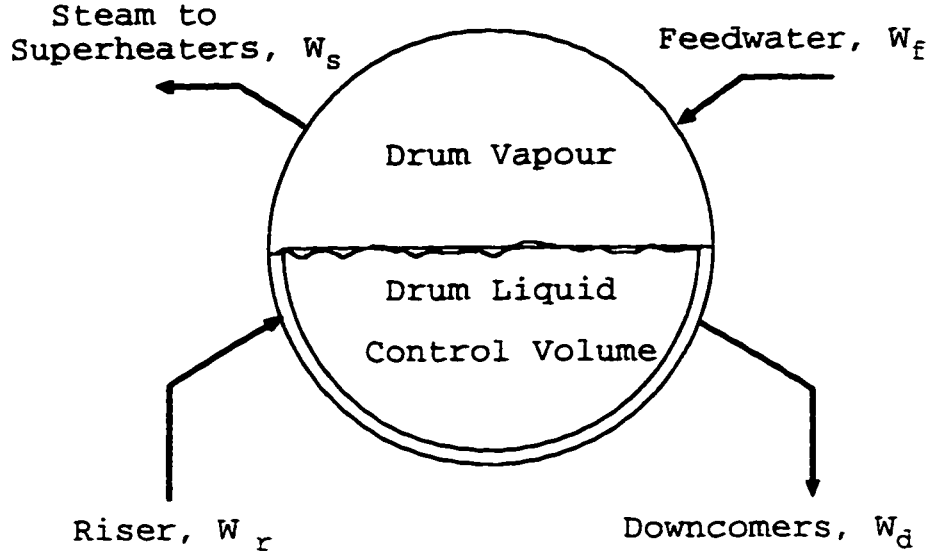


Figure 2.3: Drum liquid-water control volume

riser section, which causes the swelling and shrinking effects in the steam drum liquid level.

Expanding the derivative term, Equation 2.42 becomes

$$\rho_l \frac{dV_l}{dt} + V_l \frac{d\rho_l}{dt} = W_f - xW_r \quad (2.43)$$

By expressing the density as a quadratic function of drum pressure, the following equations are derived

$$\rho_v = a_0 + a_1 P + a_2 P^2 \quad (2.44)$$

$$\rho_l = b_0 + b_1 P + b_2 P^2 \quad (2.45)$$

$$\frac{d\rho_v}{dP} = K_1 = a_1 + a_2 P \quad (2.46)$$

$$\frac{d\rho_l}{dP} = K_2 = b_1 + b_2 P \quad (2.47)$$

a_0 , a_1 , a_2 , b_0 , b_1 , and b_2 are constants obtained by correlating the physical properties data in Perry [18] and Çengel [3].

With these correlations, the liquid phase material balance equation at the drum becomes

$$\rho_l \frac{dV_l}{dt} + V_l K_2 \frac{dP}{dt} = W_f - xW_r \quad (2.48)$$

where the subscripts l and v , denote the saturated liquid and vapour in the steam drum respectively, ρ is the density, P is the drum pressure, V_l is the volume of saturated liquid in the drum, V_v is the volume of steam in the steam drum and the superheaters, W_f is the feedwater flow, x is the average steam quality at the exit of the riser section, and W_r is the total flow rate of the two-phase streams of the riser section into the steam drum.

For the sake of convenience, Equation 2.48 is expressed in terms of a controlled variable, for instance the drum level, rather than in terms of the liquid volume. Therefore, an equation for V_l in terms of the drum level D is found. Assuming the steam drum is a right cylinder

$$\frac{V_l}{L} = R^2 \cos^{-1}\left(\frac{R-D}{R}\right) - (R-D)\sqrt{2RD - D^2} \quad (2.49)$$

D is the drum liquid level, R is the drum radius, and L is the length of the drum. Differentiating the above equation and simplifying, the following expression is

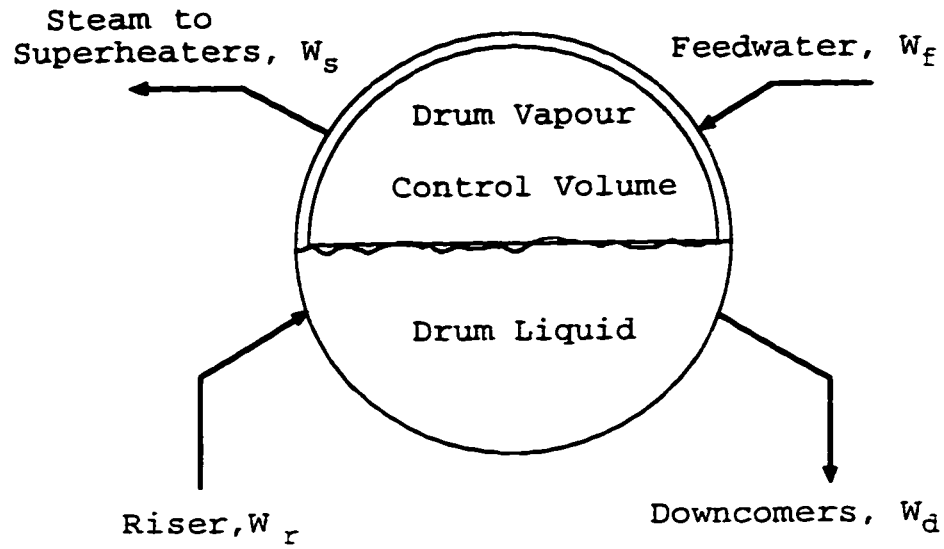


Figure 2.4: Drum vapour control volume

obtained

$$\frac{dV_l}{dt} = 2L\sqrt{2RD - D^2} \frac{dD}{dt} \quad (2.50)$$

By letting

$$\frac{dV_l}{dt} = A_0 \frac{dD}{dt} \quad (2.51)$$

an intermediate expression for the liquid mass balance at the drum is

$$\rho_l A_0 \frac{dD}{dt} + V_l K_2 \frac{dP}{dt} = W_f - xW_r \quad (2.52)$$

For the vapour phase in Figure 2.4. the material balance is

$$\frac{d\rho_v V_v}{dt} = xW_r - W_s \quad (2.53)$$

$$\rho_v \frac{dV_v}{dt} + V_v \frac{d\rho_v}{dt} = xW_r - W_s \quad (2.54)$$

Since the total volume of the liquid and vapour phases is constant, therefore,

$$\frac{dV_l}{dt} = -\frac{dV_v}{dt} = A_0 \frac{dD}{dt} \quad (2.55)$$

With the use of Equation 2.46, Equation 2.54 can be rewritten as

$$-\rho_v A_0 \frac{dD}{dt} + V_v K_1 \frac{dP}{dt} = xW_r - W_s \quad (2.56)$$

where W_s is the steam flow at the drum outlet. This steam flow can be treated as a function of the steam drum pressure and the common steam header pressure, and can be established via an empirical equation derived from the steady state data provided in the design specification sheet as

$$W_s = 4.15 \sqrt{P - P_{header}} \quad (2.57)$$

where P and P_{header} are the steam drum pressure and the common steam header pressure respectively in kPa , and the steam flow W_s is in kg/s .

Finally, by adding the material balance equations for the liquid and vapour phases in the steam drum, an overall material balance equation for the steam drum can be written as

$$A_1 A_0 \frac{dD}{dt} + A_2 \frac{dP}{dt} = W_f - W_s \quad (2.58)$$

where

$$A_1 = \rho_l - \rho_v \quad (2.59)$$

$$A_2 = V_l K_2 + V_v K_1 \quad (2.60)$$

Equation 2.58 cannot be applied directly to determine the liquid level and the pressure of the steam drum because there are two unknowns — the drum level and pressure. Therefore, one more equation required to solve for the liquid level and pressure of the steam drum. This can be obtained by performing energy balances for the steam drum.

Energy Balance of Steam Drum

The following dynamic equation can be obtained by performing an energy balance for the entire steam drum

$$\frac{d}{dt} \rho_l h_l V_l + \frac{d}{dt} \rho_v h_v V_v = W_f h_f - W_s h_v - W_d h_d + x W_r h_v + (1 - x) W_r h_l \quad (2.61)$$

where h denotes the specific enthalpies of the streams, and the subscripts l , v , f , d ,

and r represent respectively saturated liquid, saturated vapour, feed, downcomer, and riser.

Assuming feedwater enters directly into the downcomers, the water enthalpy at the downcomer inlet, h_d , can be determined from Equation 2.26.

Again, by expressing the saturated enthalpies of water and steam as functions of pressure as

$$h_r = c_0 + c_1 P + c_2 P^2 \quad (2.62)$$

$$h_l = d_0 + d_1 P + d_2 P^2 \quad (2.63)$$

$$\frac{dh_r}{dP} = K_3 = c_1 + 2c_2 P \quad (2.64)$$

$$\frac{dh_l}{dP} = K_4 = d_1 + 2d_2 P \quad (2.65)$$

where c_0 , c_1 , c_2 , d_0 , d_1 , and d_2 are constants of the enthalpy correlations.

Expanding the derivative terms in Equation 2.61, the energy balance equation for the entire steam drum becomes

$$\begin{aligned}
(K_4 \rho_l V_l + K_2 h_l V_l + K_3 \rho_v V_v + K_1 h_v V_v) \frac{dP}{dt} + (\rho_l h_l - \rho_v h_v) A_0 \frac{dD}{dt} \\
= W_f h_f - W_s h_v + Q_{swr} \quad (2.66)
\end{aligned}$$

Here, Q_{swr} is the total amount of energy transferred to the riser section as calculated in Section 2.5.2.

Therefore, solving Equations 2.58 and 2.66, the derivatives of the steam drum liquid level and pressure are

$$\frac{dD}{dt} = \frac{W_s \left(\frac{A_4}{A_2} - h_v \right) - W_f \left(\frac{A_4}{A_2} - h_f \right) + Q_{swr}}{A_3 A_0 - \frac{A_1 A_4 A_0}{A_2}} \quad (2.67)$$

$$\frac{dP}{dt} = \frac{W_s \left(\frac{A_3}{A_1} - h_v \right) - W_f \left(\frac{A_3}{A_1} - h_f \right) + Q_{swr}}{A_4 - \frac{A_3 A_2}{A_1}} \quad (2.68)$$

where A_3 and A_4 are defined respectively as

$$A_3 = \rho_l h_l - \rho_v h_v \quad (2.69)$$

$$A_4 = K_4 \rho_l V_l + K_2 h_l V_l + K_3 \rho_v V_v + K_1 h_v V_v \quad (2.70)$$

Flashing of liquid water to steam in the steam drum as a result of changes in the steam drum pressure is not included explicitly in these equations: nonetheless, it is accounted for implicitly in the boiler model itself. The flash terms in the liquid

and vapour phases cancel each other in both the material and energy balance equations and thus do not manifest themselves in the final equations.

2.5.4 Superheaters and Economizer

The primary and secondary superheaters, and the economizer are modelled identically since they can all be treated as heat exchangers. In all cases, heat is transferred from the flue gas to the metal wall, and from the metal wall into the steam or water streams.

An energy balance equation is required to describe each of the above boiler sections

$$\frac{dT_w}{dt} = \frac{Q_g - Q_s}{MC} \quad (2.71)$$

This equation is identical to Equation 2.41. The heat transfer rates can also be determined as previously from the following equations

$$Q_g = h_o A (T_g - T_w) \quad (2.72)$$

$$Q_s = h_i A (T_w - T_s) \quad (2.73)$$

$$h_o = 0.287 \left(\frac{G^{0.61}}{D^{0.39}} \right) \left(\frac{C_p^{0.33} k^{0.67}}{\mu^{0.28}} \right) F_a \quad (2.74)$$

$$h_i = 0.0279 \left(\frac{k}{D} \right) \left(\frac{GD}{\mu} \right)^{0.8} \left(\frac{\mu C_p}{k} \right)^{0.4} \left(\frac{T_s}{T_f} \right)^{0.8} \quad (2.75)$$

T_g and T_s refer to the bulk or average temperatures of the flue gas and the steam/water streams, and the physical properties are evaluated at the film temperature T_f which is given by

$$T_f = \frac{1}{2}(T_s + T_w) \quad (2.76)$$

Temperature of the flue gas and steam/water streams at the exit of the various boiler sections can be determined as given in Equations 2.38.

2.5.5 Attemperator

The attemperator is located between the two superheaters on the steam side. Steam exiting the primary superheater is mixed with subcooled spray water, at conditions of the economizer exit, and is fed to the secondary superheater for further heat transfer. The subcooled water flow rate is manipulated in such a way that the exit steam temperature of the secondary superheater is regulated at a prescribed setpoint.

Since the attemperator is assumed adiabatic and mass accumulation is neglected, the attemperator can be modelled with the steady state energy balance equation

$$m_{psh}h_{psh} + m_{sp}h_{sp} = m_{att}h_{att} \quad (2.77)$$

where m and h are the mass flow rate and the specific enthalpy of steam or water at the various boiler sections. The subscripts psh , sp , and att denote the primary superheater, spray water, and attemperator respectively. From Equation 2.77, the specific enthalpy of steam at the attemperator exit h_{att} can be determined, given the spray water flow and enthalpy, and the specific enthalpy and mass flow rate of steam at the primary superheater exit.

A correlation of the specific enthalpy of superheated steam as a function of temperature and pressure is obtained

$$h = A(P - P_0)^2 + B(T - T_0)(P - P_0) + C(T - T_0)^2 \quad (2.78)$$

where the constants A , B , and C are determined by correlating data from the steam table, h is the specific enthalpy of superheated steam, P_0 is a reference pressure of 6.0 MPa, T_0 is a reference temperature of 500 °C. P and T are the pressure and temperature of steam at the attemperator respectively. This eliminates iterations at each time step to solve for the steam temperature from its specific enthalpy at the exit of the superheater.

From Equation 2.78, assuming the attemperator pressure to be equal to the steam drum pressure, the exit steam temperature of the attemperator T can be calculated by rearranging the above quadratic equation to

$$T = \frac{1}{2C}[-X_1 + \sqrt{X_1^2 - X_2}] \quad (2.79)$$

where

$$X_1 = B(P - P_0) - 2CT_0 \quad (2.80)$$

$$X_2 = 4C(CT_0^2 + A(P - P_0)^2 - h) \quad (2.81)$$

Note here the negative root is rejected as before.

2.5.6 Common Steam Header

The common steam header is modelled exclusively from material and energy balances. The steam exiting the utility boilers is fed directly into this steam header as the input, and the steam drawn by the turbogenerators and other parts of the plant are the outputs from this steam header. Steam flow at a constant rate of 189.0 kg/s and a constant temperature of 510 °C is assumed for the two CO boilers.

Treating the header volume as a single, lumped capacity, the material balance can easily be written as

$$V \frac{d\rho}{dt} = m_i - m_o \quad (2.82)$$

where ρ is the density of steam in the header, V is the volume of the header, m is the total mass flow rate of steam, and the subscripts i and o refer to the inlet and

outlet of the steam header respectively. Hence, an equation pertaining the rate of change of steam density is obtained. Equation 2.82 will be used in conjunction with the following equations to provide the state equations for the temperature and pressure of the steam in the header.

The energy balance for the steam header can be expressed as

$$V \frac{d\rho h_o}{dt} = m_i h_i - m_o h_o \quad (2.83)$$

The enthalpy of steam inside the steam header is assumed to be the same as that at the outlet of the header based on the well-mixed assumption.

Since the specific enthalpy of steam is a weak function of pressure, and the pressure variation in the steam drum is assumed to be small, the specific enthalpy of steam can further be approximated as a function of temperature only

$$h = C_p(T - T_{ref}) \quad (2.84)$$

where T is the steam temperature and T_{ref} is a reference temperature which is chosen to be 0°C .

Combining Equations 2.83 and 2.84 gives the rate of change of the steam temperature with respect to time

$$\rho V \frac{dT_o}{dt} = m_i T_i - m_o T_o - V T_o \frac{d\rho}{dt} \quad (2.85)$$

If the superheated steam is assumed to behave as an ideal gas and the

relationship between the steam pressure and temperature can be described by the ideal gas law

$$PV = \frac{M}{M_w} RT = \frac{\rho V}{M_w} RT \quad (2.86)$$

where M is total the mass of steam in the header, M_w is the molar mass of steam, and R is the universal gas constant.

The final step is to obtain the state equation for the header pressure. This can simply be evaluated by differentiating the ideal gas law

$$\frac{dP}{dt} = \frac{RT}{M_w} \frac{d\rho}{dt} + \frac{R\rho}{M_w} \frac{dT}{dt} \quad (2.87)$$

The derivatives of steam density and temperature can be obtained from Equations 2.82 and 2.85.

To summarize, the state equations for the header temperature and pressure respectively are

$$\frac{dT}{dt} = \frac{1}{\rho V} (m_i T_i - m_o T_o - V T_o \frac{d\rho}{dt}) \quad (2.88)$$

$$\frac{dP}{dt} = RT \frac{d\rho}{dt} + R\rho \frac{dT}{dt} \quad (2.89)$$

where $\frac{d\rho}{dt}$ is calculated from Equation 2.82.

2.5.7 Swelling and Shrinking in the Steam Drum

Swelling and shrinking are complicated phenomena that occur in the steam generation section as the steam drum pressure increases or decreases. As the drum pressure decreases, the steam bubbles in the riser section expand, and as a result, the specific volume of the two-phase mixture increases. This net increase in specific volume effectively raises the liquid level in the steam drum, which defies the intuition that water level decreases as the steam pressure decreases because of the increased flashing rate. Shrinking is the exact opposite to swelling as the steam drum pressure is increased.

Modifications ought to be made to the equations describing the steam drum and the riser section in order to incorporate these effects into the boiler model. Material and energy accumulation in the riser section is now important in the model development.

Material Balance for the Riser Section

As can be seen in Figure 2.5, the material balance for the control volume CV_2 is easily obtained as

$$W_d - W_r = \frac{dM_{CV2}}{dt} \quad (2.90)$$

where M_{CV2} is the total mass storage in the riser section.

Since the water stream in the riser section can be divided into two parts, a subcooled part and a two-phase part as alluded to previously in Section 2.5.2,

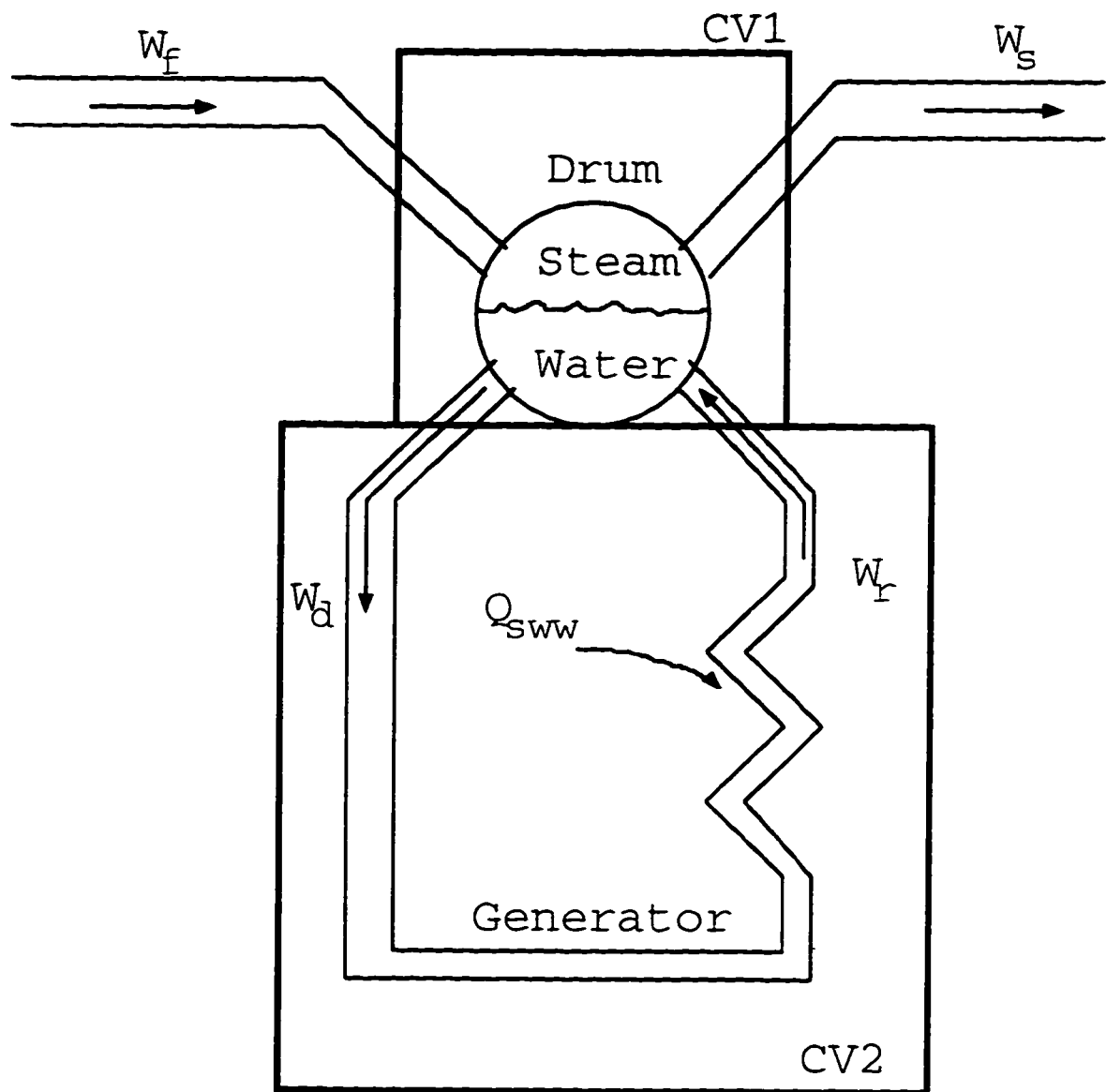


Figure 2.5: Control volumes of the steam generation section

the mass storage in this section can thus be evaluated as

$$M_{CV2} = [\rho_{ec}L_{ec} + \rho_{ev}L_{ev}]A_r \quad (2.91)$$

where ρ is the density of the fluid, L is the length of the subcooled and two-phase sections in the risers, and the subscripts ec and ev denote the subcooled and two-phase respectively. ρ_{ec} is approximated as the water density at the inlet of the riser section, and ρ_{ev} is the mean density of the two-phase stream.

Energy Balance for the Riser Section

Instead of the steady state energy balance equation used in the previous section, the energy balance equation for the control volume CV_2 in Figure 2.5 is required.

$$Q_{swr} - xW_r(h_v - h_l) + h_l(W_d - W_r) - W_f(h_l - h_f) = \frac{dE_{CV2}}{dt} \quad (2.92)$$

where E_{CV2} is the total amount of energy storage in the control volume CV_2 .

Material Balances for the Steam Drum

The material balance equations for the steam drum can be obtained as in Equation 2.42 and 2.53, only that the mass flow rates in the riser and the downcomer sections are not equal; that is,

$$W_d \neq W_r \quad (2.93)$$

The material balances for the liquid and vapour phases in the steam drum can thus be written respectively as

$$\frac{d\rho_l V_l}{dt} = W_f + (1 - x)W_r - W_d \quad (2.94)$$

$$\frac{d\rho_v V_v}{dt} = xW_r - W_s \quad (2.95)$$

Therefore, by substituting Equation 2.90, and combining Equations 2.94 and 2.95, the overall material balance for the steam drum and the riser section is

$$\frac{d}{dt}(\rho_l V_l + \rho_v V_v) = W_f - W_s - \frac{dM_{CV2}}{dt} \quad (2.96)$$

Energy Balance for the Steam Drum

Performing an energy balance for the entire steam drum for both the liquid and vapour phases as in Dieck-Assad [6],

$$\frac{d}{dt}[h_l \rho_l V_l + h_v \rho_v V_v] = W_f h_f - W_s h_v - W_d h_l + W_f (h_l - h_f) + xW_r (h_v - h_l) + W_r h_l \quad (2.97)$$

and substituting Equation 2.92, the following is obtained

$$\frac{d}{dt}[h_l \rho_l V_l + h_v \rho_v V_v] = W_f h_f - W_s h_v + Q_{swr} - \frac{dE_{CV2}}{dt} \quad (2.98)$$

The energy storage E_{CV2} in the riser section can be determined as the summation of the energy storage in the saturated vapour and liquid phases, and the subcooled liquid phase in the bottom part of the riser section.

$$E_{CV2} = [h_f \rho_l L_{ev}(1 - \alpha) + h_g \rho_g L_{ev} \alpha + \frac{h_f + h_{dc.o}}{2} L_{ec}] A_r \quad (2.99)$$

where h_f and h_g are the saturated specific enthalpies of the liquid and vapour phases respectively, ρ_l and ρ_v are the densities of the saturated liquid and vapour. α is the volumetric steam quality, $h_{dc.o}$ is the specific enthalpy of the subcooled water stream exiting the downcomer. and A_r is the total cross sectional area of the riser section.

Combining Equations 2.98, and 2.99, the overall energy balance for the steam drum and the riser section is

$$\begin{aligned} \frac{d}{dt}[h_l \rho_l V_l + h_v \rho_v V_v] &= W_f h_f - W_s h_v + Q_{swr} \\ &- A_r \frac{d}{dt}[h_f \rho_l L_{ev}(1 - \alpha) + h_g \rho_g L_{ev} \alpha + \frac{h_f + h_{dc.o}}{2} L_{ec}] \end{aligned} \quad (2.100)$$

By simplifying the overall material and energy equations (Equations 2.96 and 2.100) as in the previous section, the resulting equations for the derivatives of the drum liquid level D and the drum pressure P are

$$\frac{dD}{dt} = \frac{Q'_{swr} + (\frac{A_4}{A_2} - h_v)W_s - (\frac{A_4}{A_2} - h_f)W_f - \frac{A_4}{A_2}(W_r - W_d)}{A_3A_0 - \frac{A_1A_0A_4}{A_2}} \quad (2.101)$$

$$\frac{dD}{dt} = \frac{Q'_{swr} + (\frac{A_3}{A_1} - h_v)W_s - (\frac{A_3}{A_1} - h_f)W_f - \frac{A_3}{A_1}(W_r - W_d)}{A_4 - \frac{A_2A_3}{A_1}} \quad (2.102)$$

where

$$Q'_{swr} = Q_{swr} - A_r \frac{dE_{CV2}}{dt} \quad (2.103)$$

and the variables A_0 , A_1 , A_2 , A_3 , and A_4 are defined as in the previous section.

The derivatives of mass and energy storage terms are obtained via numerical differentiation. The derivative block in Simulink, which uses the first-order backward difference approach, is employed in the simulation. Numerical differentiation generally is undesirable for practical use because it amplifies noise that is present in the system; however, noise does not exist in this simulation, and therefore, it is justified to use numerical differentiation. Further, since the boiler system has fairly slow dynamics, given the small integration step size used in the simulation, numerical differentiation should give good estimates of the derivatives of variables.

2.6 Summary

The development of the state space model for the Syncrude boiler system, including the utility boilers and the common steam header, is outlined in this chapter. A first principles approach is taken to model this boiler system so that this model could be utilized for the study of the dynamic behaviour of the entire system during large transient excursions.

The utility boiler is divided into several boiler sections on both the flue gas and the steam/water sides to facilitate its modelling. The principles of heat transfer, combustion, and material and energy balances are used in the development of this model. The common steam header is modelled as a single, lumped capacity using material and energy balances only. The steam inside the header is assumed to be an ideal gas. This simulation model is first developed by assuming negligible swelling and shrinking effects, and is later extended to include both of these phenomena. All the assumptions and equations that are used to describe the boiler system are provided in this chapter.

Chapter 3

Evaluation of Methods for Simulating Heat Transfer in an Industrial Boiler

3.1 Introduction

The basic principle of boiler operation is to transfer energy, or heat, from the hot side to the relatively cold water side. As a result of this energy transfer, water is transformed into steam which could then be utilized for purposes such as power generation or as process steam for usage in other parts of an industrial plant. Therefore, heat transfer is among the most important physical phenomena involved in boiler operation.

An industrial boiler can be viewed as several heat exchangers connected in series, and it is modelled as a combination of heat exchangers in this project. Therefore, the method of heat exchanger modelling would affect the efficiency and accuracy of the overall simulation model. The need to identify a reliable and efficient method is apparent.

Gould [10] and Franks [9] provided background for dynamic modelling of heat exchangers. An extensive literature review of different methods for modelling the heat exchanger phenomenon has been performed by Kohlenberg [15]. These methods, however, are for two-dimensional analysis of heat exchangers, and are therefore not suitable for use in this boiler model because of the high computational requirement.

This chapter presents three methods for modelling heat exchangers. These methods are discussed in the first part of the chapter. The most effective method is then identified based on simulation results which are provided in the latter half of this chapter.

3.2 Methods for Modelling Heat Exchangers

In this section, three different methods are discussed, namely

1. the direct feedback method:
2. the energy balance method (used in the existing boiler simulation model):
and
3. the differential energy balance (DEB) method.

Discussions of the above methods are based on a single heat exchange unit with a schematic diagram as shown in Figure 3.1.

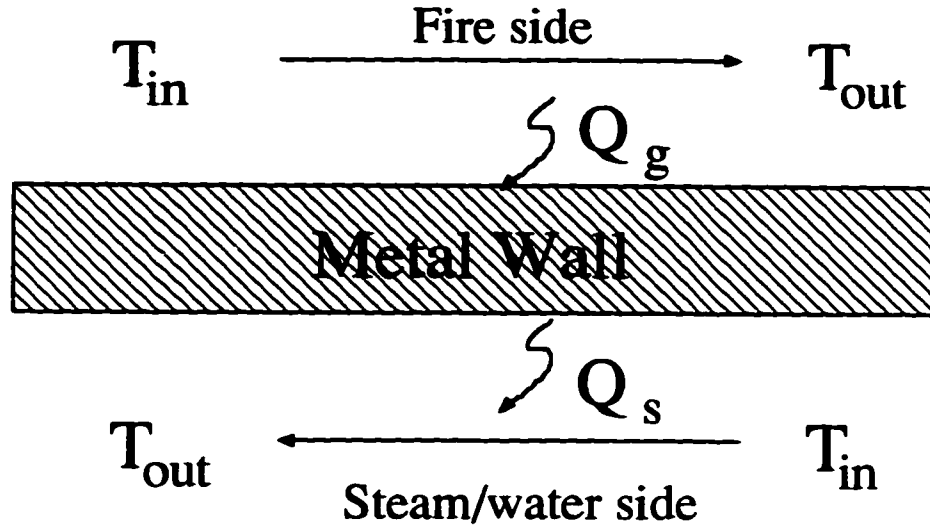


Figure 3.1: Schematic diagram showing a counter flow heat transfer component in a boiler

3.2.1 Direct Feedback Method

The direct feedback method is the simplest of the three methods that are presented in this chapter. The heat transfer rates on the outside and inside of the metal wall are calculated assuming no energy accumulations on the gas side and the steam sides, and thus can be determined respectively as in the previous chapter as

$$Q_g = h_g A (T_{gb} - T_w) \quad (3.1)$$

$$Q_s = h_s A (T_w - T_{sb}) \quad (3.2)$$

where T_{gb} and T_{sb} are calculated respectively as

$$T_{gb} = \frac{1}{2}(T_{gi} + T_{go}) \quad (3.3)$$

$$T_{sb} = \frac{1}{2}(T_{si} + T_{so}) \quad (3.4)$$

Here, Q is the heat transfer rate, h is the heat transfer coefficient. T is the temperature, and the subscripts g , s , b , and w denote the gas side, the steam side, the bulk fluid, and the metal wall respectively. The heat transfer coefficients can be calculated from Equations 2.40 and 2.75.

The outlet temperatures on the gas and steam sides of the heat exchanger can therefore be determined respectively from the steady state energy balance equations as

$$T_{go} = T_{gi} - \frac{Q_g}{m_g C_{pg}} \quad (3.5)$$

$$T_{so} = T_{si} + \frac{Q_s}{m_s C_{ps}} \quad (3.6)$$

where T_{go} and T_{so} are the exit temperatures of the gas and steam sides respectively. m_g and m_s are respectively the mass flow rates of gas and steam, and C_{pg} and C_{ps} are the specific heat capacities of gas and steam respectively.

The metal wall temperature is then obtained from the ordinary differential equation

$$\frac{dT_w}{dt} = \frac{Q_g - Q_s}{MC} \quad (3.7)$$

where MC is the heat capacity of the metal walls.

This wall temperature, T_w , is in turn used in Equations 3.1 and 3.2 for use to determine the rate of heat transfer.

This method can be represented as the flow chart provided in Figure 3.2. As can be seen from this figure, the exit temperatures on both the gas and steam sides at the previous time step are fed back directly to the calculation scheme to determine the exit temperatures for the next time step. Only one integration operation is required in this method.

3.2.2 Energy Balance Method

The energy balance method is very similar to the direct feedback method, except that the energy accumulation terms are not neglected. All the calculations for heat transfer coefficients and heat transfer rates are identical. The only differences are the exit temperatures of gas and steam.

By performing energy balances on both the gas and steam sides, the exit temperatures on the gas and steam sides can be determined respectively from

$$\frac{dT_{go}}{dt} = \frac{m_g C_{pg}(T_{go} - T_{gi}) - Q_g}{M_g C_{pg}} \quad (3.8)$$

$$\frac{dT_{so}}{dt} = \frac{m_s C_{ps}(T_{so} - T_{si}) + Q_s}{M_s C_{ps}} \quad (3.9)$$

where M_g and M_s are the mass storage of fluid in the heat exchanger.

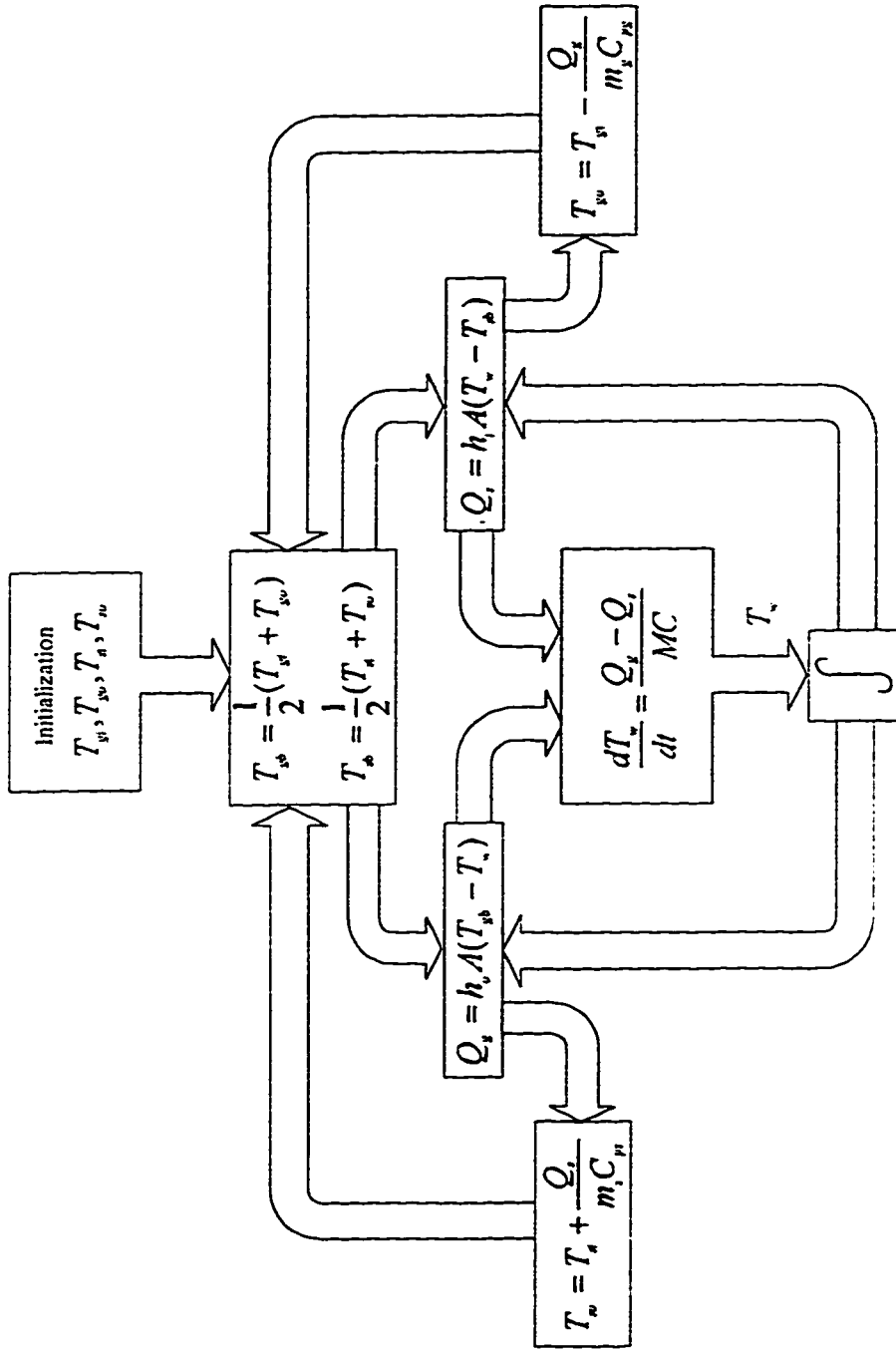


Figure 3.2: Flow chart showing the direct feedback method.

The flow chart of this energy balance method is given in Figure 3.3. The exit temperatures on both sides of the heat exchangers are obtained by integrating the derivative terms determined from Equations 3.8 and 3.9, and are then fed back to the calculation scheme. A total of three integrators are required to model one heat exchange unit.

3.2.3 Differential Energy Balance (DEB) Method

The derivation of the differential energy balance (DEB) method is presented in this section. This derivation is to determine heat transfer on both sides of the heat exchanger by convection only, and is therefore applicable only for the economizer and generator sections of the boiler. To simulate the superheater section in the boiler, in which both radiative and convective heat transfer mechanisms are important, a separate derivation of this method has to be performed. The distribution of radiative heat transfer has to be specified in this case.

Steady State Analysis

This DEB method is derived first assuming steady state heat transfer on both sides of the heat exchanger; that is

$$Q_g = Q_s \quad (3.10)$$

or

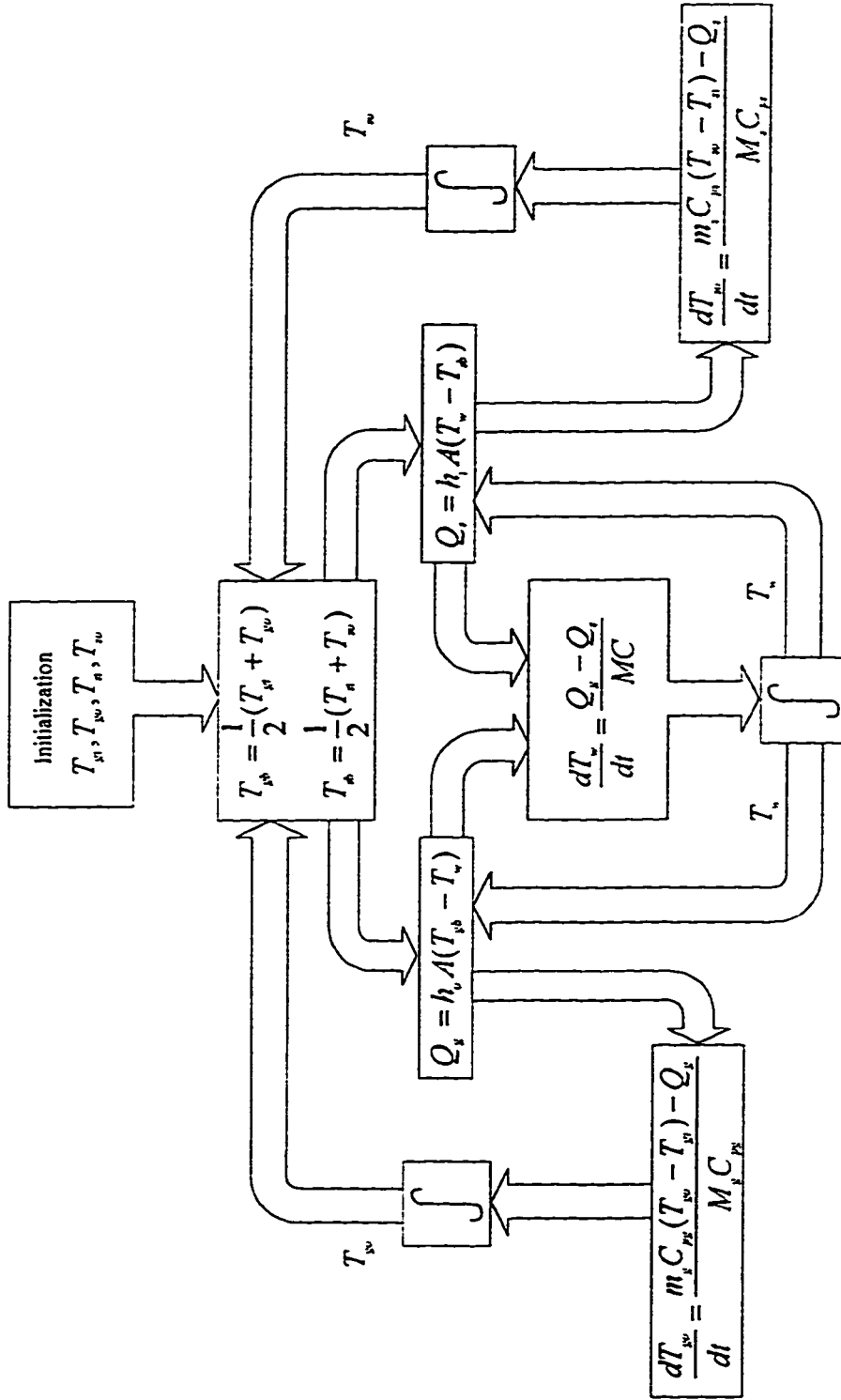


Figure 3.3: Flow chart showing the energy balance method.

$$C_{pg}m_g(T_{g,0} - T_{g,L}) = C_{ps}m_s(T_{s,0} - T_{s,L}) \quad (3.11)$$

The subscripts 0 and L denote the two ends of the heat exchanger. As can be seen from Figure 3.4, $x = 0$ denotes the inlet on the flue gas side and the outlet on the steam side, and $x = L$ denotes the outlet of the flue gas side and the inlet on the steam side.

For a differential element δx along the length of the heat exchanger: that is, in the x -direction, the differential gas side heat transfer rate can be represented in two different ways as

$$\delta Q_{g,x} = h_{gm}(A\frac{\delta x}{L})(T_{g,x} - T_{w,x}) \quad (3.12)$$

and

$$\delta Q_{g,x} = C_{pg}m_g(T_{g,x-\delta x} - T_{g,x}) = C_{pg}m_g\delta T_{g,x} \quad (3.13)$$

where

$$\frac{1}{h_{gm}} = \frac{1}{h_g} + \frac{1}{2} \frac{1}{k} + \frac{1}{h_{fouling,g}} \quad (3.14)$$

h_g is the gas side heat transfer coefficient, k is the thermal conductivity of the metal, $h_{fouling,g}$ is the fouling factor on the gas side. The subscript x denotes the position along the length of the heat exchanger. The multiplier of 1/2 to the thermal conductivity term is to account for half of the tube wall thickness. This is

lumped with the gas side heat transfer coefficient to determine the overall outside heat transfer coefficient, h_{gm} . The other half of the tube thickness is lumped with the inside heat transfer coefficient.

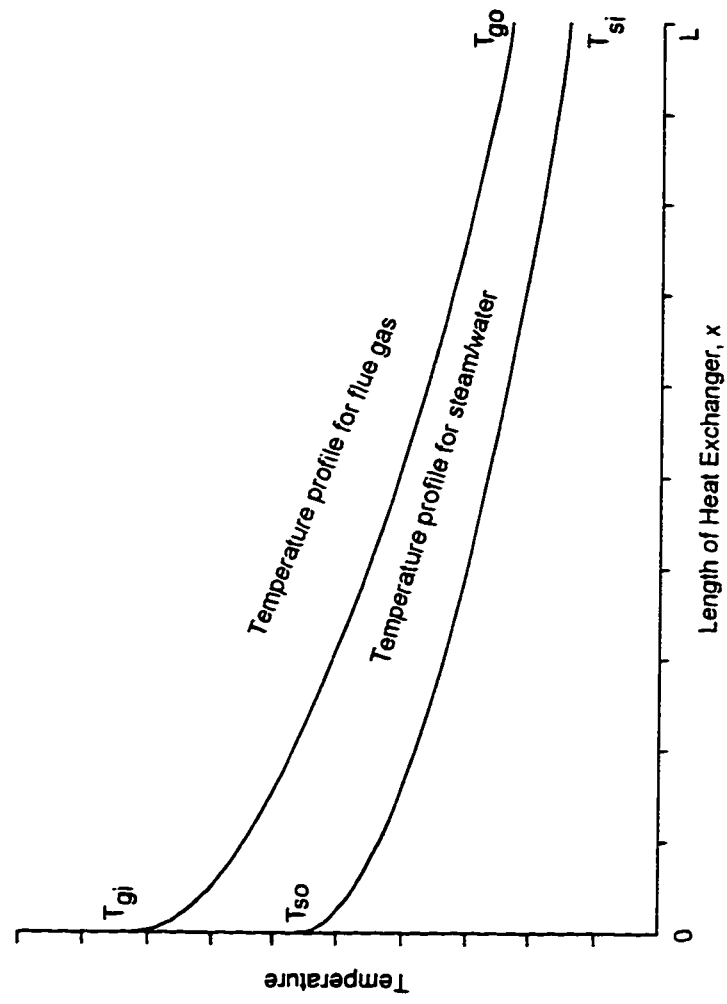


Figure 3.4: Temperature profile of the flue gas and steam/water sides along the length of heat exchanger.

In the development of the dynamic simulation model for the boiler, the last two terms are assumed to be negligible for simplicity. Hence,

$$h_{gm} = h_g \quad (3.15)$$

The subscript x in Equation 3.12 represents the position along the length of the heat exchanger.

Likewise, the differential steam side heat transfer rate is

$$\delta Q_{s,x} = h_{ms} \left(A \frac{\delta x}{L} \right) (T_{w,x} - T_{s,x}) \quad (3.16)$$

or

$$\delta Q_{s,x} = C_{ps} m_s (T_{s,x-\delta x} - T_{s,x}) = C_{ps} m_s \delta T_{g,x} \quad (3.17)$$

with h_{ms} defined similarly to Equation 3.14 as

$$\frac{1}{h_{ms}} = \frac{1}{h_s} + \frac{1}{2} \frac{1}{k} + \frac{1}{h_{fouling,s}} \quad (3.18)$$

h_s is the heat transfer coefficient on the steam side, and $h_{fouling,s}$ is the fouling factor on the steam side. Again, h_{ms} is assumed to be equal to h_s .

Since the heat transfer problem is assumed to be at steady state: that is,

$$\delta Q_{g,x} = \delta Q_{s,x} \quad (3.19)$$

Thus,

$$h_g(T_{g,x} - T_{w,x}) = h_s(T_{w,x} - T_{s,x}) \quad (3.20)$$

This can be simplified to give

$$T_{w,x} = h_a \left(\frac{T_{g,x}}{h_s} + \frac{T_{s,x}}{h_g} \right) \quad (3.21)$$

where

$$h_a = \frac{1}{\frac{1}{h_s} + \frac{1}{h_g}} \quad (3.22)$$

By substituting Equation 3.21 into Equations 3.12, 3.13, 3.16, and 3.17, and simplifying,

$$\frac{\delta T_{g,x} - \delta T_{s,x}}{T_{g,x} - T_{s,x}} = \frac{A \delta x}{L} h_1 \quad (3.23)$$

where

$$h_1 = h_a \left(\frac{1}{m_s C_{ps}} - \frac{1}{m_g C_{pg}} \right) \quad (3.24)$$

Integrating from 0 to x ,

$$\frac{T_{g,x} - T_{s,x}}{T_{g,0} - T_{s,0}} = \frac{\Delta T_x}{\Delta T_0} = e^{h_1 A \frac{x}{L}} \quad (3.25)$$

By noting that

$$\delta Q_{g,x} = -m_g C_{pg} \delta T_{g,x} = -m_g C_{pg} (T_{g,x} - T_{g,x-\delta x}) \quad (3.26)$$

$$\delta Q_{s,x} = -m_s C_{ps} \delta T_{s,x} = -m_s C_{ps} (T_{s,x} - T_{s,x+\delta x}) \quad (3.27)$$

and using Equation 3.19,

$$T_{s,x} = T_{s,0} + \frac{C_{p,g} m_g}{C_{p,s} m_s} (T_{g,x} - T_{g,0}) \quad (3.28)$$

Substituting into Equation 3.25 and solving for the flue gas temperature at position x , or $T_{g,x}$, as a function of flue gas inlet temperature, $T_{g,0}$ and the metal wall temperature at $x = 0$, or $T_{w,0}$,

$$T_{g,x} = T_{g,0} - \frac{h_g}{C_{p,g} m_g h_1} (T_{g,0} - T_{w,0}) (e^{h_1 A \frac{x}{L}} - 1) \quad (3.29)$$

The temperature of gas at the outlet of the heat exchanger can then be evaluated by substituting $x = L$ into the equation

$$T_{g,L} = T_{g,0} - \frac{h_g}{C_{p,g} m_g h_1} (T_{g,0} - T_{w,0}) (e^{h_1 A} - 1) \quad (3.30)$$

The exit temperature of steam, that is, the temperature of steam at position $x = 0$, can be determined by back substituting Equation 3.29 into Equation 3.28 as

$$T_{s,0} = \frac{T_{s,L}}{D} + \frac{D-1}{D} T_{m,0} \quad (3.31)$$

where

$$D = 1 + \frac{h_s}{C_{p,s} m_s h_1} (e^{h_1 A} - 1) \quad (3.32)$$

As can be seen in Equations 3.30 and 3.31, the exit temperatures on both sides of the heat exchanger can be solved directly from the inlet temperatures of flue gas and steam, and the metal wall temperature at the flue gas inlet. Feedback of the previous exit temperatures does not affect the calculation of the current exit temperatures directly.

Transient Analysis

The development of the DEB method up to this point is based on the assumption that the heat transfer is at steady state. However, one could conjecture that since the dynamics of heat transfer on the gas and steam sides are much faster than that of the energy accumulation in the metal walls, the dominant dynamics of the system is therefore the energy storage in the metal walls [6].

The metal wall temperature along the length of the heat exchanger is not assumed to be uniform in this derivation; however, for the sake of being consistent with the approach of boiler simulation development as provided in the previous chapter, the metal wall temperature will be assumed constant throughout the

length of the heat exchanger; that is,

$$T_{w,x} = T_w \quad (3.33)$$

Thus, the dynamics of the heat exchanger can be approximated as

$$\frac{dT_w}{dt} = \frac{Q_g - Q_s}{MC} \quad (3.34)$$

The exit temperatures on both sides of the heat exchanger can be calculated directly using this method from the inlet temperatures and the wall temperature without requiring information of the exit temperatures at the previous time step. A flow chart for this method is shown in Figure 3.5.

3.3 Evaluation of the Three Methods

3.3.1 Simulation Setup

The above methods were evaluated in terms of their efficiency by means of simulations. Two sets of simulations, s1 and s2, were performed. Each of the above methods was implemented in turn in s1 to simulate a single counter flow heat exchanger. In the second set of simulations, a fictitious plant consisting of three identical counter flow heat exchangers in series was assumed. Again, the different modelling methods were implemented in turn. Two schematic diagrams showing different arrangements of connecting a series of counter flow heat exchangers are

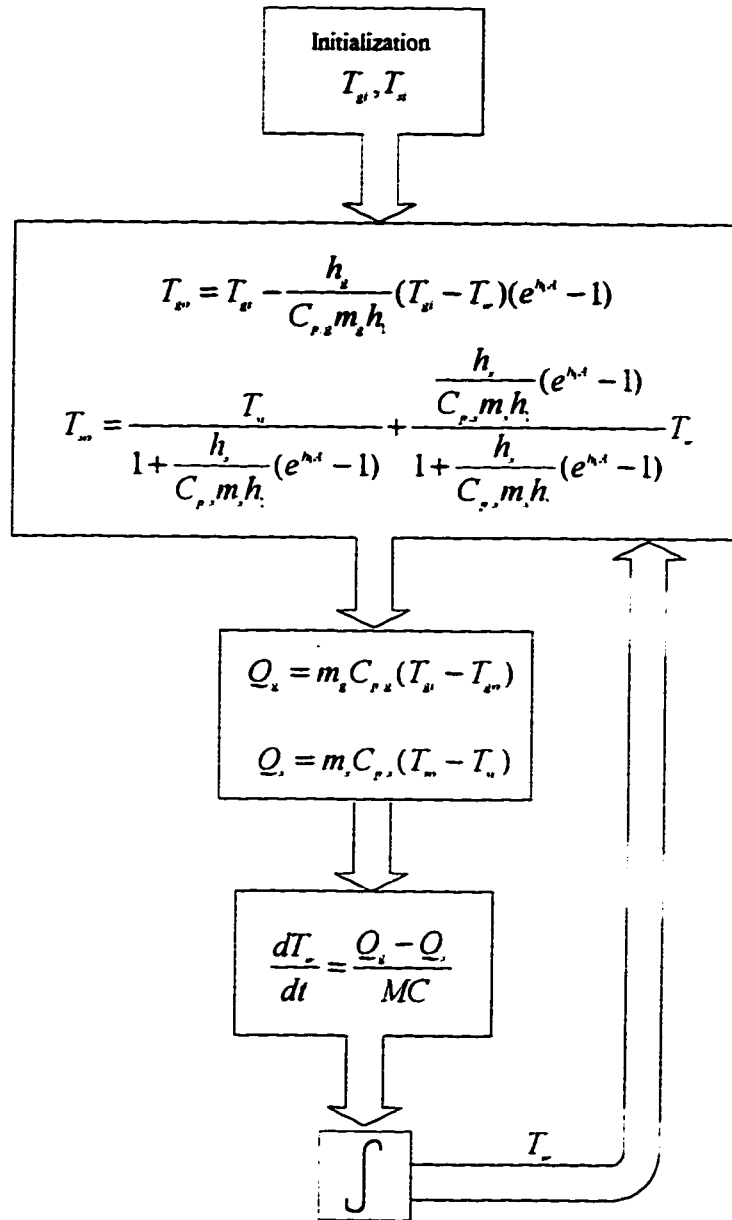


Figure 3.5: Flow chart showing the DEB method.

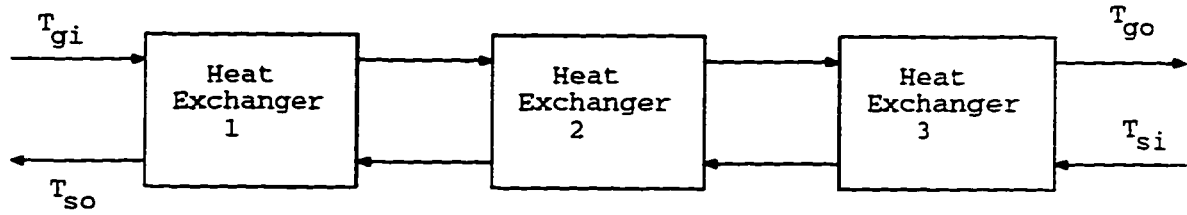


Figure 3.6: A schematic diagram showing an arrangement for connecting counterflow heat exchangers in series.

shown in Figures 3.6 and 3.7. The arrangement given in Figure 3.6 is the same as that of the boiler as discussed in the previous chapter; however, one difficulty in implementing the direct feedback and the DEB methods in an arrangement like this lies in the fact that the intermediate temperatures between the boilers are not known, and therefore, no information is provided to the down stream heat exchanger blocks for heat transfer calculations. If the heat exchangers were identical as is the case in this second simulation set, the three heat exchangers connected in series can be lumped into one heat exchanger which has a heat transfer area three times its original size. Nonetheless, this is not the case in general, and thus, the direct feedback and the DEB methods cannot be implemented directly for this type of heat exchanger arrangement. Further research is required if one desires to implement this method in an industrial boiler. The arrangement of a series of heat exchanger given in Figure 3.7 does not post the same problem as mentioned for the DEB method, and is thus utilized as the basis for simulation set s2. Two separate simulation runs, *i* and *ii*, were performed for each of the two simulation sets, using different heat transfer areas for the the heat exchangers.

Identical excitations were employed for all the simulations. The efficiency

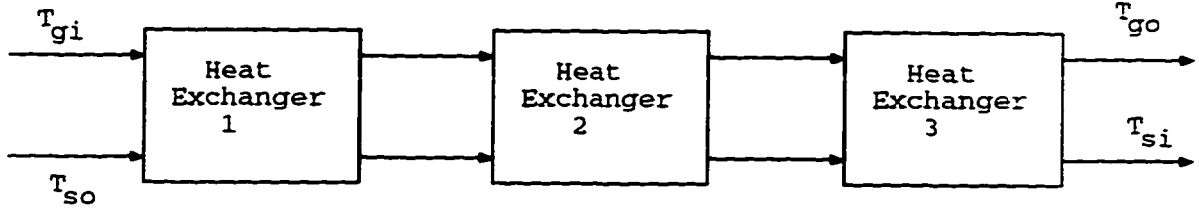


Figure 3.7: A schematic diagram showing another arrangement for connecting counterflow heat exchangers in series.

of the methods was determined based on the number of floating point operations (FLOPS) that had to be performed to simulate a fixed period of time.

The economizer section in the dynamic boiler simulation described in the previous chapter was utilized as the heat exchanger model in the fictitious plant. The heat transfer area, A , of the heat exchanger in the two sets of simulations was reduced from 1675 m^2 to 200 m^2 and 300 m^2 respectively in simulations *i* and *ii*, so that the fluid temperatures are within reasonable ranges. This reduction in area effectively reduced the length of the tubes. Other parameters were adjusted accordingly. There are four inputs to the system:

1. mass flow rate of flue gas, m_g ;
2. mass flow rate of water, m_s ;
3. inlet temperature of flue gas, $T_{g,i}$; and
4. inlet temperature of water, $T_{s,i}$.

The plant was simulated for 5000s with arbitrary step changes in the above inputs as shown in Table 3.1.

Table 3.1: Excitations to the series of heat exchangers

| Variable | Initial Value | Final Value | Step Time |
|-----------|---------------|-------------|-----------|
| m_g | 125.2 kg/s | 100.0 kg/s | 1000 s |
| m_s | 94.5 kg/s | 80.0 kg/s | 4000 s |
| $T_{g,i}$ | 800.0 °C | 900.0 °C | 2000 s |
| $T_{s,i}$ | 50.0 °C | 80.0 °C | 3000 s |

3.3.2 Results and Discussions

The simulation results are summarized in Table 3.2. The direct feedback method is the simplest among the three methods presented in this chapter in terms of its derivation and implementation: however, as can be seen in Table 3.2, this method is not reliable. In the first set of simulations, the number of FLOPS increased drastically by 83.5 times as the heat transfer area increased from 200 m^2 to 300 m^2 . The simulation even went unstable for the second set of simulations when the heat transfer areas of the three heat exchangers in series were increased. The flue gas and steam exit temperatures and the wall temperature of the heat exchanger in simulation s1 ii is given in Figure 3.8. Poor numerical stability can be observed in the figure. The various variables showed similar oscillatory responses on a separate simulation run with the minimum integration step sized decreased from 0.5 s to 0.1 s. The heat transfer rates on both sides are assumed to be so fast in this direct feedback method that the dynamics of heat transfer is negligible compared with the dynamics of energy storage in the metal wall. This assumption essentially creates a numerically stiff system, since the dynamics present in the heat exchanger are either extremely fast (the heat transfer mechanisms) or very

Table 3.2: Number of floating point operations performed to simulate the series of heat exchangers for 5000 s.

| Simulation | Energy Balance | DEB | Direct Feedback |
|--------------|----------------|--------|-----------------|
| s1 <i>i</i> | 45980 | 35156 | 38346 |
| s1 <i>ii</i> | 49248 | 36379 | 3205093 |
| s2 <i>i</i> | 238944 | 215730 | 240570 |
| s2 <i>ii</i> | 250800 | 198528 | unstable |

slow (the energy storage capacity in the metal wall). The stiffness therefore results in oscillatory responses as shown in the figure. This type of response was not observed when the other methods were employed. Energy storage on both sides of the heat exchangers, as well as in the metal wall was taken into account in the energy balance method. As a result, the dynamics of heat transfer and energy storage are not in such a contrast as in the direct feedback method. The DEB method will always yield stable results since the original third-order description of the heat exchanger is reduced to a first-order system. The states representing the exit temperatures on the steam and gas sides are removed.

The energy balance method, which is the method that is currently being used in the existing boiler simulation, was satisfactory as far as numerical stability was concerned. Nonetheless, the number of FLOPS performed in all the simulations were at least 10.8 % more than that using the DEB method. The reduction in the number of FLOPS using the DEB method could be attributed to the elimination of some of the integrators that were utilized in the simulation, and therefore, less computational effort was required. Although it is feasible that the DEB method would improve the efficiency of the overall boiler simulation,

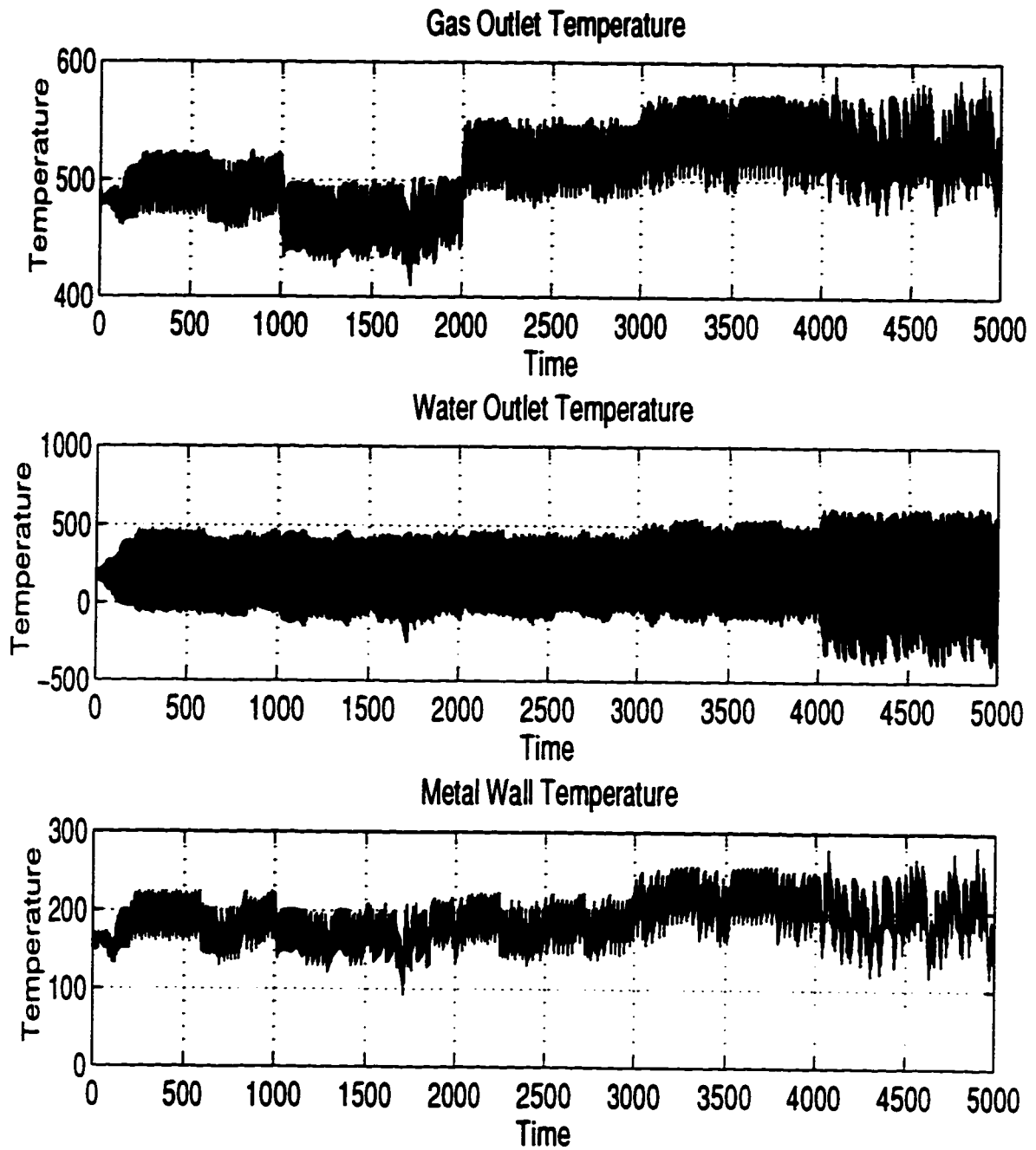


Figure 3.8: Flue gas and steam exit temperatures and wall temperature of the heat exchanger in simulation *sl ii* using the Direct Feedback Method.

the difficulty in implementing this method in the setting of a boiler renders this method as unsatisfactory. Results of simulation *s1ii* using the energy balance and DEB methods are shown respectively in Figures 3.9 and 3.10 for comparisons.

The flue gas and steam exit temperatures, and the wall temperature of the third heat exchanger in simulation *s2ii* using the energy balance and DEB methods are shown in Figures 3.11 and 3.12. Both methods show similar numerical stability and the results are close. The gas and water exit temperatures calculated by the DEB method are both within 1.2 % of those by the energy balance method, and the metal wall temperature calculated by the DEB method is 30.9 % higher than that by the energy balance method. The transient responses of the gas and water exit temperatures are slower in the energy balance method than the DEB method. The time constants of the gas and water exit temperatures in Simulation *s2ii* are approximately 100 s for both the energy balance and DEB methods.

The DEB method, in theory, is more rigorous and should therefore provide more accurate results. The temperature variations on both sides along the length of the heat exchanger are taken into consideration. This method is also more efficient than the energy balance method as far as the number of FLOPS is concerned. However, the derivation of the DEB method is much more complicated than the previous methods. It requires lengthy algebraic manipulation to attain the final equations for use in the simulation. This method also has to be re-derived for heat transfer involving both convection and radiation by assuming a certain distribution of radiative heat transfer. Moreover, this method cannot be utilized

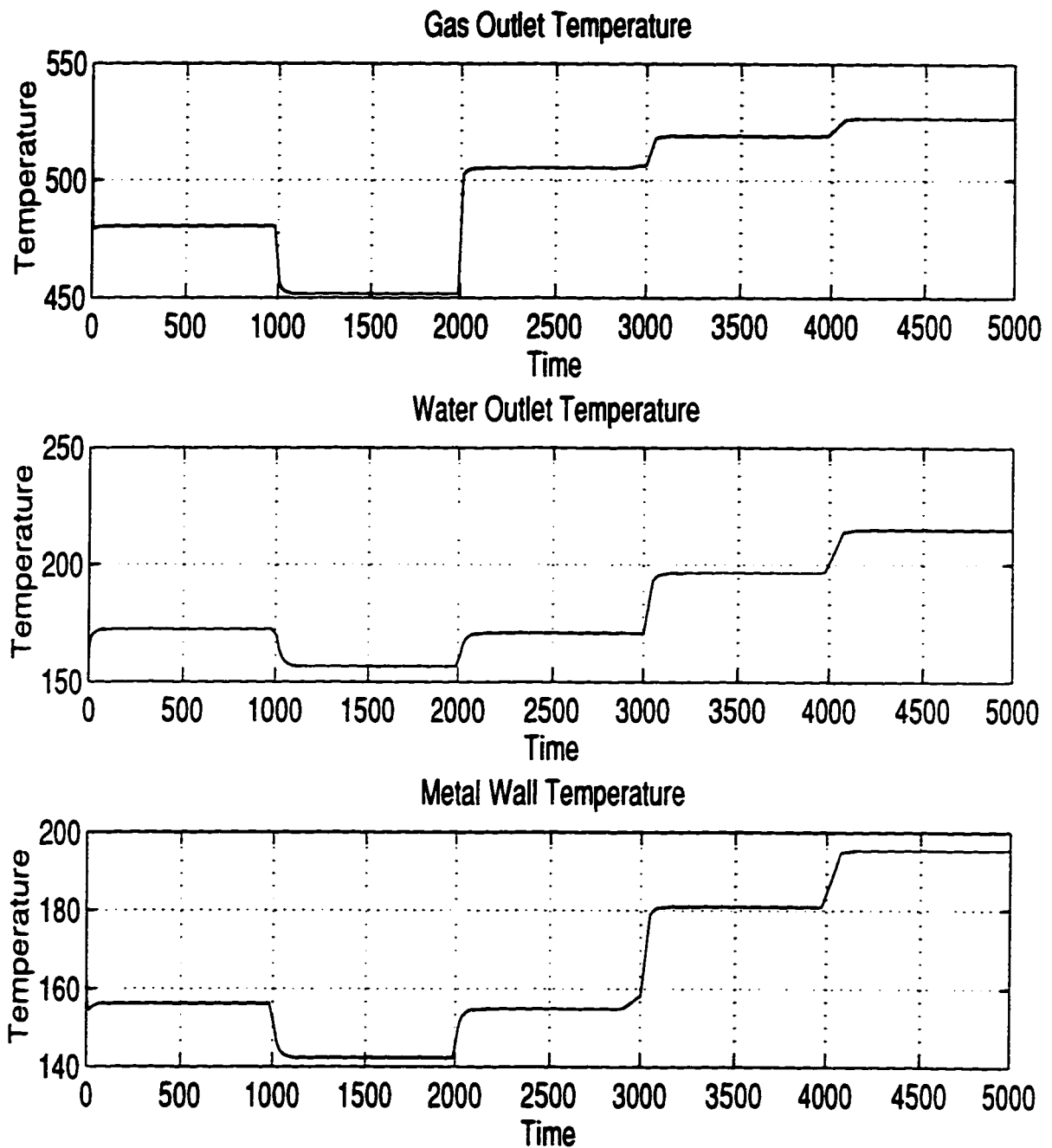


Figure 3.9: Flue gas and steam exit temperatures and wall temperature of the heat exchanger in simulation *slu* using the Energy Balance Method.

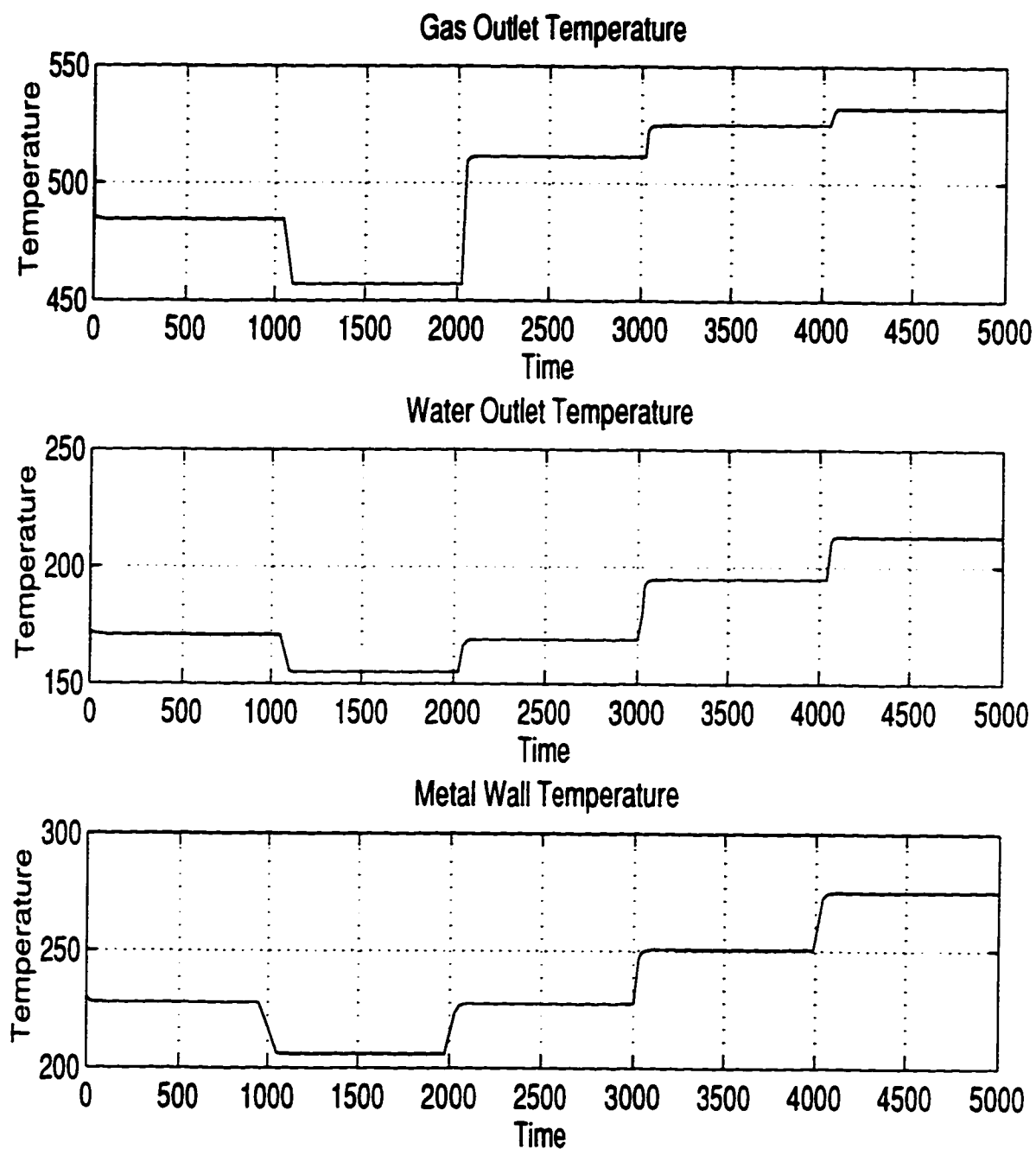


Figure 3.10: Flue gas and steam exit temperatures and wall temperature of the heat exchanger in simulation s11i using the DEB Method.

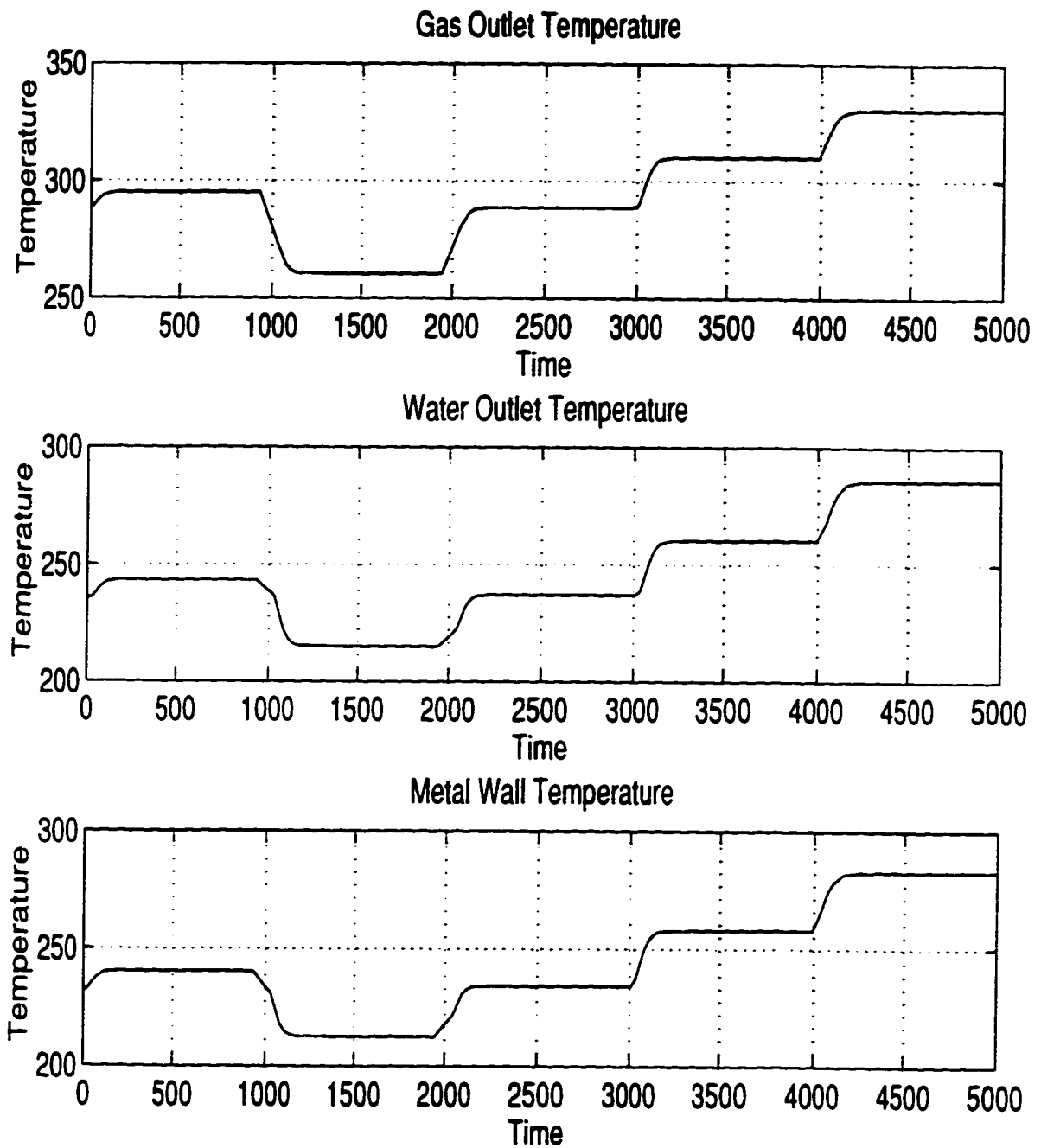


Figure 3.11: Flue gas and steam exit temperatures and wall temperature of the heat exchanger in simulation *s2ii* using the Energy Balance Method.

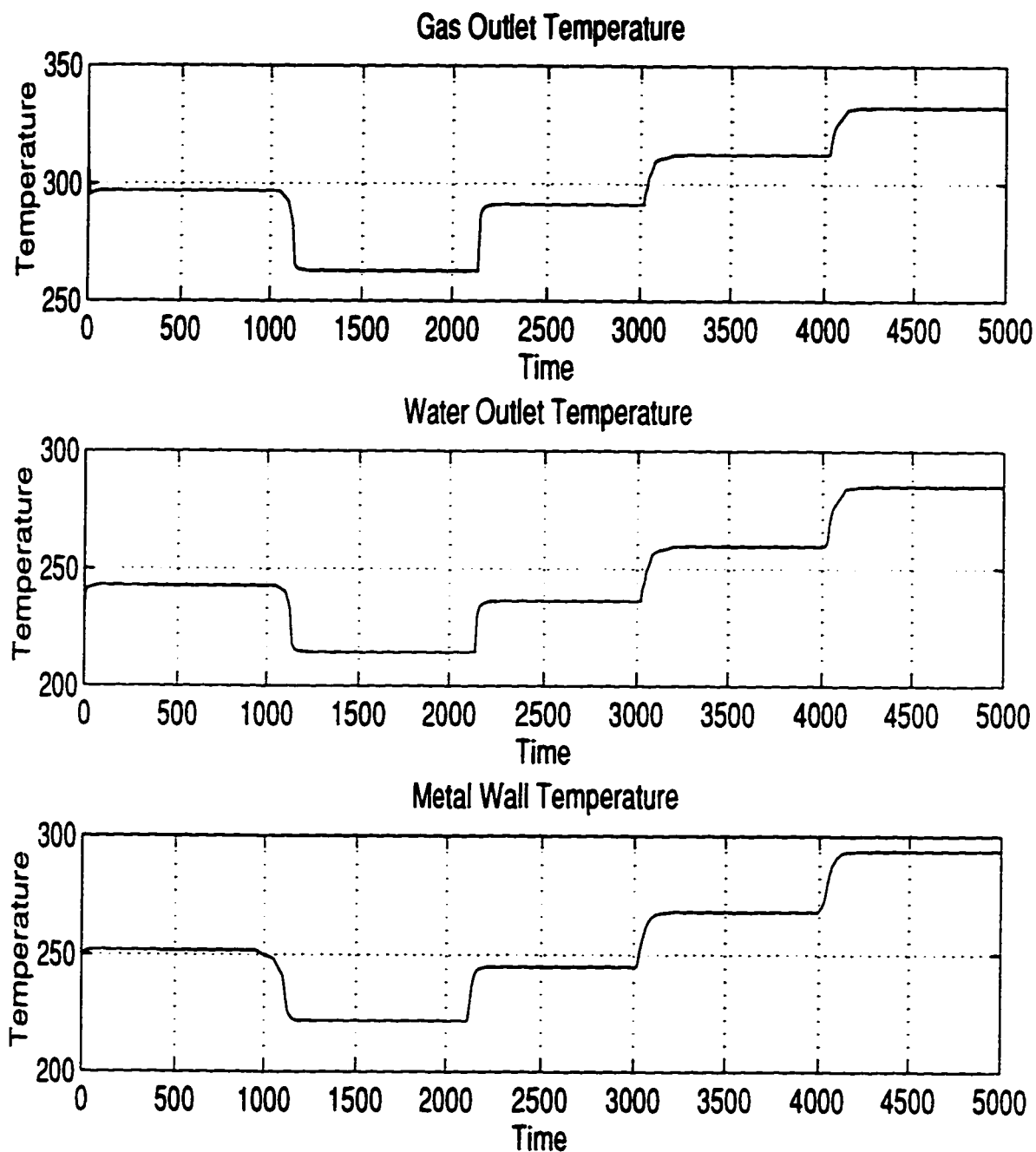


Figure 3.12: Flue gas and steam exit temperatures and wall temperature of the heat exchanger in simulation s2ii using the DEB Method.

for heat exchangers connected in series as in the setting of a boiler, therefore, it cannot be implemented in the boiler model at this stage. Further research is required if this method is to be employed in the heat transfer calculations for the boiler model.

3.4 Summary

Three heat transfer calculation methods were studied in this chapter, namely the direct feedback method, the energy balance method, and the DEB method. Each was presented in turn, and the numerical efficiency was investigated.

The direct feedback method was numerically unstable for simulating heat exchangers, especially for a system of heat exchangers in series. This method is not recommended for use in dynamic simulation of the industrial boiler system.

The energy balance method, which is the method being used in the existing boiler model, and the DEB method showed numerical stability in the simulation runs. Both methods can thus be utilized in dynamic simulation of heat exchangers to provide satisfactory results.

The DEB method is the most efficient method among the three presented in this chapter based on the number of FLOPS. However, due to the difficulty in implementing this method in the heat exchangers in the setting of a boiler, and the complexity and involved algebraic manipulations in the derivation of this method, it is not recommended for use in the developed boiler model.

Chapter 4

Control and Validation of the State Space Model of the Boiler System

4.1 Introduction

The main motivation in developing the state space model for the Syncrude boiler system is to obtain a means for studying its dynamic behaviour, which includes the stability and interactions of the entire boiler system, without disturbing the plant. The dynamic model utilized has to be accurate and reliable for the studies to be effective. Thus, the validity of the developed model has to be established. This chapter primarily deals with the validity of the dynamic model for the steam side of the boiler system including the utility boiler and the common steam header.

There is one difficulty, however, in validating the boiler model as developed thus far — it is open-loop unstable. Proper control loops have to be incorporated into the model to generate any result for comparisons with the real process. Therefore, the existing control schemes for four key areas are simplified and augmented

to the state space model. This not only allows for comparisons of the simulated and the actual conditions of the boiler system, but also facilitates the studies of interactions and stability of the boiler system subjected to different disturbances with the existing control algorithms. Proportional and integral (PI) controllers are used exclusively in the existing control schemes. The control valves are assumed to be linear and have very fast or no dynamics at all.

The first section of this chapter will be dedicated to the study and implementation of the existing control schemes. The validity of the state space model will be discussed afterwards.

4.2 Boiler Control

Boiler control systems are normally multivariable with the control loops for fuel, combustion air, and feedwater interacting in the overall system. Because of these interactions, the existing Syncrude boiler control system is very complicated. Simplifications to the existing control schemes are made to capture only the most important ingredients. There are four key control areas that arise:

1. Feedwater control:
2. Main steam and attemperator steam temperature control;
3. Firing rate demand; and
4. Combustion control.

These simplified control schemes will be introduced and discussed in detail in the subsequent sections.

4.2.1 Feedwater Control

The flow of feedwater to the boiler drum is normally controlled in order to hold the level of water in the steam drum close to the normal water level set point, and to ensure adequate water supply to the boiler for steam generation.

According to Dukelow [7], the main objectives of feedwater control are to:

1. control the drum level to a set point:
2. minimize the interaction with the combustion control system:
3. make smooth changes in the boiler water inventory as boiler load changes:
4. properly balance the boiler steam output with the feedwater input: and
5. compensate for the feedwater pressure variation without process upset or set point shift.

The existing feedwater control is the three-element control scheme as given in Dukelow [7]. A schematic of the feedwater control scheme is depicted in Figure 4.1. The low load water valve in the actual configuration is ignored in the simulation because it is mainly used during start-up. The temperature and pressure corrections for the steam flow signal in the existing scheme are also ignored.

One difficulty in feedwater control lies in the swelling and shrinking of water level in the steam drum. Swelling results when the steam load on a boiler

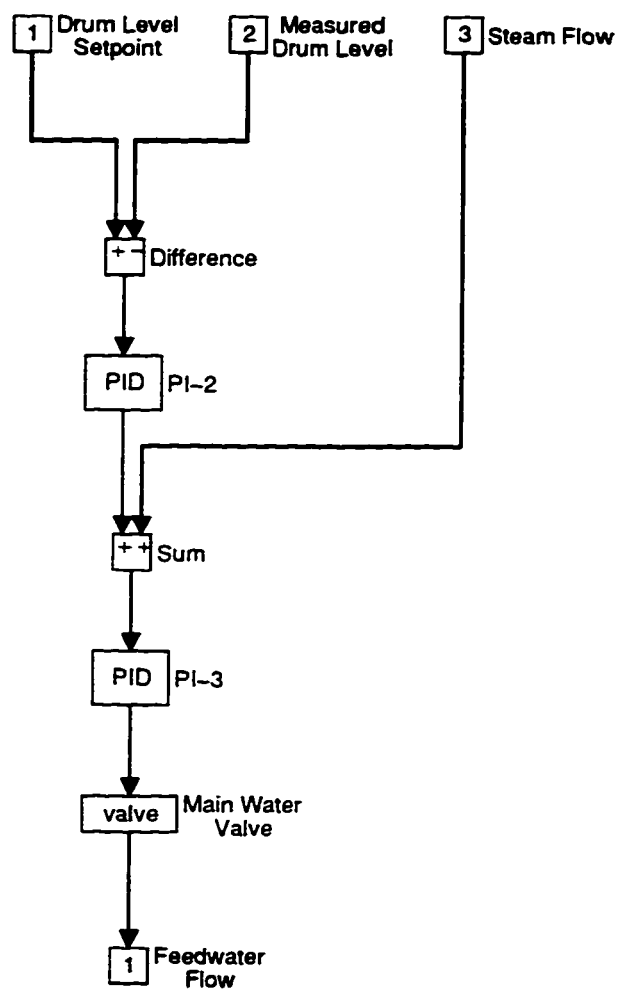


Figure 4.1: Feedwater Control

increases. This decreases the pressure in the steam drum and therefore increases steam generation in the riser section, which in turn decreases the average density of the riser two-phase mixture. This leads to an increase in the drum liquid volume, causing the liquid level to increase. Shrinking is the exact opposite which occurs when the steam load is decreased.

At a constant steam drum level, that is, without swelling or shrinking effects, an increase in the steam load on the boiler would result in an increase in feedwater demand. On the other hand, with a constant steam load, an increase in drum level would cause a reduction in feedwater flow. Since, in reality, an increase in steam load always results in an increase in the steam drum liquid level, namely the swelling effect, these effects conflict with one another.

A properly adjusted feedwater control system balances these opposing influences so that the basic control objectives listed above are met. For an increase in steam load, if the influence of drum level is too strong, the initial control action will be to reduce feedwater flow because of the swelling effect. As the swelling effect settles and the drum level falls below the set point, feedwater demand will increase to compensate for its reduction during swelling, causing the drum level to move beyond the control set point to make up for the lost water flow causing oscillatory drum level response. On the other hand, if the influence of steam flow is too strong, the initial control action will be to increase feedwater flow. The drum level would therefore stay above the set point for a prolonged period of time.

The desired action is for the feedwater to hold its flow rate initially during a load change and change only as the drum level begins to return to its set point. In this manner, water inventory can be smoothly adjusted to its new desired value.

Since the drum level control signal calls for a feedwater decrease as the steam flow signal is calling for an increase, the proper gain settings on steam flow and drum level should cause them to offset each other, and no immediate change in the water flow control valve signal should result. As the drum level begins to change, the feedwater valve control signal is manipulated to keep the system in continuous balance until steam flow and water flow are again equal and the drum level is at the set point. At this point, since steam flow and water flow are equal, there is no driving force to cause further changes in boiler drum water level. In this three-element arrangement, steam flow is the feedforward signal that anticipates a need for additional feedwater flow.

4.2.2 Main Steam and Attenuator Temperature Control

The superheated steam temperature at the exit of the boiler is bound to vary unless the boiler is equipped with a control mechanism. The primary purpose of the control mechanism is to adjust the superheating capacity as the steam load changes. The boiler steam temperature is also affected by several other factors such as the cleanliness factor, the fuel being fired, the imbalance between the fuel energy input and steam energy output, and the excess combustion air. The

control mechanism must also have the capability of adjusting for these secondary influences in order that the steam temperature at the boiler exit may be controlled at a desired value.

The purpose of steam temperature control is usually to maintain as nearly as possible a constant superheat temperature at all boiler loads. The primary benefit in constant steam temperature is in improving the economy of conversion of heat to mechanical power while not exceeding the temperature limits for the piping. Control capability increases the lower load temperature, resulting in the potential for higher thermal efficiency of the power generation process [7].

In addition, maintaining a constant temperature minimizes the unequal expansion or contraction due to unequal mass of material between the static and the various rotating parts of the power generation machines. This makes possible the use of smaller clearances between the parts and results in higher thermal efficiency in the energy conversion process.

The simplified version of the existing control scheme is shown in Figure 4.2. A cascade arrangement is employed to control both the main steam temperature and the steam temperature at the attemperator exit. The modification of the set point to the attemperator temperature controller (the secondary controller in the control loop) by the air flow and steam drum pressure in the actual algorithm is ignored in the simulation model.

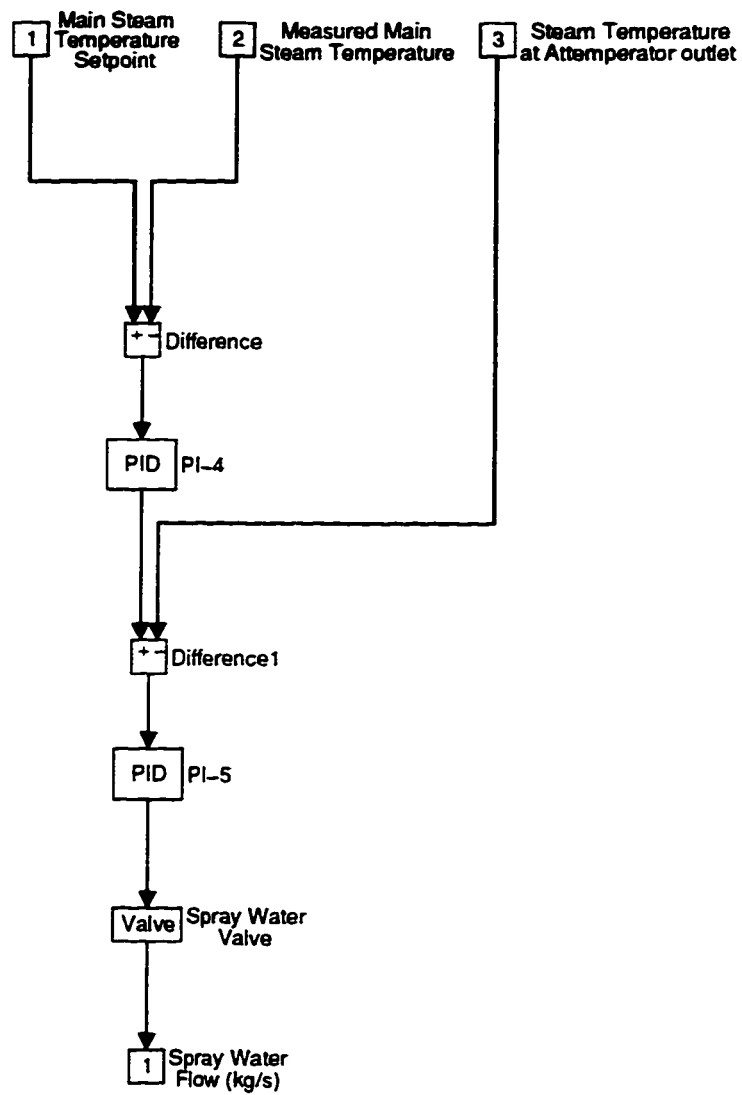


Figure 4.2: Main Steam and Attemperator Temperature Control

4.2.3 Firing Rate Demand

The combustion, feedwater, and steam temperature control systems determine how a boiler actually operates and whether it achieves its efficiency potential. The controls should be designed to regulate fuel, air, and water flow to a boiler and maintain a desired steam pressure while simultaneously optimizing the boiler efficiency.

The firing rate demand for the utility boilers is manipulated such that the steam header pressure is maintained at a constant level through a simple feedback configuration with a PI controller. This is shown in Figure 4.3. The output signal from the controller is the demand firing rate which is fed as a set point to the combustion control loop. This signal determines the requirements of fuel and air flows to the boiler.

4.2.4 Combustion Control

The objective of combustion control is to ensure enough fuel supply to the boiler for steam generation and ample air supply for the complete combustion of the fuel. The simplified control scheme is shown in Figure 4.4. This control arrangement is now generally recognized as a standard control arrangement [7]. The existing control configuration accounts for the variations in fuel composition, fuel heating value, fuel and air temperatures, and the ratio of which fuel and air are fed. Nonetheless, all of the above, except for the fuel and air ratio, are assumed constant in the simulation, and thus, these arrangements in the original control

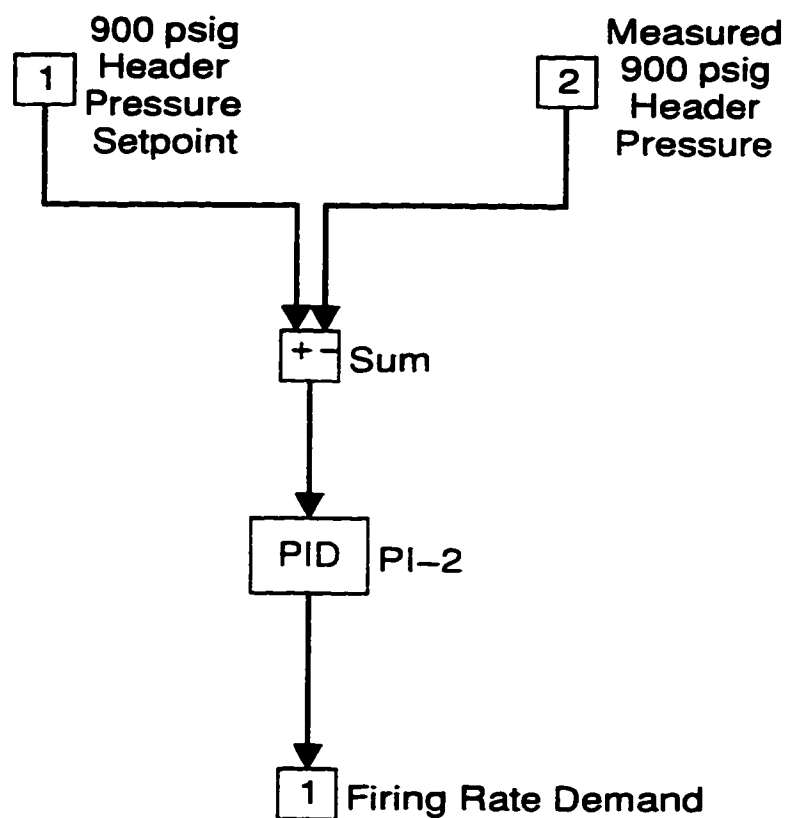


Figure 4.3: Firing Rate Demand (Plant Master)

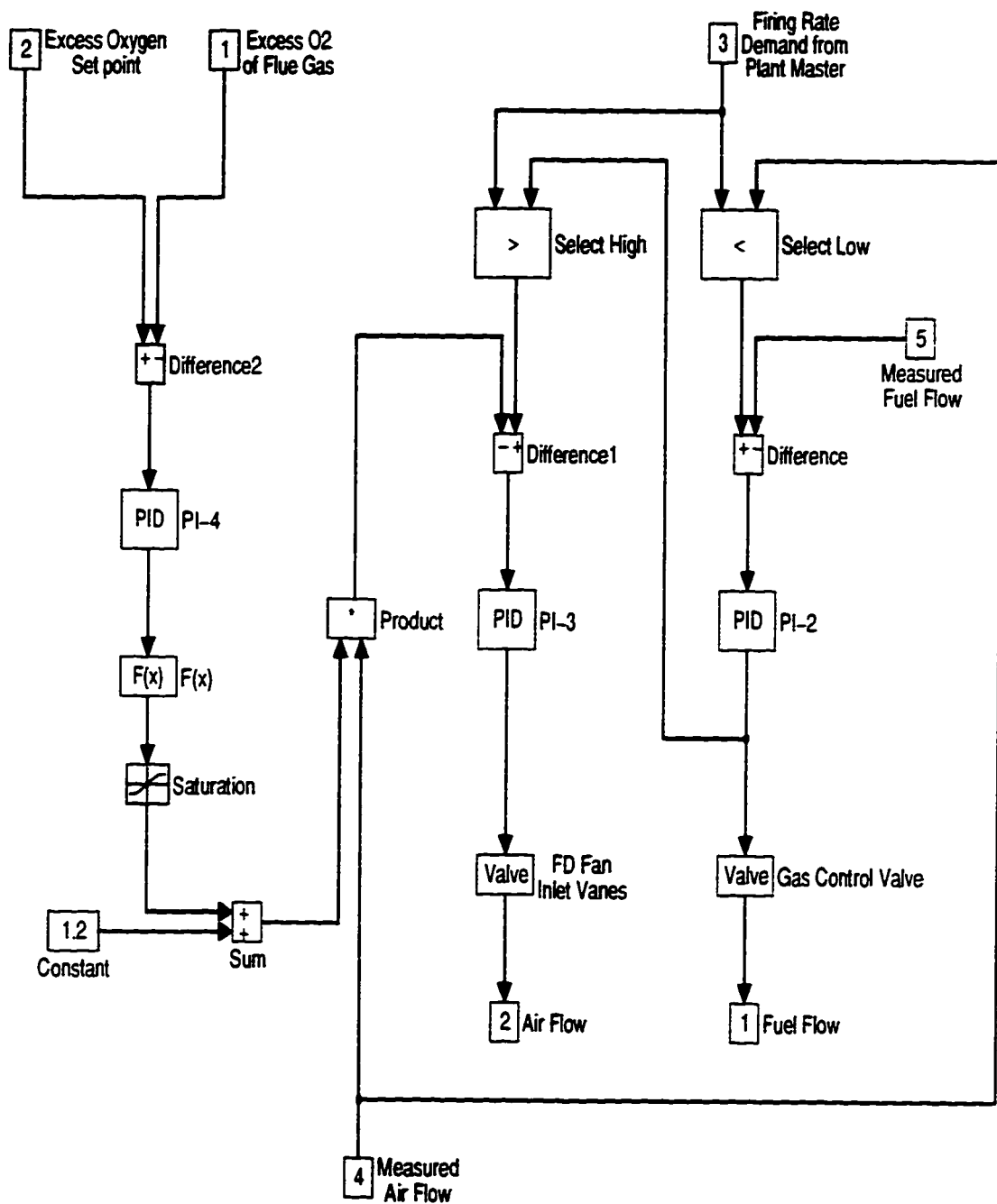


Figure 4.4: Combustion Control

scheme for all these variations are eliminated in the model.

The select high and select low functions are present to add active safety constraints to the system. The low select function compares the firing rate demand signal to the air flow measurement signal, and the lower of the two becomes the set point of the fuel controller. The result is that the fuel flow set point is limited to the level of the signal representing available combustion air flow. Similarly, the high select function forces the air flow set point to the higher of the two signals that represent firing rate demand and fuel flow. The result is that actual fuel flow sets the minimum air flow demand.

Figure 4.4 also shows the application of an oxygen trim control loop. By its control action, the air flow measurement signal is continuously adjusted so that the excess oxygen level is maintained at a specified level. The firing rate demand signal from the plant master (Figure 4.3) is used as the input signal in the arrangement shown.

4.3 Model Validation

The dynamic model developed is open loop unstable if the steam demand, and the fuel and air flow rates to the system do not match. These variables have to be specified and matched exactly in order for the system to reach a steady state. If the steam demand from the steam header is fixed, an excess in fuel and air flow to the boilers will result in an excess in steam generation, causing in an increase in the steam header pressure and the drying up of the steam drum at constant rates.

If the specified fuel and air flow rates are insufficient, steam generation would be too low and that will result in a constant rate of decrease in the steam header pressure and a constant rate of increase in the steam drum liquid level.

Therefore, control loops have to be incorporated into the simulation in order to obtain any form of comparisons between the simulated data and the actual process data of the Syncrude boiler system. However, validation of the model is still difficult due to the unavailability of data at present and the lack of measurements of some variables. The results of simulations will be compared with data obtained from Syncrude engineering personnel through personal communications. These data, which are also based on simulations, provides steady state values of the variables at three different steam loads, and is regarded as the basis of validation of the developed model.

4.3.1 Simulation Setup

At present, validation is performed only on the developed dynamic model of the boiler system, including the utility boilers and the 6.6 *MPa* common steam header. This model will later be connected to the electrical side of the power generation system for further validation. In this section, model validation only pertains to the boiler system, in particular, the utility boilers and the common steam header.

All the variables in this dynamic model for the boiler side are controlled except the steam demand out of the common steam header which is the only

input to the boiler system. This variable will be manipulated and the transient responses of the other variables are studied. The simulations are divided into two parts: steady state validation and dynamic validation. In the first part, the boiler system is subjected to three different steam loads and the results are compared with the report mentioned above. The transient behaviour of this boiler system is then studied by implementing a series of step changes in the steam load to the boiler system.

The steam generation of the two CO boilers connected to the steam header is assumed to be each at a constant rate of 94.5 kg/s and at a constant temperature of 510°C .

4.3.2 Simulation Results

Steady State Results

Simulations were performed at three different steam loads to obtain steady state results for comparison with the obtained data. Cases 1, 2, and 3 in the following tables correspond to steam loads of 94.5 kg/s , 100.8 kg/s , and 108.9 kg/s respectively for each of the utility boilers.

The mean temperatures of the metal walls of the various boiler sections at three different steam loads from the simulations of the dynamic model developed are shown in Table 4.1.

A comparison of fuel composition between the simulation and the obtained data is shown as Table 4.2. The lower heating value of the fuel is 834.8 kJ/mol

Table 4.1: Mean temperatures of metal walls at various boiler sections

| | Units | Case 1 | Case 2 | Case 3 |
|-----------------------|-------|--------|--------|--------|
| Economizer | °C | 160.5 | 160.9 | 161.4 |
| Generator | °C | 304.3 | 305.3 | 306.7 |
| Primary superheater | °C | 387.4 | 390.5 | 394.2 |
| Secondary superheater | °C | 484.2 | 484.4 | 484.7 |

Table 4.2: Comparison of fuel composition of the simulation and the Syncrude report

| | Report | Simulation |
|-----------------|--------|------------|
| Component | Mole % | Mole % |
| Hydrogen | 30.01 | 33.88 |
| Propane | 7.26 | 8.20 |
| Propene | 5.85 | - |
| n-Butane | 1.14 | - |
| i-Butene | 2.93 | - |
| Methane | 33.30 | 37.59 |
| Nitrogen | 0.92 | - |
| Carbon Monoxide | 0.45 | - |
| Carbon Dioxide | 0.12 | - |
| Ethene | 5.70 | 6.42 |
| Ethane | 12.32 | 13.91 |
| Total | 100.0 | 100.0 |

from the simulation compared with 827.5 kJ/mol from the obtained data, showing a difference of 0.88 %.

Table 4.3 shows some important simulation results for determining the overall energy balance of the boiler. The results in the obtained data are also included in the table for comparisons.

Comparisons between the simulation results and the obtained data of the flue gas temperatures at various locations in the boiler for the three cases are given in Table 4.4.

Table 4.3: Comparison of the reported and simulated variables of the boiler system at steam loads of 94.5 kg/s, 100.8 kg/s, and 108.9 kg/s

| | Case 1 | | | Case 2 | | | Case 3 | | |
|-----------------------------|--------|------------|--------------|--------|------------|--------------|--------|------------|--------------|
| | Report | Simulation | % Difference | Report | Simulation | % Difference | Report | Simulation | % Difference |
| Flow rates (kg/s) | | | | | | | | | |
| Steam to header | 94.5 | 94.5 † | - | 100.8 | 100.8 † | - | 108.9 | 108.9 † | - |
| Fuel | 5.27 | 5.14 | 2.28 | 5.62 | 5.51 | 1.96 | 6.09 | 5.98 | 1.81 |
| Flue gas | 115.3 | 100.1 | 13.2 | 123.1 | 107.4 | 12.8 | 133.4 | 116.6 | 12.6 |
| Temperatures (°C) | | | | | | | | | |
| Feedwater to boiler | 141.7 | 141.7 † | - | 141.7 | 141.7 † | - | 141.7 | 141.7 † | - |
| Final steam | 510.0 | 510.0 † | - | 510.0 | 510.0 † | - | 510.0 | 510.0 † | - |
| Flue gas to stack | 208.3 | 194.0 | 6.87 | 211.7 | 197.0 | 6.94 | 216.1 | 200.8 | 7.08 |
| Pressures (MPa(abs)) | | | | | | | | | |
| Steam drum | 7.17 | 7.27 | 1.39 | 7.23 | 7.36 | 0.41 | 7.34 | 7.49 | 2.04 |
| Common steam header | 6.65 | 6.65 † | - | 6.65 | 6.65 † | - | 6.65 | 6.65 † | - |

Notes: †denotes specified input ‡denotes controlled variable

Table 4.4: Flue gas temperatures (°C) at the exits of the various boiler sections at three steam loads

| | Case 1 | | | Case 2 | | | Case 3 | | |
|-------------|--------|------------|--------------|--------|------------|--------------|--------|------------|--------------|
| | Report | Simulation | % Difference | Report | Simulation | % Difference | Report | Simulation | % Difference |
| Furnace | 1515.6 | 1378.9 | 9.02 | 1543.3 | 1399.6 | 9.31 | 1571.1 | 1424.6 | 9.32 |
| Superheater | 932.2 | 1063.7 | 14.1 | 959.4 | 1085.3 | 13.2 | 990.6 | 1111.5 | 12.2 |
| Generator | 329.4 | 369.6 | 12.2 | 334.4 | 382.7 | 14.4 | 342.8 | 399.1 | 16.4 |
| Economizer | 208.3 | 194.0 | 6.87 | 211.7 | 197.0 | 6.94 | 216.1 | 200.8 | 7.08 |

Transient Response of the Boiler System

A series of step changes in the steam demand from the common steam header was implemented as the input to the simulation model to obtain the dynamic behaviour of the system. The boiler system was allowed to reach steady state at its designed maximum capacity at a steam load of 94.5 kg/s before it was subjected to step inputs. Therefore, the initial transients of all the variables from time $t = 0 \text{ s}$ to $t = 2000 \text{ s}$ should be ignored.

The steam load was increased by 9.45 kg/s , or 10 % of the nominal steam demand, at 2000 s . Two step decreases in the steam demand from the common steam header, each of a magnitude of 10 % of the maximum designed capacity, were added at 5000 s and 8000 s . The boiler system was then allowed to return to the maximum capacity of a steam demand of 94.5 kg/s at 11000 s . The steam loads refer to the steam demand for each of the utility boilers. Figure 4.5 shows the steam demand for each utility boiler versus time.

Figures 4.6 to 4.18 show the dynamic behaviour of a selection of important variables of the boiler system when the above step changes are made to the boiler system.

Figures 4.19 to 4.22 show the transient responses of the metal wall temperature at the various boiler sections.

Most of the variables stabilize within 1500 s of each step change in the steam load.

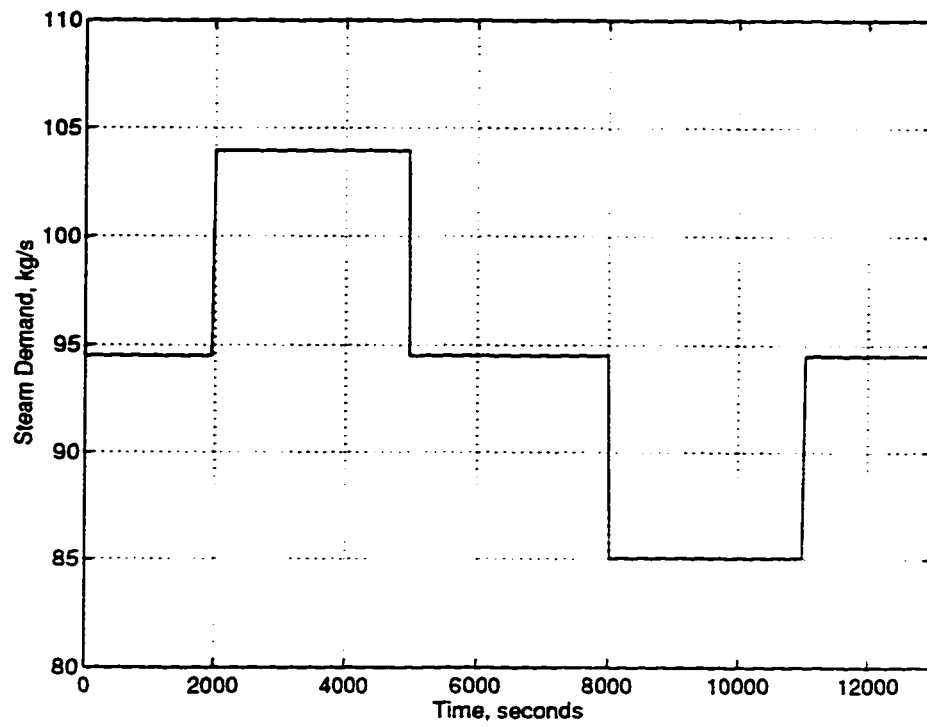


Figure 4.5: Steam demand from the boiler system

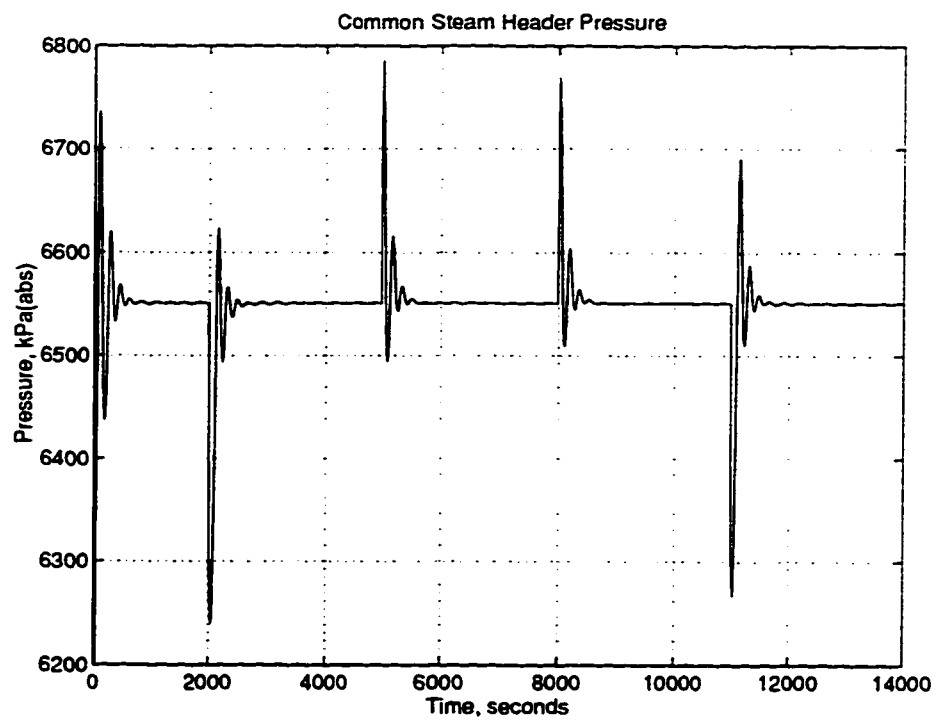


Figure 4.6: Pressure variation of the common steam header

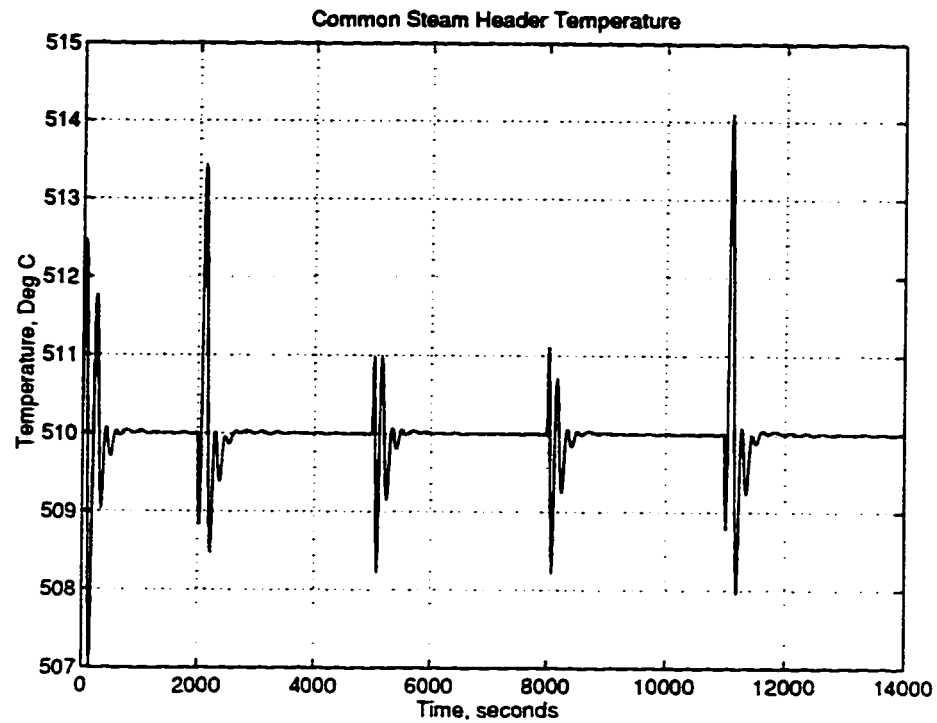


Figure 4.7: Temperature variation of the common steam header

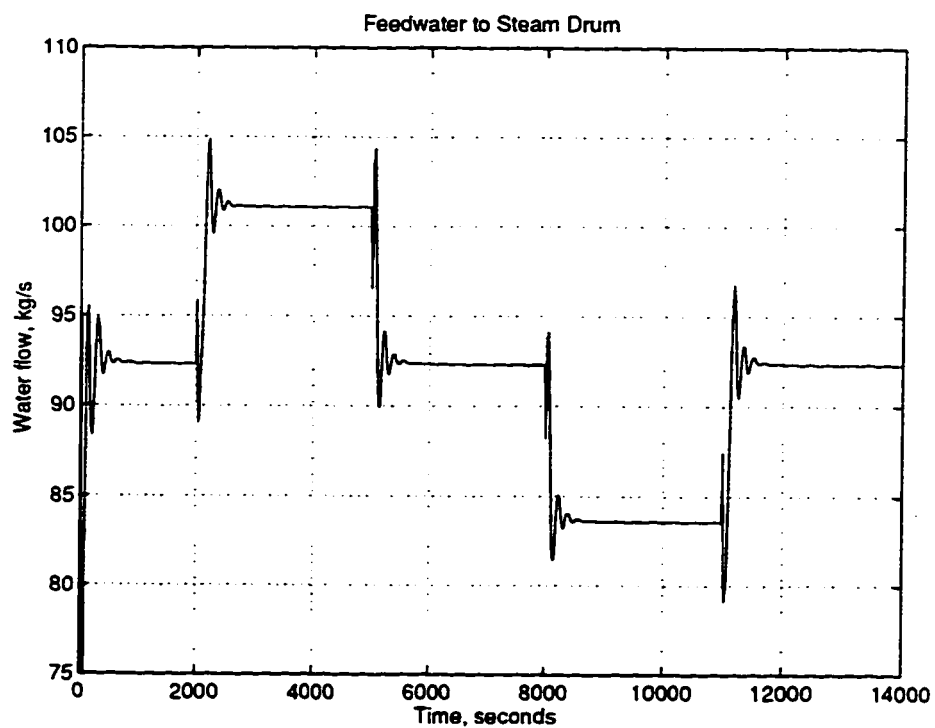


Figure 4.8: Transient response of feedwater flow

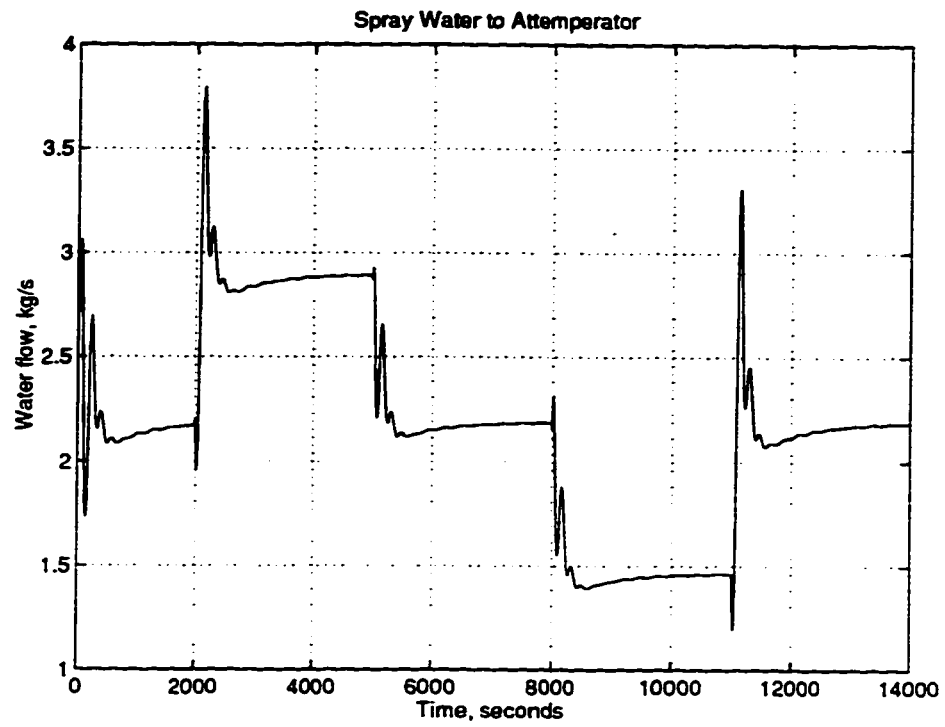


Figure 4.9: Transient response of attenuator water flow

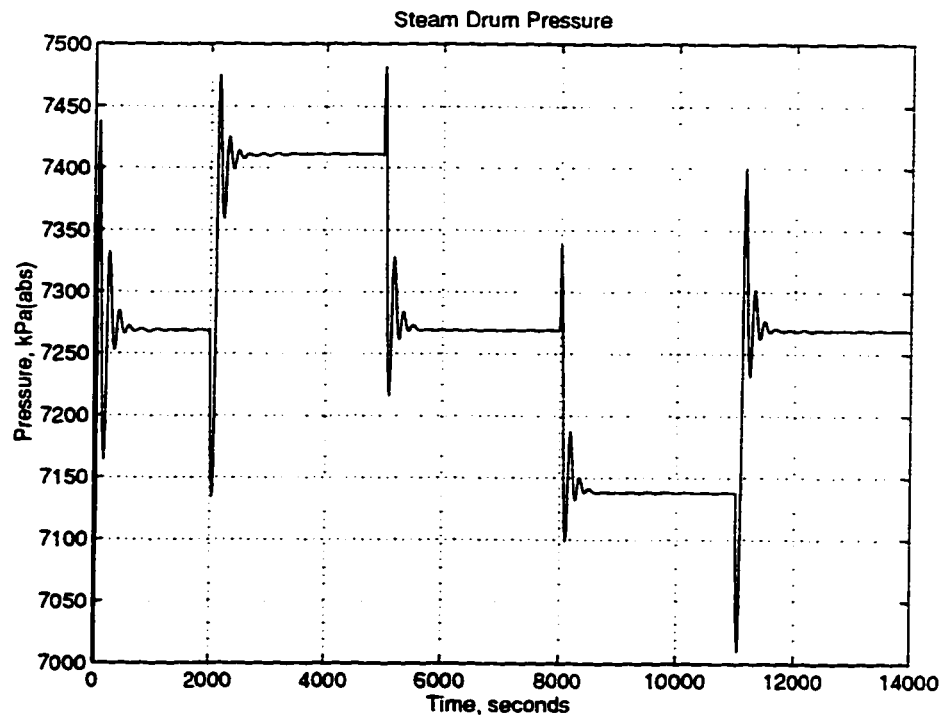


Figure 4.10: Transient response of steam drum pressure

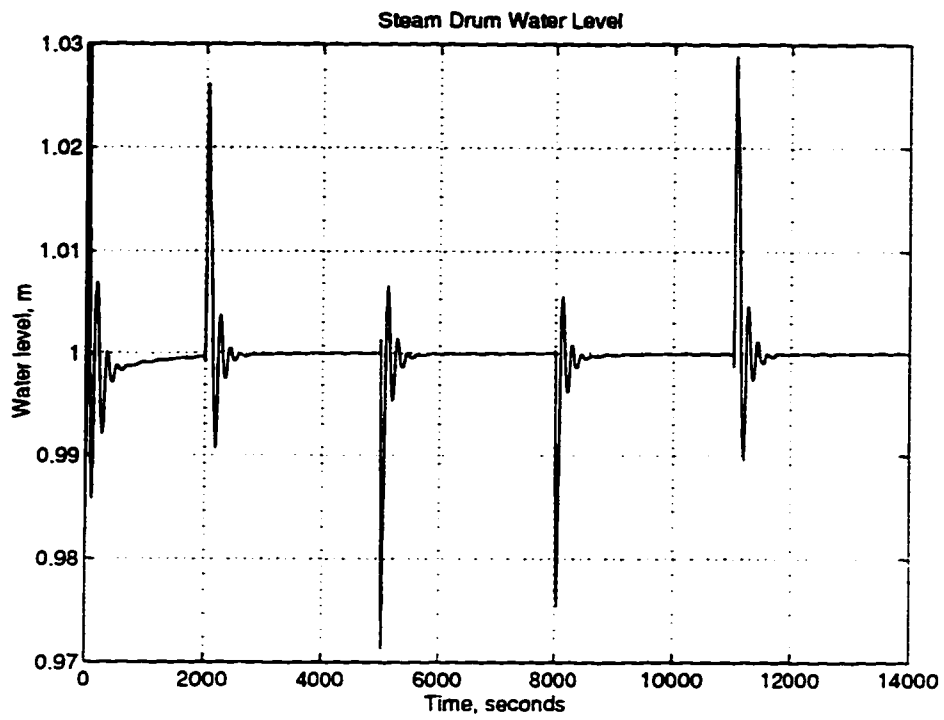


Figure 4.11: Transient response of steam drum liquid level

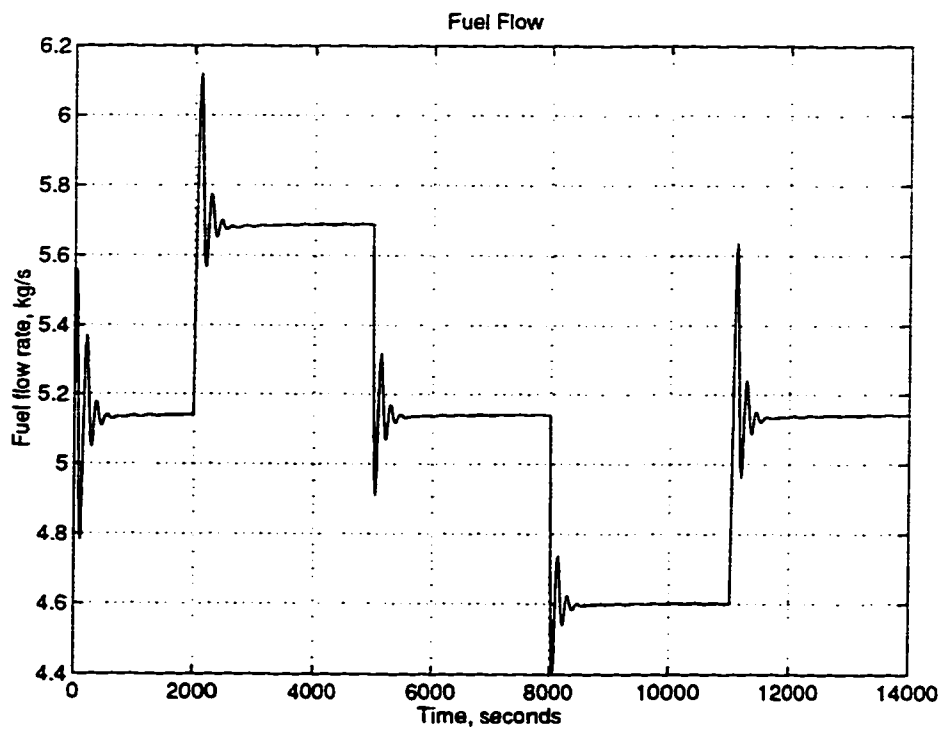


Figure 4.12: Transient response of fuel flow

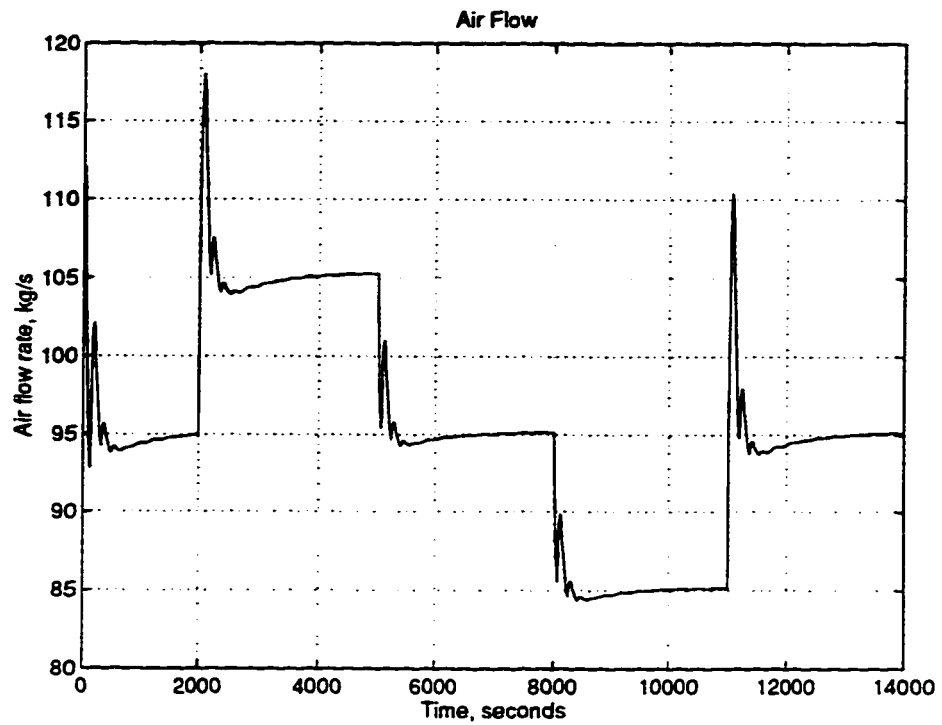


Figure 4.13: Transient response of air flow

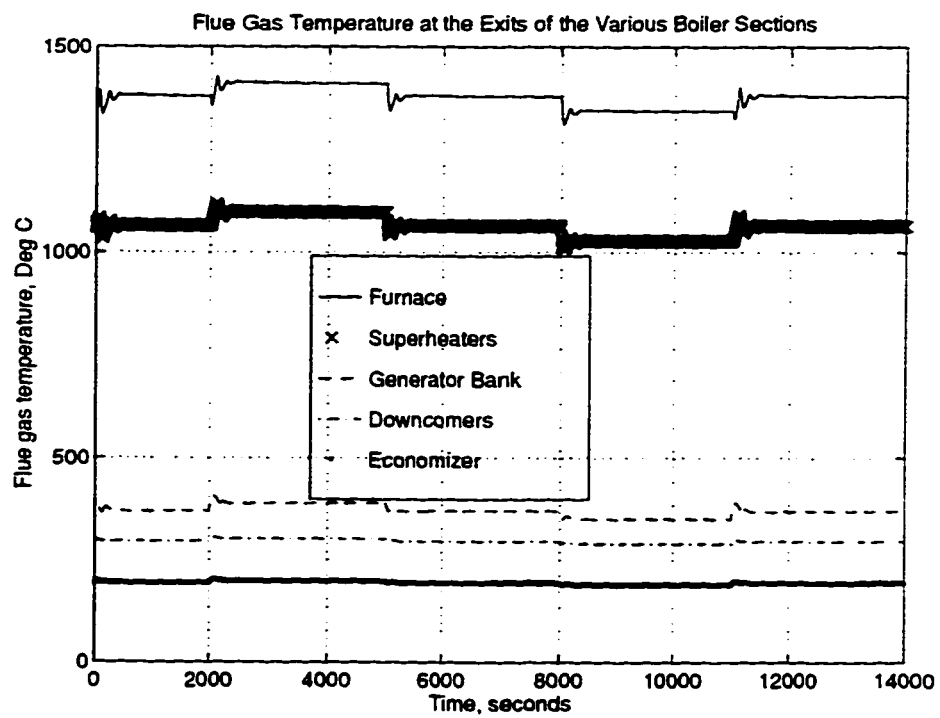


Figure 4.14: Transient response of flue gas temperature at various boiler sections

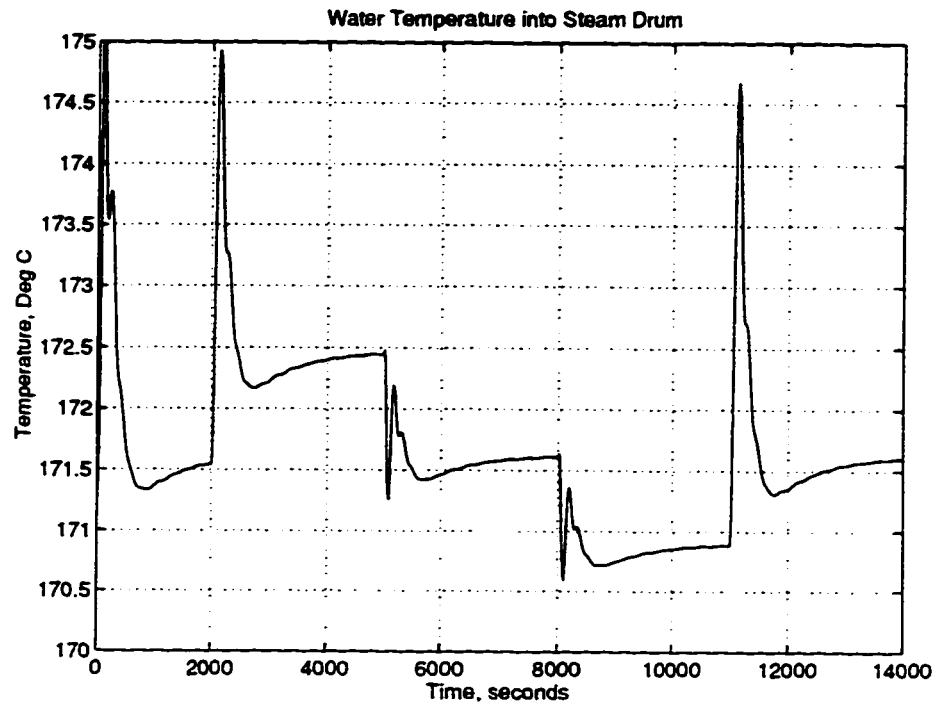


Figure 4.15: Transient response of water temperature at the economizer exit

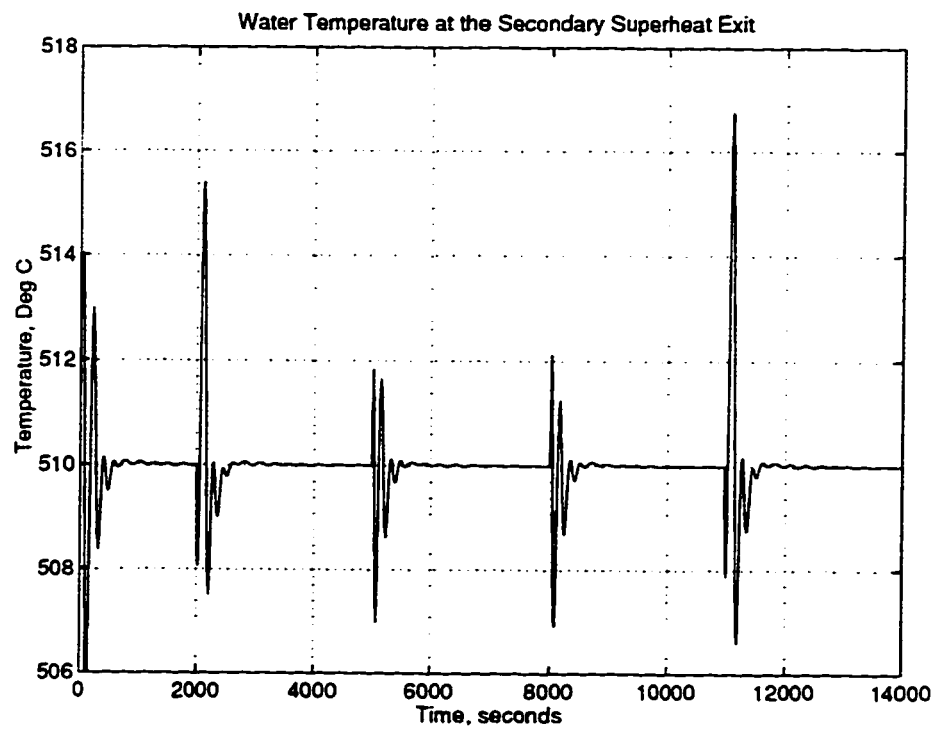


Figure 4.16: Transient response of steam temperature at the secondary superheater exit

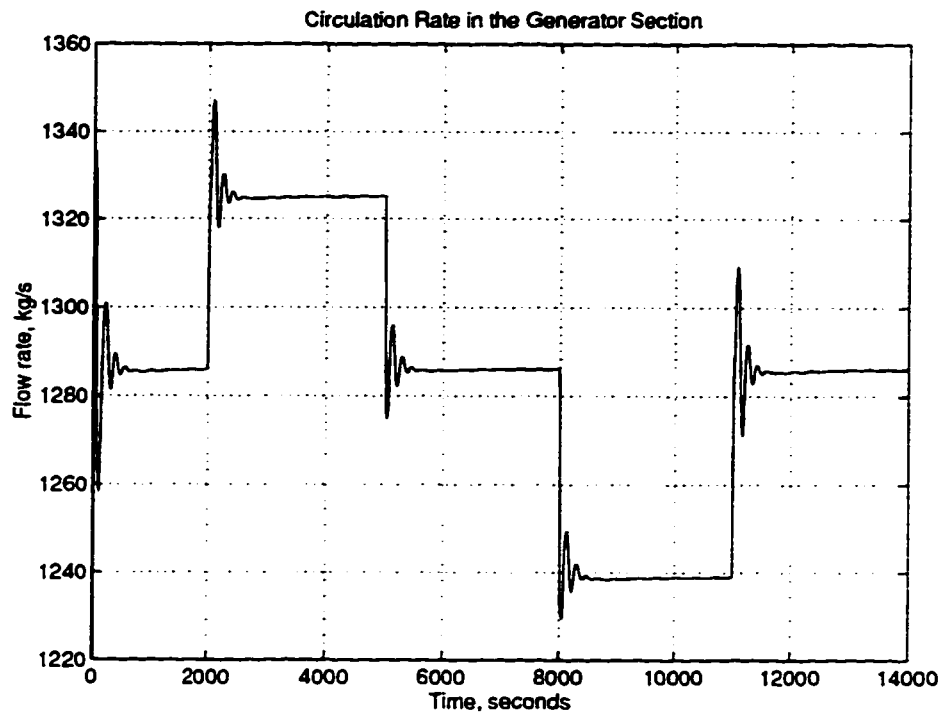


Figure 4.17: Transient response of circulation rate

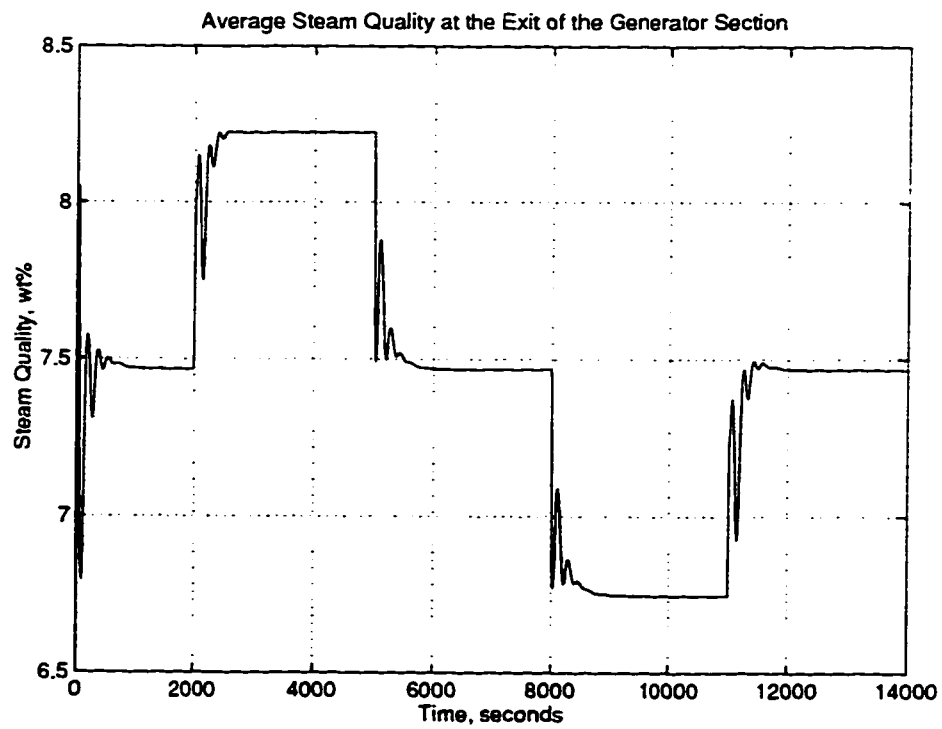


Figure 4.18: Transient response of the average steam quality at the exit of risers

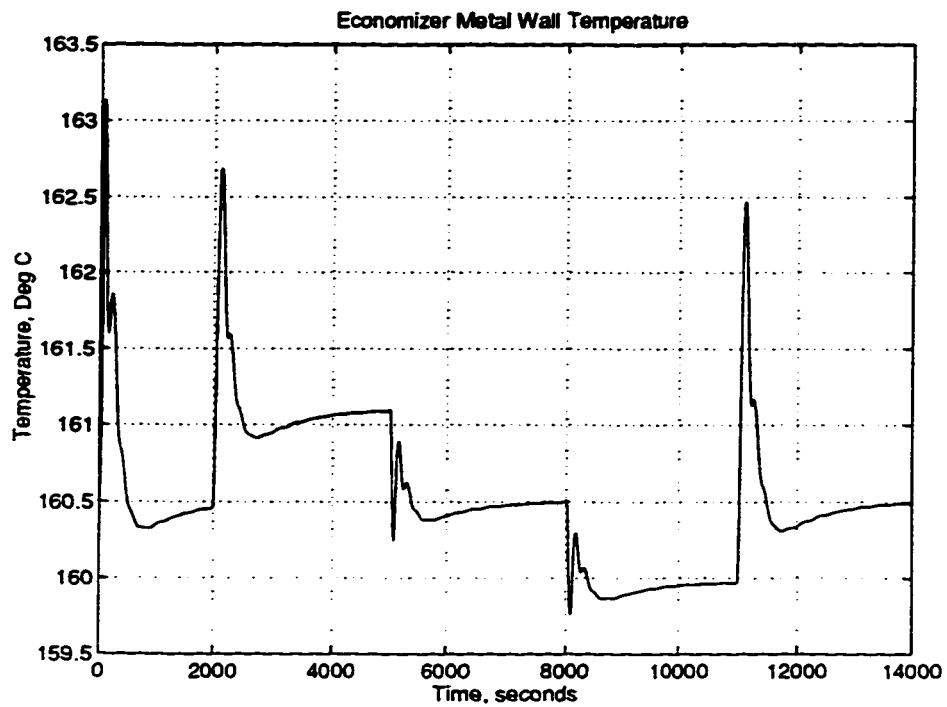


Figure 4.19: Transient response of the economizer metal wall temperature

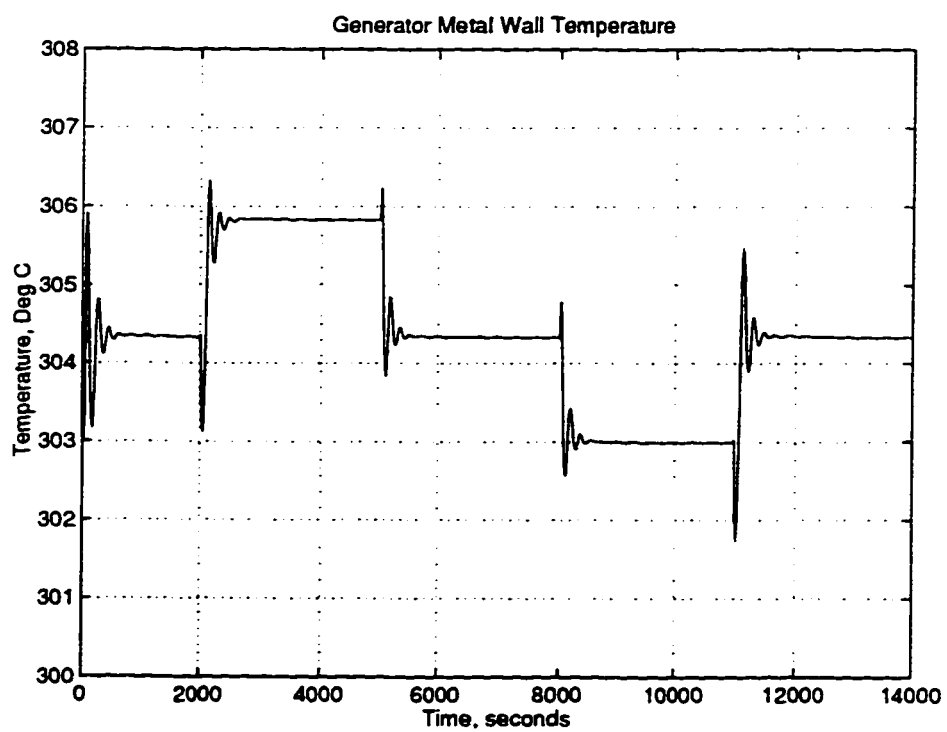


Figure 4.20: Transient response of the generator metal wall temperature

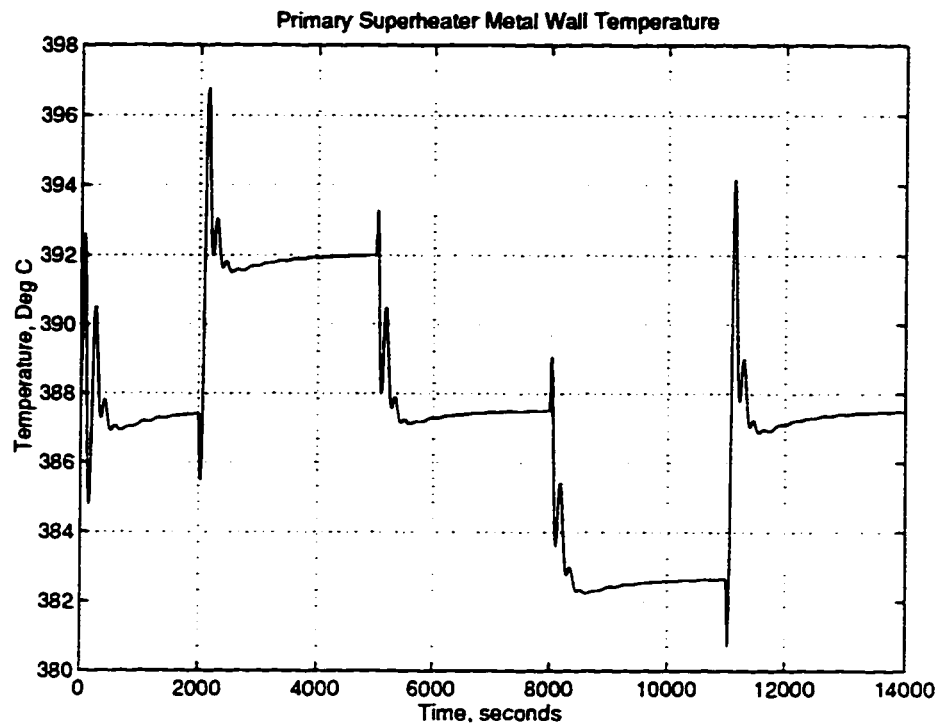


Figure 4.21: Transient response of the primary superheater metal wall temperature

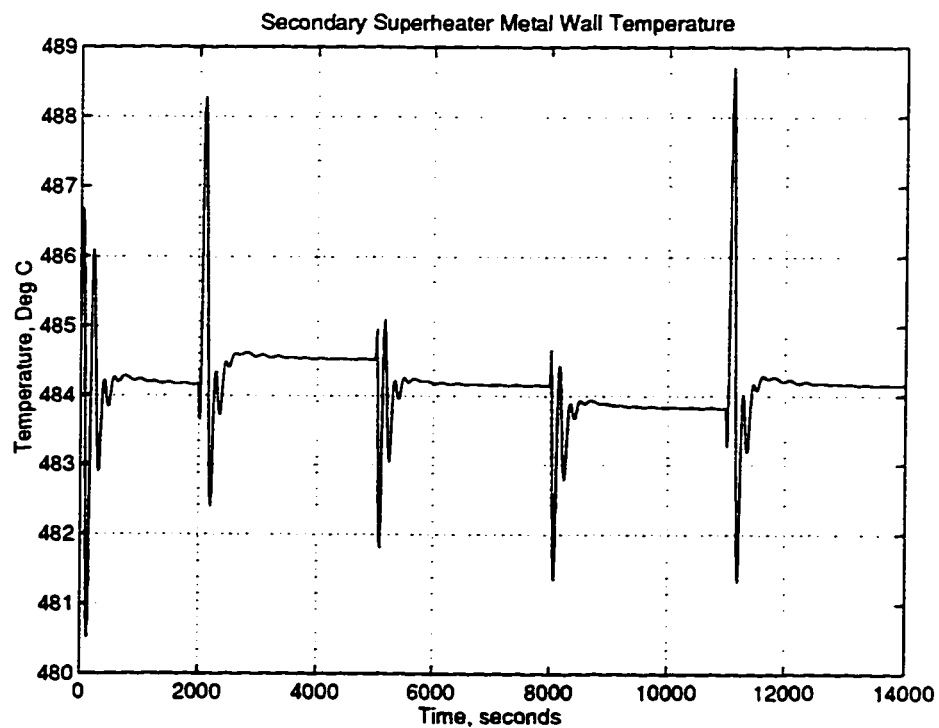


Figure 4.22: Transient response of the secondary superheater metal wall temperature

4.3.3 Discussions on the Simulation Results

Steady State Results

The mean wall temperatures of the various boiler sections shown in Table 4.1 could not be used directly to predict tube failure. The calculated wall temperatures cannot be regarded as the true wall temperatures because the temperature variation along the tube was ignored in the simulation. These wall temperatures could merely be used to infer the transient temperature variations of the metal walls at different steam loads.

The run time of the dynamic model can be improved by converting the various functions in the simulation from MATLAB code to "C". MATLAB interprets the various functions line by line as they are executed each time if they are written in MATLAB code. By converting the MATLAB code to "C", the time required for interpreting the functions is reduced significantly, thereby improving the speed of the simulation. Currently, the run time is approximately 2.3 times slower than real-time. This has to be sped up if this boiler simulation is to be used as a basis of a real-time operator training simulator.

Table 4.3 shows all the important results in determining the overall energy balance of the simulation. Since the feedwater inlet temperature and the inlet conditions of fuel and air were specified inputs, and the steam load, the final steam exit temperature and pressure from the boiler were controlled variables, the fuel requirement and the exit temperature of the flue gas to stack could be used as indicators on the closure of the overall energy balance. As can be seen

in Table 4.3, the fuel flow rates were within 2.28 % of the obtained data for all three cases. Flue gas exit temperatures to stack were 6.87 % to 7.08 % lower than those given in the Syncrude report. This is due to the fact that the flue gas mass flow rates were 12.6 % to 13.2 % lower than those in the report. This difference could in turn be attributed to the fewer heavy components in the fuel in the simulation. Propylene, n-butene, i-butene, and a few other heavy components were ignored in the simulation (see Table 4.2). These heavy components not only increase the molecular weight of the fuel, they also react with oxygen at higher stoichiometric ratios. As a result, more oxygen is required for the complete combustion of the fuel, thereby increasing the amount of flue gas flow. Therefore, it can be concluded that the overall energy balance in the simulation model is reasonably correct. The deviations in the flue gas exit temperature and the flue gas mass flow can be reduced by using the same fuel content in the report.

The flue gas exit temperatures at the various boiler sections from the simulation also showed agreement with the obtained data within 16.4 %. These discrepancies could all be reduced or even eliminated by fine-tuning the model, for example, by adjusting the values of certain parameters that appear in the physical laws which are not accurately known, so as to minimize the various discrepancies. This has not been done, since the validity of a first-principles model rests on the faithfulness of the physical phenomena descriptions, as demonstrated by qualitatively-correct behaviour over a wide range of conditions, not on the accuracy with which a given, limited set of data can be matched by model outputs.

Transient Response of the Boiler System

There are no dynamic process data available for the Syncrude boiler system at present, and as a result, dynamic validation of the model is impossible. However, the model could still be validated qualitatively, for example, changes in variables can be validated based on observations of the dynamic behaviour of the system.

In Figure 4.6, as the steam demand was increased at 2000 s and 11000 s, the pressure in the common steam header decreased initially before recovering to the set point, as would be expected in the real situation. The sudden increase in steam demand results in a net decrease in the amount of steam accumulated in the header, and thus a decrease in the header pressure. The header pressure soon returned to the desired set point due to the increases in firing rate and feedwater flow to the boiler in response from the decreases in header pressure and drum level. As the steam load was decreased at 5000 s and 8000 s, the exact opposite happened — an initial increase in the header pressure was observed. The header pressure was able to recover to the set point in approximately 1500 s after each perturbation.

The deviation of the header pressure from the set point after each step was different in magnitude even though the magnitudes of the step changes are the same. Therefore, it could be concluded that the boiler system is nonlinear. Such nonlinear behaviour was displayed in other variables of the boiler system such as the steam temperature exiting the secondary superheater (Figure 4.16), the spray water flow to the attemperator (Figure 4.9), the steam drum pressure and liquid

level (Figures 4.10 and 4.11), the circulation rate in the downcomers and risers (Figure 4.17), and the fuel and air flow rates (Figures 4.12 and 4.13).

Figure 4.10 shows the transient response of the steam drum pressure. The steam drum pressure decreased initially when the steam load was increased, and increased initially when the steam load was decreased. This behaviour was identical to that of the steam header. However, the steam drum pressure was not controlled at any set point, it was allowed to vary so that the steam flow from the boiler to the common header matched the steam demand. The steam flow into the steam header (exiting the boiler) was determined from the steam drum and header pressures based on the empirical relationship given in the previous chapter.

The steam drum liquid level increased initially after each step increase in the steam demand, and decreased initially after the step decreases in the steam demand. These are the evidents of the swelling and shrinking effects. As described previously, swelling refers to the increase in drum liquid level as the steam drum pressure decreases after each step increase in steam demand. Shrinking is the opposite effect to swelling. The transient response of the steam liquid level is shown in Figure 4.11.

Figures 4.8 and 4.9 are the feedwater flow rate to the steam drum and the spray water flow to the attemperator respectively. The sum of these flow rates was equal to the steam demand in the steady state. Spray water flow was adjusted according to the change in the steam temperature at the attemperator and the

secondary superheater exit.

As shown in Figures 4.12 and 4.13, fuel and air flows also exhibited correct changes in order to compensate for the pressure variations in the steam header. The fuel rate decreased with an increase in the header pressure, and increased with a decrease in header pressure. Air flow was also adjusted to maintain a 1.5 mole percent of excess oxygen in the flue gas.

From Figure 4.14, the flue gas temperature in the boiler decreased as the fuel rate decreased and increased as the fuel rate increased. This is also observed in the real process.

All the variables stabilized within 1500 s, except for the water temperature at the economizer outlet and the economizer metal wall temperature. The economizer wall temperature required a large amount of time to settle because of its large thermal storage capacity. This slow response in the metal wall temperature also affected the water exit temperature of the economizer as it was dependent on the economizer wall temperature.

The actual PI tuning parameters in the existing control scheme are able to provide satisfactory responses in all of the variables, therefore, the dynamic behaviour of the dynamic model can be concluded indirectly to be accurate.

4.4 Summary

This chapter presents the existing control algorithms for four key areas in the Syncrude boiler system:

1. Feedwater control;
2. Main steam and attemperator control;
3. Firing rate demand; and
4. Combustion control.

Discussions on the various control schemes are provided in the first part of this chapter.

Steady state and transient responses of the various variables of interest are presented in the second part of this chapter. The simulation model can be concluded to be accurate based on a report on the Syncrude boiler system. The overall energy balance was correct — with specified conditions for the feedwater and final steam temperatures matching those given in the Syncrude report, the fuel requirement was within 2.28 % and the flue gas exit temperature within 13.2 % of those given in the Syncrude report.

The dynamic properties of the simulation model also appeared correct as the responses of the various variables were satisfactory with the actual PI controller parameters in the existing control scheme. Therefore, the assumptions imposed in developing this dynamic model are justified. The swelling and shrinking effects in the steam drum liquid level appeared to be correctly modelled.

The dynamic model could be fine-tuned to better match the actual process. This could be achieved by changing parameters that appear in the physical laws. for example, the heat transfer areas and thermal masses of the various boiler

sections.

The exit temperatures of both the flue gas and the steam-water sides at each boiler section were solved using energy balances rather than algebraic iteration because of the improved numerical stability.

The run time of the simulation could be reduced if all the functions are coded in "C" rather than MATLAB script.

Chapter 5

Conclusions

The main objective of this thesis was to develop a dynamic model for the Syncrude boiler system to:

1. provide a means of investigating the dynamic behaviour of the Syncrude power generation system.
2. provide a basis for the development of a simulator for operator training.
3. provide estimates of transient variations of metal wall temperatures at various boiler sections for use in studying boiler life expectancy.

Chapter 2 provided the theoretical background and assumptions and simplifications imposed for the development of the dynamic model for the steam side of the entire Syncrude boiler system, including the utility boilers and the 6.6 *MPa* common steam header.

Three methods for simulating heat exchange units were presented in Chapter 3. The derivations of these methods were also incorporated in this chapter. These methods were evaluated based on numerical stability and efficiency.

Chapter 4 provided discussions of the control schemes for four key areas including feedwater control, main steam and attemperator control, firing rate demand, and combustion control were implemented in the model. Validation of the dynamic model was provided in the second part of Chapter 4.

5.1 Conclusions

1. The direct feedback method is not adequate for dynamic simulation of heat exchange units, especially for systems with a series of heat exchangers.
2. The energy balance and the DEB methods are both acceptable for dynamic simulation of heat exchangers. Both showed numerical stability. The DEB method was demonstrated to be more efficient than the energy balance method based on the number of FLOPS required in the heat exchanger simulations discussed in Chapter 3.
3. The DEB method cannot be implemented directly for a series of heat exchangers connected as in the setting of a boiler because of the lack of intermediate temperatures between the heat exchangers. Therefore, this method cannot be utilized in the heat transfer calculations in the dynamic boiler model.
4. The dynamic model developed was accurate in the steady state. The results of simulations were compared with data obtained through Syncrude engineering personnel. The steady state results were close, within 16.4 % for all

variables, to those given in the report.

5. The transient characteristics of the dynamic model were also fairly accurate.

The responses of all the variables were satisfactory and reached steady state within 1500 s when the actual PI controller parameters from the Syncrude boiler system were used.

6. The behaviour of important variables such as the steam drum and common header pressures, the fuel and air flow, and the temperatures of the flue gas and steam/water, in the various boiler sections also matched those observed in the real process. The swelling and shrinking effects on the steam drum liquid level were also correctly modelled.

5.2 Recommendations for Future Work

1. Further research is required if the DEB method is to be incorporated into the heat transfer calculations for a series of heat exchangers connected as in the boiler.
2. The dynamic model is accurate based on the steady state and dynamic validations.
3. Further validation of the model should be performed by comparing the simulated results with actual process data from the plant.

4. This dynamic model for the utility boiler and the common steam header need to be combined with that for the electrical side in order to facilitate studies on the entire Syncrude boiler system.
5. A user interface needs to be developed should this dynamic model be used for operator training.
6. The run-time of this boiler model can be reduced by converting the MATLAB codes into "C" code.

Bibliography

- [1] A. G. Blokh. *Heat transfer in steam boiler furnaces*. Hemisphere Publishing Corporation, New York, 1988.
- [2] D. Butterworth and G.F. Hewitt. *Two-phase flow and heat transfer*. Oxford University Press, Oxford, 1978.
- [3] Y. A. Çengel and M. A. Boles. *Thermodynamics*. McGraw-Hill Publishing Company, Toronto, 1989.
- [4] E. Cheres. Small and medium size drum boiler models suitable for long term dynamic response. *IEEE Transactions on Energy Conversion*, 5(4):686–692, 1990.
- [5] N. de Nevers. *Fluid mechanics for chemical engineers*. McGraw-Hill, Inc., Toronto, 2 th edition, 1991.
- [6] G. Dieck-Assad. Development of a state space boiler model for process optimization. *Simulation*, 55(4):201–213, 1990.

- [7] S. G. Dukelow. *The control of boilers*. Instrument Society of America, North Carolina, 2 nd edition, 1991.
- [8] R. M. Felder and R. W. Rousseau. *Elementary principles of chemical processes*. John Wiley & Sons, Inc., New York, 2 nd edition, 1986.
- [9] R. Franks. *Modeling and Simulation in Chemical Engineering*. John Wiley & Sons, Inc., Toronto, 1972.
- [10] L. A. Gould. *Chemical Process Control: Theory and Application*. Addison-wesley Publishing Company, Don Mills, Ontario, 1969.
- [11] H. C. Hottel and A. F. Sarofim. *Radiative transfer*. McGraw-Hill Book Company, Toronto, 1967.
- [12] F. P. Incropera and D. P. De Witt. *Introduction to heat transfer*. John Wiley & Sons, Inc., Toronto, 2 nd edition, 1990.
- [13] S. Kakaç, editor. *Boilers, evaporators and condensers*. John Wiley & Sons, Inc., New York, 1991.
- [14] J. B. Knowles. *Simulation and control of electrical power stations*. John Wiley & Sons, Inc., Toronto, 1990.
- [15] M. Kohlenberg. Analysis of transient responses of steam flow in power plant piping networks. Master's thesis, University of Alberta, 1993.
- [16] R. Leung. Dynamic simulation of natural circulation in a boiler. Master's thesis, University of Alberta, 1997.

- [17] G. Y. Masada. *Modeling and Control of Power Plant Boiler-Turbine-Generator Systems*. PhD thesis, Massachusetts Institute of Technology, 1979.
- [18] R. H. Perry and D. Green, editors. *Perry's chemical engineers' handbook*. McGraw-Hill Book Company, Toronto, 6 th edition, 1984.
- [19] L. Pujol and A. H. Stenning. Effect of flow direction on the boiling heat transfer coefficient in vertical tubes. *Int. Symp. research in cocurrent gas - liquid flow*, 1969.
- [20] G. Rackette. A combustion and heat transfer model of a medium-sized power boiler. M. Eng. Project, Mechanical Engineering, University of Alberta, 1994.
- [21] S. C. Stultz and J. B. Kitto, editors. *Steam — its generation and use*. The Babcock & Wilcox Company, U.S.A., 40 th edition. 1992.

Appendix A

Parameters for the Dynamic Model

This appendix provides the various parameters that are used in the dynamic model. Table A.1 of this appendix is a summary of the heat transfer areas and thermal capacities of the different boiler sections. These can be treated as tuning parameters of the model itself. Table A.2 is a list of PI controller tuning parameters used in the model. These PI parameters are the same as those used in the actual process.

A.1 Different Parameters for the Various Boiler Sections

Table A.1: Various parameters used in the simulation

| | Heat Transfer Area | Thermal Capacity of Metal Wall | Number of Tubes |
|-----------------------|-----------------------|-----------------------------------|--------------------|
| Units | m^2 | $10^7 J/C$ | |
| Economizer | 1672.3 | 3.0 | 88 |
| Risers | 2406.1 | - | 874 |
| Downcomers | 2291.0 | 9.8 | - |
| Primary superheater | 511.0 | 1.3 | 152 |
| Secondary superheater | 464.5 | 1.3 | 156 |
| Waterwalls | 580.6 | - | 480 |

A.2 Tuning Parameters for the PI controllers in the Dynamic Model

The transfer function of the PI controllers used in the dynamic model is as follows

$$G_c(s) = K_p(1 + \frac{K_i}{s})$$

The tuning parameters given in Table A.2 are according to this transfer function. These parameters are obtained through personal communication with Syncrude engineering personnel.

Table A.2: PI tuning parameters

| Description | Control Diagram | PI controller Number | Proportional Gain (K_p) | Integral Gain (K_i) |
|--------------------------------------|-----------------|----------------------|-----------------------------|-------------------------|
| Plant Master | A1 | PI-2 | 2.67 | 0.0067 |
| Combustion Control and Oxygen Trim | A3 | PI-2 | 0.2 | 0.083 |
| | | PI-3 | 0.65 | 0.025 |
| | | PI-4 | -0.3 | 0.0083 |
| Feedwater control | A8 | PI-1 | 0.6 | 0.1 |
| | | PI-2 | 4.0 | 0.00083 |
| Final Steam and Attemperator Control | A9 | PI-2 | -7.5 | 0.0125 |
| | | PI-4 | 1.5 | 0.017 |

Appendix B

Simulink Block Diagrams of the Dynamic Model

All the Simulink block diagrams in the dynamic model are provided in this appendix. The block diagrams for the various boiler sections of the utility boiler, the common steam header, and the various control diagrams for the boiler system are included in this appendix.

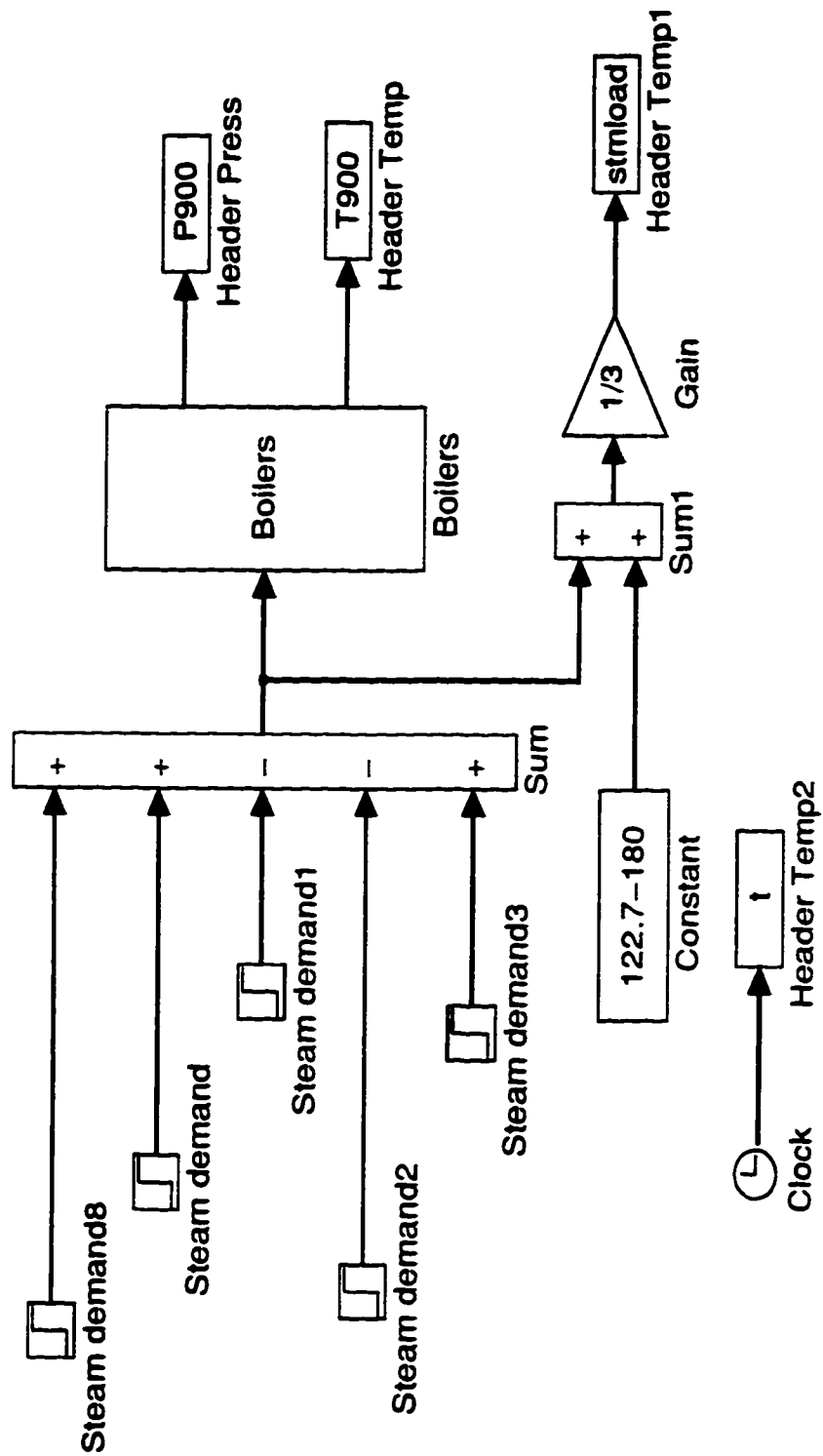


Figure B.1: First level of the model

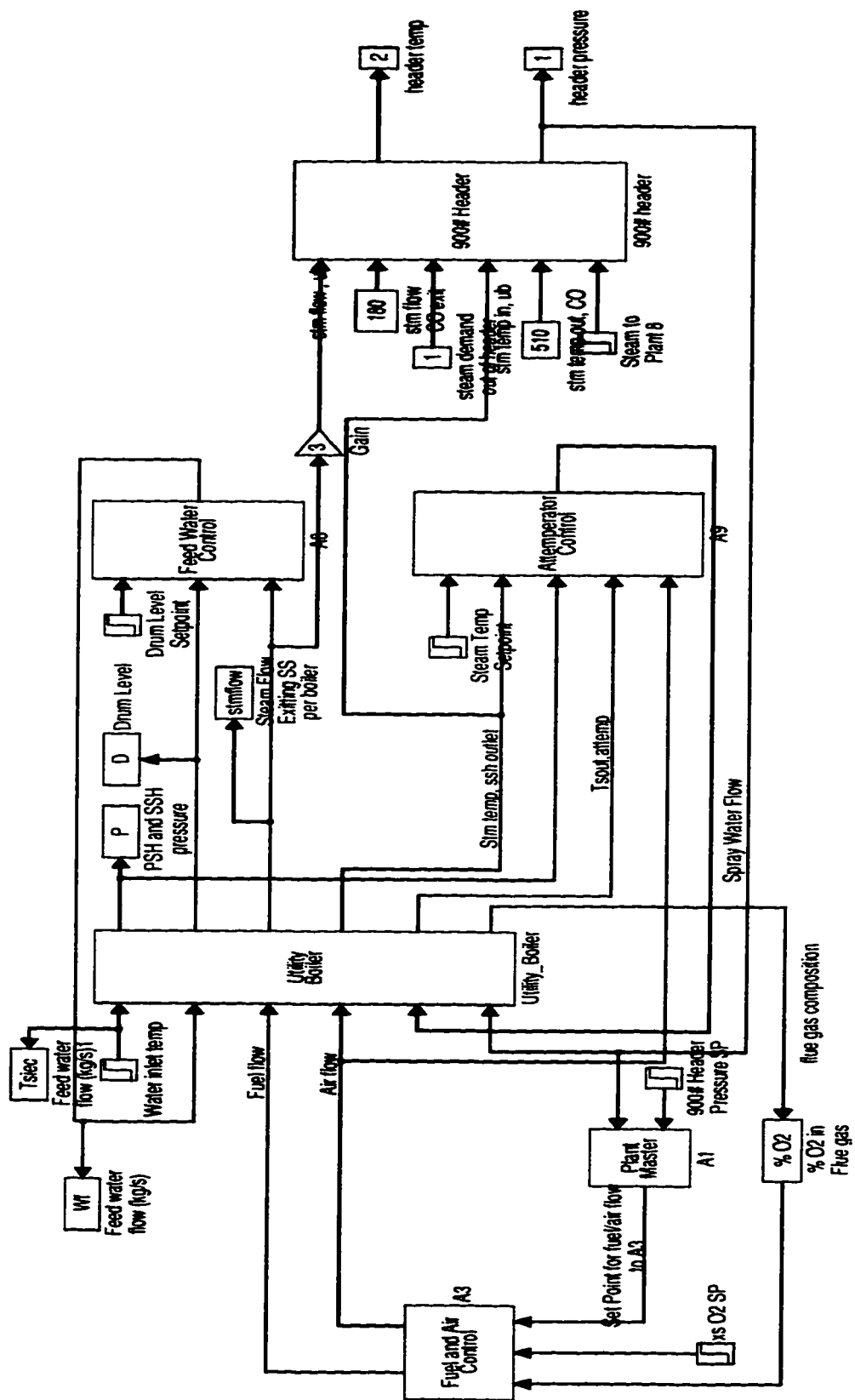
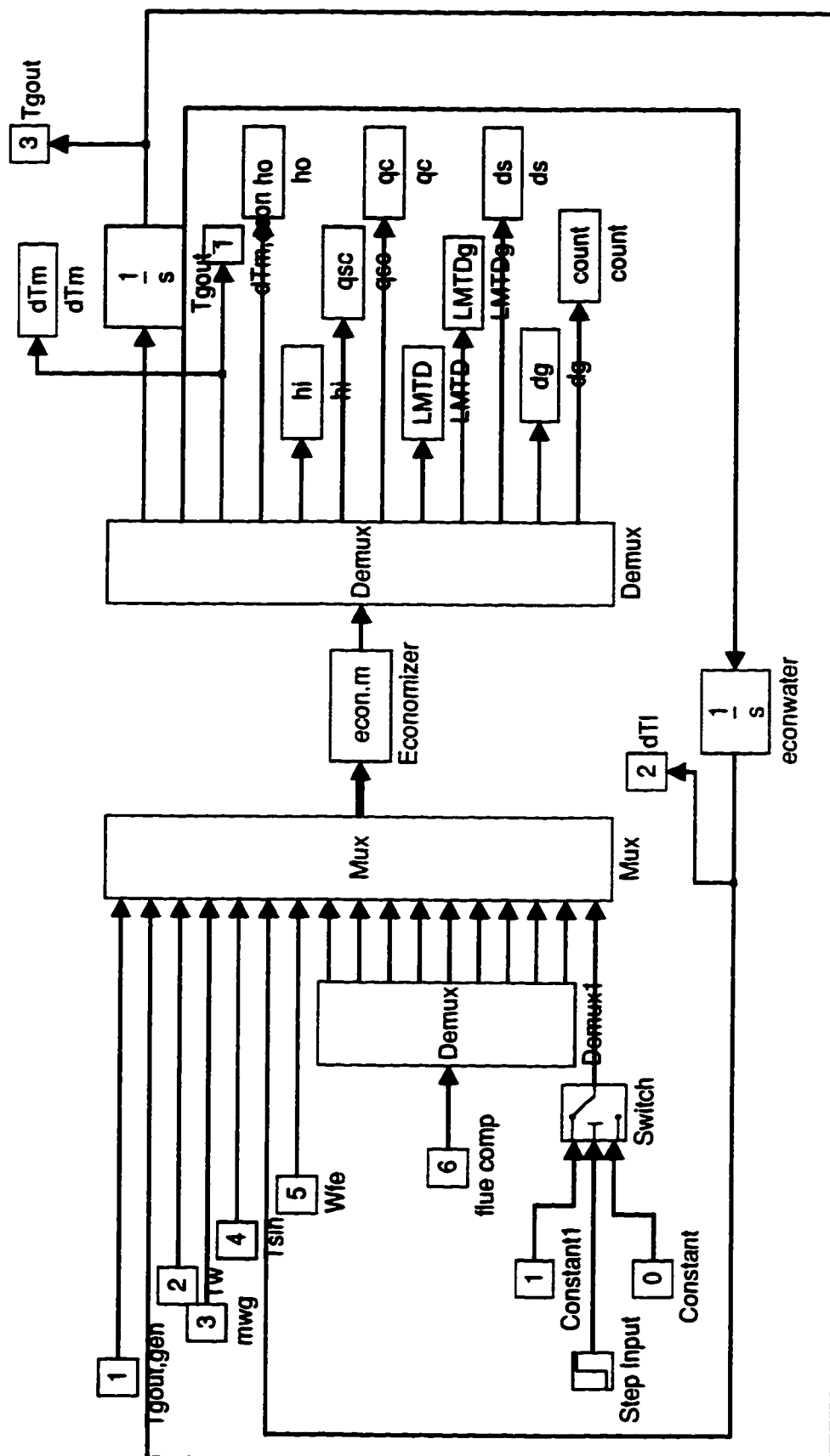


Figure B.2: Second level of the model including the utility boiler, the common steam header and the control schemes



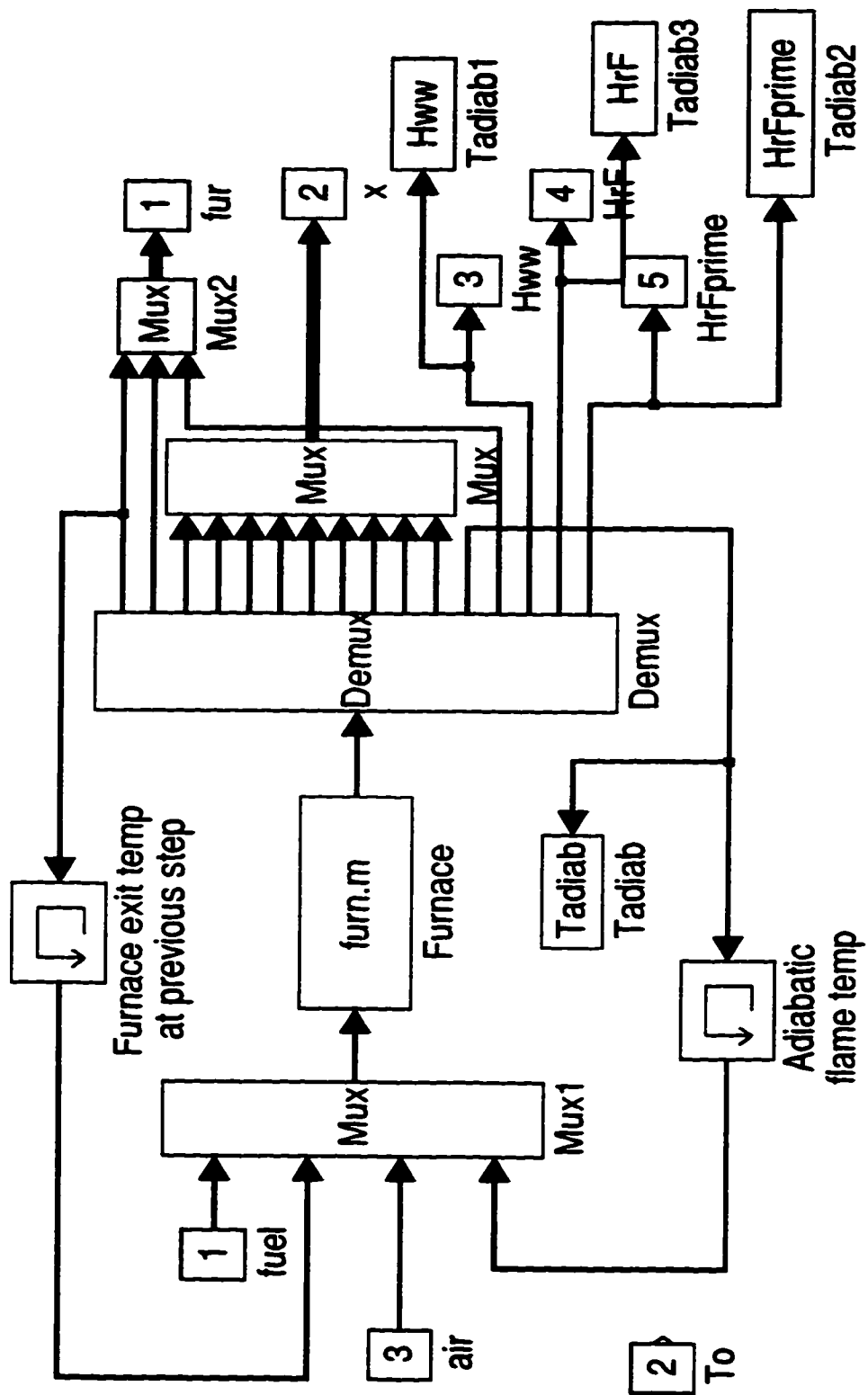


Figure B.5: This block diagram shows the furnace section in the utility boiler

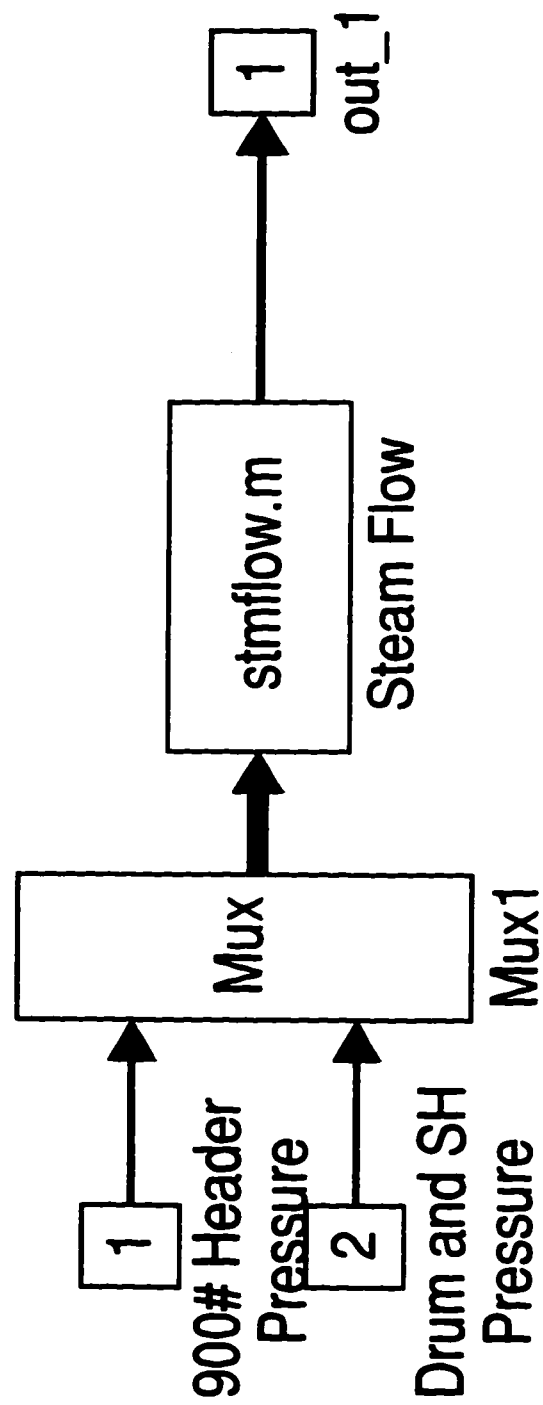


Figure B.6: This block calculates the steam flow from the steam drum to the common steam header using the steam drum and header pressures

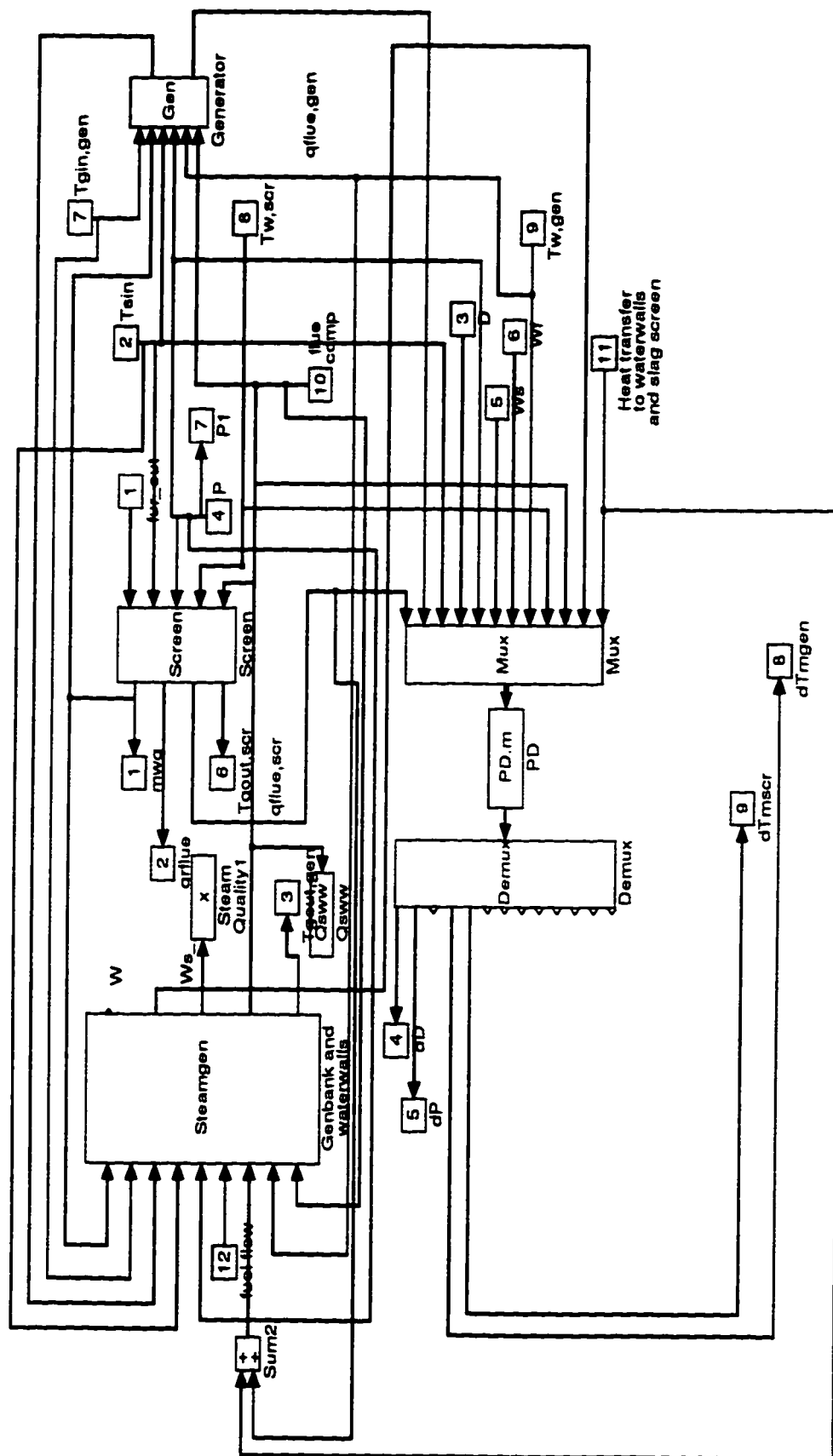


Figure B.7: This block diagram contains the slag screen and the generator sections in the utility boiler

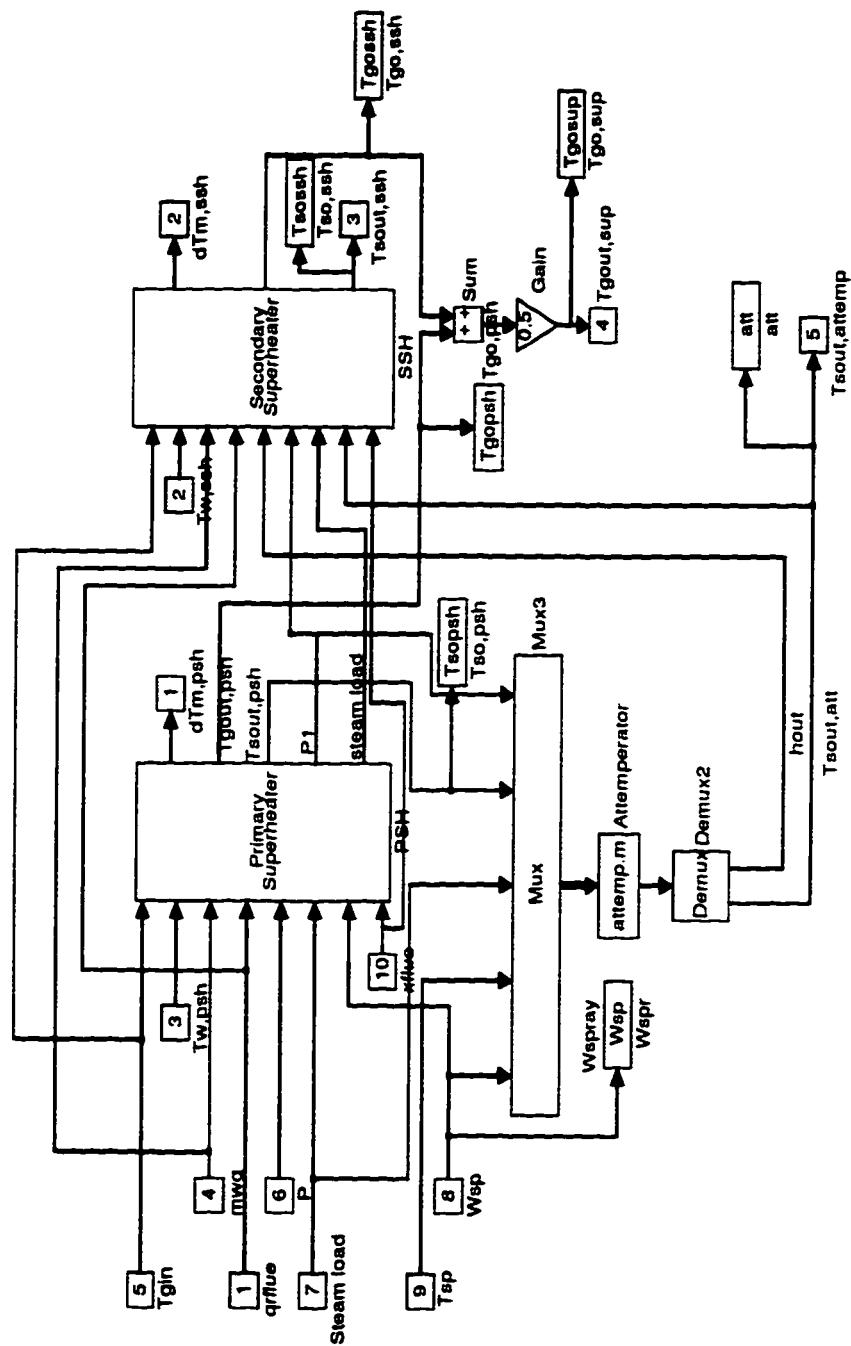


Figure B.10: This block diagram contains the superheaters and the attempator in the utility boiler

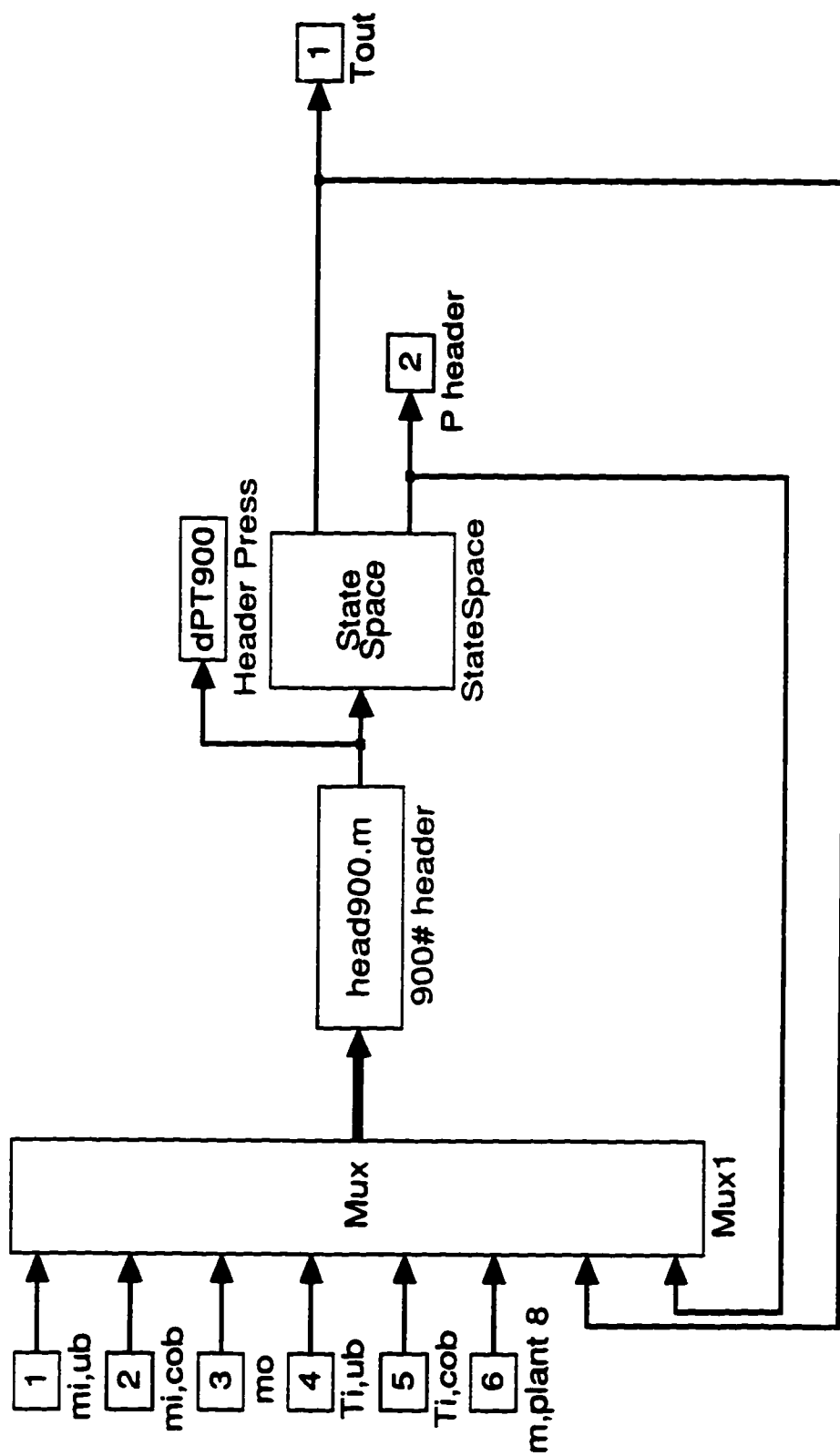


Figure B.13: This block diagram shows the common steam header in the dynamic model

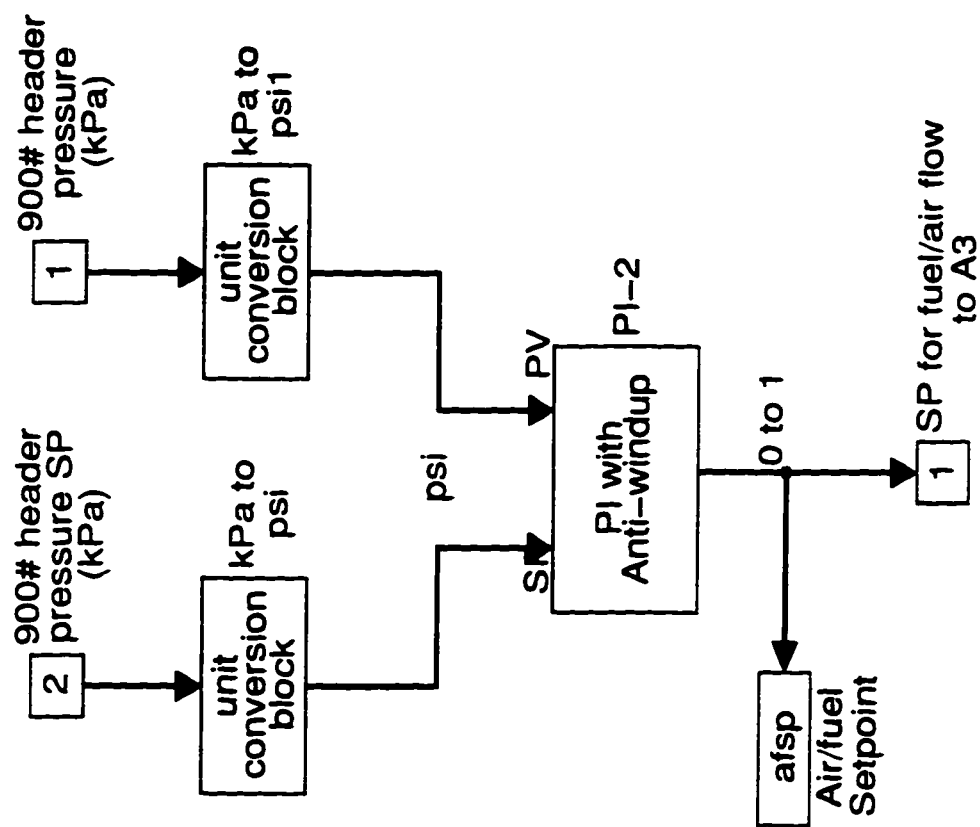


Figure B.14: This block diagram shows the plant master (firing rate demand) control scheme

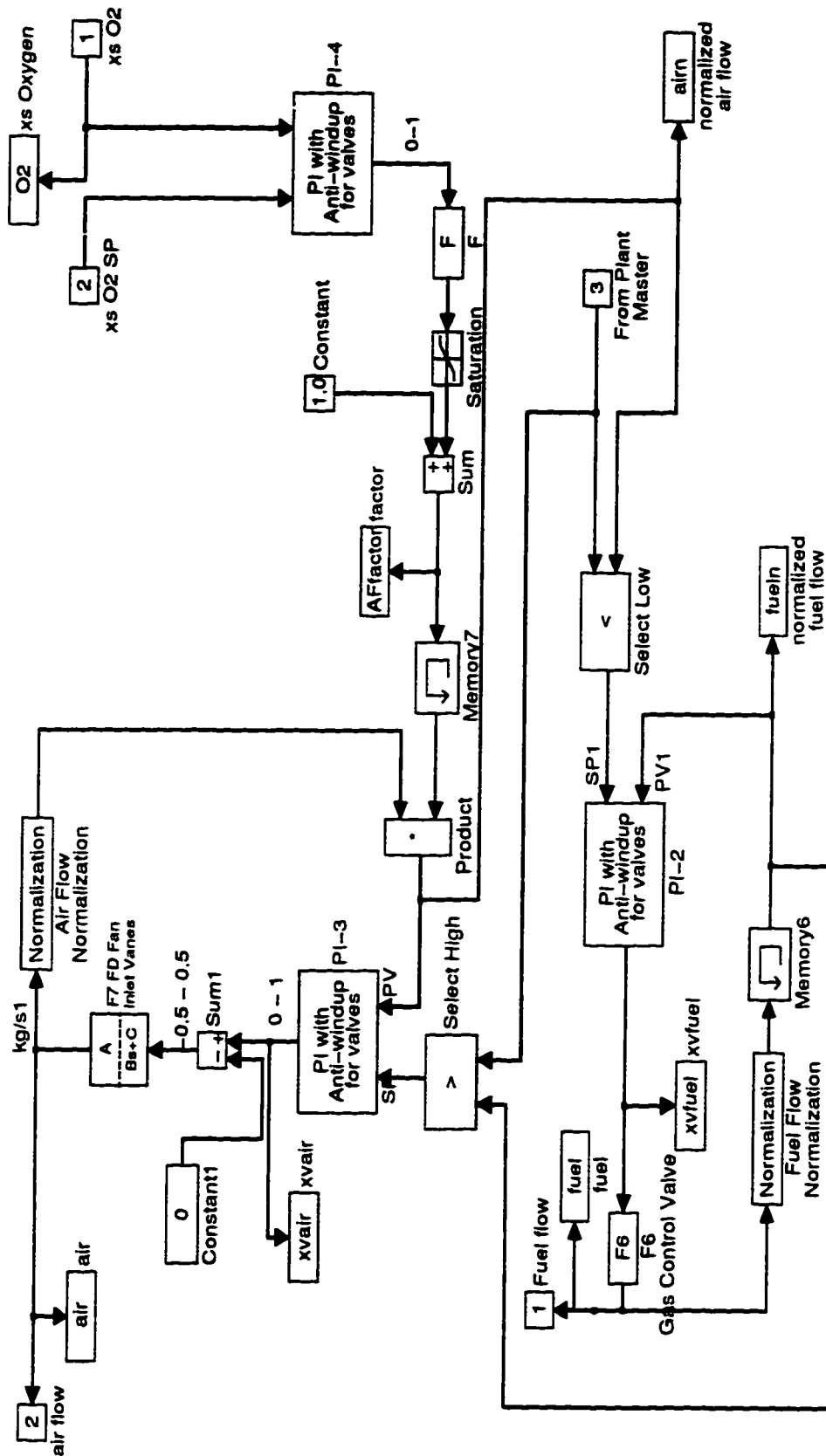


Figure B.15: This block diagram shows the combustion and oxygen trim control schemes

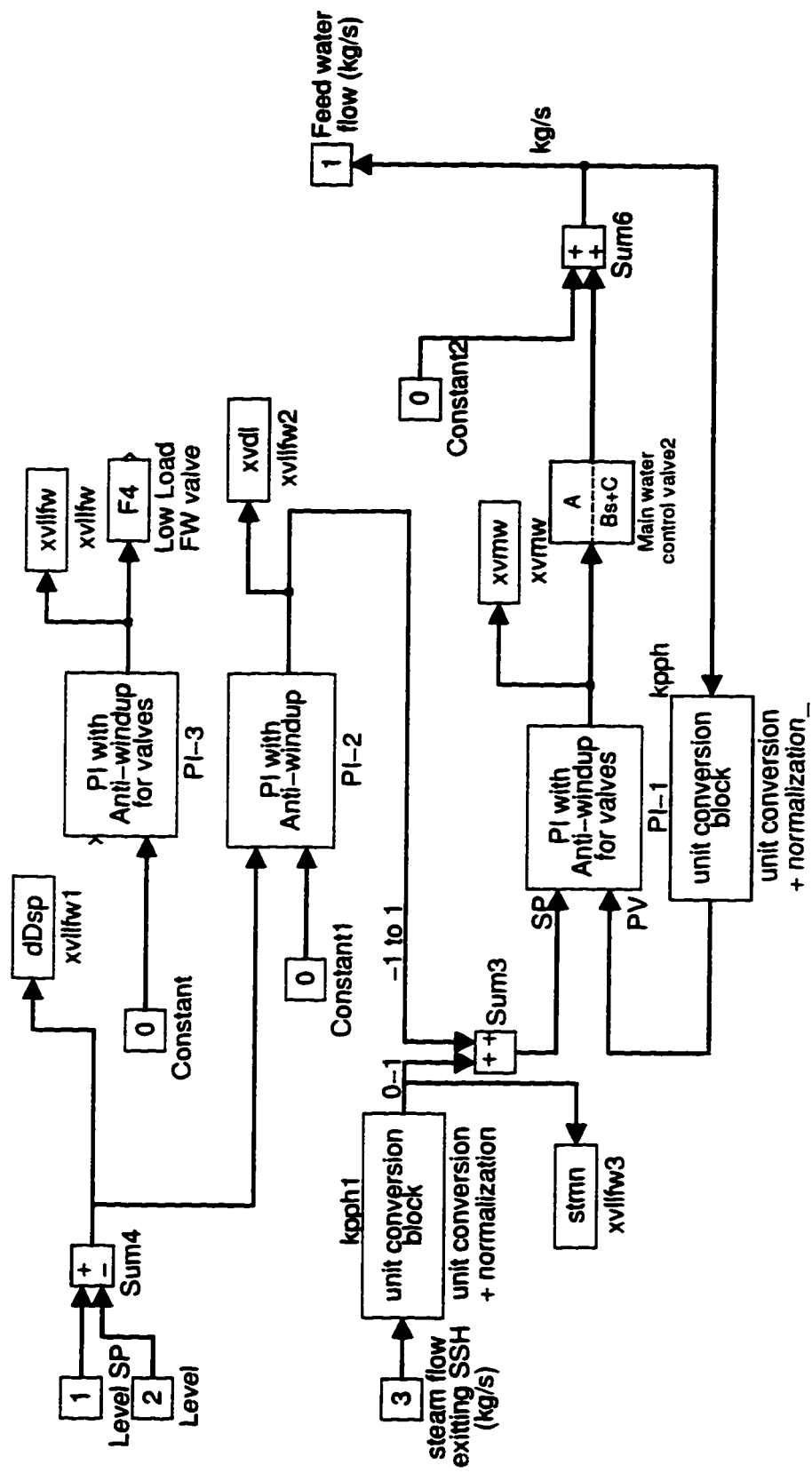
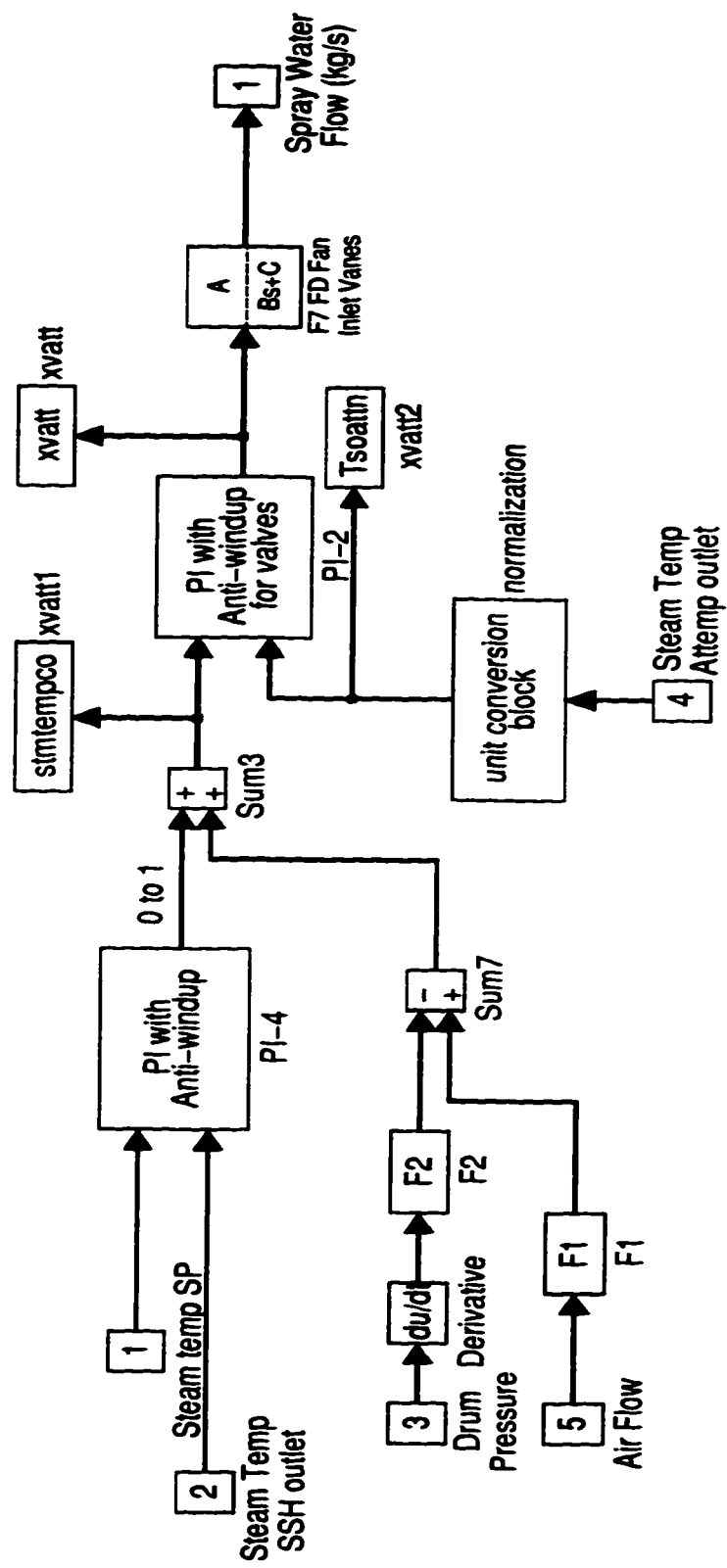


Figure B.16: This block diagram shows the feedwater control scheme



Appendix C

MATLAB Script Files

This appendix lists MATLAB script files that were used to simulate the various boiler sections in the dynamic model of the Syncrude boiler system.


```

function fur=furn(u)

% Calculates the furnace section heat transfer and flue gas
% temperature at furnace exit

global nflue xflue nfeed xfeed vf DHc nfuel

% INITIALIZATION

fur = zeros(16,1);

vf = u(1);
va = u(3);
Tp = u(2); % gas temp at furnace exit (pre)
Tpa = u(4); % adiab temp (previous step)

Afur = 580.644; % Furnace area, m2
Ascr = 78.252; % Screen area, m2
sigma = 5.6705e-8; % J/s.m2.K4
ef = 0.318; % Furnace emissivity
psiw = 0.644; % water wall thermal eff
M = 0.5;
phi = 0.99;

MWair = 29;
MW = [ 32 28  2  44  16 28  30 44 18 ]';
%   O2 N2 H2 C3H8 CH4 C2H4 C2H6 CO2 H2O

DHc0 = [ -241.83 -2043.96 -802.34 -1322.97 -1427.87 ]; %H2O(g) (LHV)
%       H2       C3H8       CH4       C2H4       C2H6

%   O2  N2
xair = [.21 .79]; % mol %

%   H2   C3H8   CH4   C2H4   C2H6
xfuel = [.3388 .0820 .3759 .0643 .1391];

Cw = (xfuel(2)*3+xfuel(3)+xfuel(4)*2+xfuel(5)*2)*12;
Hw = (xfuel(1)*2+xfuel(2)*8+xfuel(3)*4+xfuel(4)*4+xfuel(5)*6);

% Molecular weight of fuel
MWfuel = xfuel*MW(3:7);

```

```
% Calculate molar flow rate of fuel(R), xs O2(P), N2(I), H2O(P),
% CO2(P)
```

```
nfuel = vf*1000/MWfuel; % mol/s
```

```
% Heat of Combustion of Fuel
```

```
DHc = (xfuel*nfuel)*DHc0'; % kW
```

```
Hu = -(xfuel*DHc0')/MWfuel*1000; % kJ/kg
```

```
% Mole of O2 required for complete combustion per mole reactant
% (ratio)
```

```
nO2req = xfuel*['.5 5 2 3 3.5'];
```

```
nO2 = va*210/MWair; % mol/s
```

```
nO2xs = nO2-nO2req*nfuel;
```

```
if nO2xs<0, nO2xs = 0; end;
```

```
nN2 = va*790/MWair;
```

```
nH2O = xfuel*[1 4 2 2 3]*nfuel;
```

```
nCO2 = xfuel*[0 3 1 2 2]*nfuel;
```

```
nflue = [nO2xs nN2 0 0 0 0 0 nCO2 nH2O];
```

```
nfeed = [nO2 nN2 xfuel*nfuel 0 0];
```

```
xflue = nflue/sum(nflue);
```

```
MWflue= xflue*MW;
```

```
xfeed = nfeed/sum(nfeed);
```

```
% Calculate total molar flow of fuel and air at inlet conditions:
```

```
% P = 101.325 kPa
```

```
% T = 25 C
```

```
% Calculate adiabatic flame temperature
```

```
C = [ 29.1    1.158e-2  -0.6076e-5   1.311e-9; % O2
      29      0.2199e-2  0.5723e-5  -2.871e-9; % N2
      28.84   0.765e-4   0.3288e-5  -0.8698e-9; % H2
      68.032  22.59e-2  -13.11e-5   31.71e-9; % C3H8
      34.31   5.469e-2   0.3661e-5  -11e-9; % CH4
      40.75   11.47e-2  -6.891e-5   17.66e-9; % C2H4
      49.37   13.92e-2  -5.816e-5   7.28e-9; % C2H6
      36.11   4.233e-2  -2.887e-5   7.464e-9; % CO2
      33.46   0.688e-2   0.7604e-5  -3.593e-9]; % H2O(g)
```

```
Cp = xflue*C; % kJ/kmol.K
```

```

Ife = (Cp*[Tp Tp^2/2 Tp^3/3 Tp^4/4]')/MWflue;
Iref = (Cp*[25 25^2/2 25^3/3 25^4/4]')/MWflue;
Ife = Ife - Iref;

%   H2   C3H8   CH4   C2H4   C2H6
xfuel = [.2762 .0677 .4667 .0635 .1259];

K = -DHc + sum(nfeed)*Cpfluem([15.7 xfeed])*(15.7-25)*1e-3;
A = sum(nflue)*1e-3;
X3 = -K/A-Cp(1)*25-Cp(2)*25^2/2+Cp(3)*(Tpa^3/3-25^3/3) ...
+Cp(4)*(Tpa^4/4-25^4/4);
Ta = (-Cp(1)+sqrt(Cp(1)^2-2*Cp(2)*X3))/Cp(2);

Ta = Ta + 273.15; % K
Tp = Tp + 273.15; % K
p = 0.1; % Furnace pressure, MPa

Vf = 920.3; % Furnace volume, m3
Aw = 580.6; % Furnace area, m2
%Aw = 468;
S = 3.6 * Vf / Aw;
rH2O = xflue(9);
rCO2 = xflue(8);
r = rH2O+rCO2;
kg = 10*((0.78+1.6*rH2O)/(10*p*S*r)-0.1)*(1-0.37*Tp/1000);
ks = 0.3*(2-1.5)*(1.6*Tp/1000-0.5)*Cw/Hw;
klum = kg * r + ks;
alum = 1 - exp(-klum*p*S);
ag = 1 - exp(-kg*r*p*S);
afl = 0.1*alum + (1-0.1)*ag;
aF = 1/(1+(1/afl-1)*0.65*0.99);
vc = (vf*Hu-(vf+va)*Ife)/vf/(Ta-Tp);
Tflo = Ta/(M*((5.67e-11*psiw*Aw*aF*Ta^3)/phi/vf/vc)^0.6+1); %Deg K

% OUTPUTS

Tflm = 0.925*sqrt((Ta)*(Tflo))-273.15;
mwg = vf+va;
Ta = Ta-273.15;
Tflo = Tflo-273.15;

Hr = phi*(vf*Hu-mwg*Ife)*1e3/vf; % Total ht from fire ball J/kg
qrF = vf*Hr/Aw; % Total heat flux in furnace
%   W/m2

```

```

HrF = 0.685*1.2*qrF*39.7; % Furnace exit area = 39.7 m2
HrFprime= HrF/0.685*(1-0.685); % Radiant heat to superheaters
Hww = (Hr-HrF/vf-HrFprime/vf)*vf;
HrFp = HrFprime/vf/1e3;

fur = [Tflo  mwg  xflue Ta Tflm Hww HrF HrFprime];

```

```

function ec=econ(u)

% Calculates economizer heat transfer

% INITIALIZATION

ec = zeros(12,1);

Tgin = u(1);
Tgout = u(2);
Tw = u(3);
mwg = u(4);
Tsin = u(5);
Tsout = u(6);
feed = u(7);
x = u(8:16)';
flag = u(17);

% GAS SIDE

Tb = 0.5*(Tgin+Tgout); % Flue gas bulk temperature, C
Tf = 0.5*(Tw+Tb); % Flue gas film temperature, C

A = 1672.25; % screen heat transfer area, m2
Ag = 10.78; % Area for flue gas (psh)
D = 2*0.0254; % PSH tube outside diameter
Fa = 1.1; % Arrangement factor
Fd = 1; % Depth factor

Atube = 3.14*D^2/4; % Cross sectional area per tube
N = 88; % Number of tubes
M = 18548; % Water holdup in econ, kg

MC = 3e7; % Heat capacity of metal wall,J/C

% FLUE GAS SIDE

[muf,kf]= flueprop([Tf x]);
Cpf = Cpflue([Tf x])*1000;
Tb = 0.5*(Tgin+Tgout);
LMTDg= Tb-Tw;
ho = 0.287*(mwg/Ag)^0.61/(D^0.39)*...
(Cpf^0.33*kf^0.67/muf^0.28)*Fa*Fd;

```

```

qc = ho*A*LMTDg;

dTgout = 1/160/337.6/Cpf*(Tgout+273.15)*...
        (mwg*Cpf*(Tgin-Tgout)-qc);
% volume on gas side = 160 m3
% 337.6 --- constant for density calc.

% STEAM / WATER SIDE

Tbs = 0.5*(Tsin+Tsout);
Tfs = 0.5*(Tw+Tbs);

mi = feed/N; % Steam flow per tube

hi = 0.0279*mi^0.8/D^1.8* ...
    ((Cpl(Tbs)*1000)^0.4*kl(Tfs)^0.6/mul(Tfs)^0.4)* ...
    ((Tbs+273.15)/(Tfs+273.15))^0.8;

LMTD = Tw-Tbs;

qsc = hi*A*LMTD;
dTl = 2/M*(feed*(Tsin-Tsout)+qsc/Cpl(Tbs)/1000);

dTm = (qc - qsc)/MC;

ds = Tsout-Tsin;
dg = Tgin-Tgout;

% OUTPUTS

ec = [dTgout dTl dTm ho hi qsc qc LMTD LMTDg ds dg count];

```

```

function ps=psh(u)

% Calculates heat transfer in primary superheater

% INITIALIZATION

Tgin = u(1);
Tgout = u(2);
Tw = u(3);
mwg = u(4);
HrFprime= u(5);
P = u(6);
Tsout = u(7);
load = u(8);
sp = u(9);
x = u(10:18)';

flow = load-sp;
Tsin = Tsat(P);

Apsh = 510.97; % PSH heat transfer area, m2
Kpsh = 0.28; % Fuel factor
D = 1.64*0.0254;
Fa = 1; % Arrangement factor
Fd = 1; % Depth factor
Fs = 1; % Intertube radiation
% effectiveness factor
Atube = 3.14*D^2/4; % Cross sectional area per tube
N = 152;

M = 239.8;

Ag = 19.2; % To calc max mass flux

MC = 1.3e7; % Heat capacity of metal wall,kJ/C

% FLUE GAS SIDE

Tb = 0.5*(Tgin+Tgout); % Flue gas bulk temperature, C
Tf = 0.5*(Tw+Tb); % Flue gas film temperature, C
LMTD = Tb-Tw;

if (LMTD>0)

```

```

[muf,kf]= flueprop([Tf x]);
Cpf = Cpflue([Tf x])*1000;

ho = 0.287*(mwg/Ag)^0.61/(D^0.39)*...
(Cpf^0.33*kf^0.67/muf^0.28)*Fa*Fd;
qc = ho*Apsh*LMTD;
qr = HrFprime/2;

Qgas = qc + qr;% + qrtube;
dTgout = 2/25.3/337.6/Cpf*(Tgout+273.15)*(mwg/2*Cpf*...
(Tgin-Tgout)-qc);
% volume on gas side = 25.3 (same for ssh)
% 337.6 --- constant for density calc.
else

    Qgas = 0;
    dTgout = 0;

end;

% STEAM / WATER SIDE

Tbs = 0.5*(Tsin+Tsout);
Tfs = 0.5*(Tw+Tbs);

mi = flow/N;
hi = 0.0279*mi^0.8/D^1.8* ...
((Cpv(Tbs)*1000)^0.4*kv(Tfs)^0.6/muvap(Tfs+273)^0.4)* ...
((Tbs+273.15)/(Tfs+273.15))^0.8;

LMTD = Tw - 0.5*(Tsout+Tsin);

if (LMTD>0)

    qsc = hi*Apsh*(Tw-Tbs);
    dTsout = 2/M*(flow*(Tsin-Tsout)+qsc/Cpv(Tbs)/1000);

else

    qsc = 0;
    dTsout = 0;

end;

```



```
dTm = (Qgas - qsc)/MC;
```

```
% OUTPUTS
```

```
ps = [dTgout dTsout dTm 0];
```

```

function ss=ssh(u)

% Calculates heat transfer in secondary superheater

% INITIALIZATION

global SpEn % Specific Enthalpy

ss = zeros(3,1);

Tgin = u(1);
Tgout = u(2);
Tw = u(3);
mwg = u(4);
HrFprime= u(5);
hin = u(6);
Tsout = u(7);
P = u(8);
load = u(9);
Tsin = u(10);
x = u(11:19)';

Tb = 0.5*(Tgin+Tgout); % Flue gas bulk temperature, C
Tf = 0.5*(Tw+Tb); % Flue gas film temperature, C
Assh = 464.52; % PSH heat transfer area, m2
Kssh = 0.3; % Fuel factor
D = 1.64*0.0254;
Fa = 1; % Arrangement factor
Fd = 1; % Depth factor
Fs = 1; % Intertube radiation
% effectiveness factor
Atube = 3.14*D^2/4; % Cross sectional area per tube
N = 156;

Ag = 19.2; % To calc max mass flux

MC = 1.3e7; % Heat capacity of metal wall,J/C

% FLUE GAS SIDE

[muf,kf]= flueprop([Tf x]);
Cpf = Cpflue([Tf x])*1000;
Tb = 0.5*(Tgin+Tgout); % Flue gas bulk temperature, C

```

```

Tf = 0.5*(Tw+Tb); % Flue gas film temperature, C
LMTD = Tb-Tw;

if (LMTD>0)
    [muf,kf]= flueprop([Tf x]);
    Cpf = Cpflue([Tf x])*1000;

    ho = 0.287*(mwg/Ag)^0.61/(D^0.39)*...
    (Cpf^0.33*kf^0.67/muf^0.28)*Fa*Fd;
    qc = ho*Assh*LMTD;
    qr = HrFprime/2;
    Qgas = qc + qr;
    dTgout = 2/25.3/337.6/Cpf*(Tgout+273.15)*...
    (mwg/2*Cpf*(Tgin-Tgout)-qc);
    % volume on gas side = 25.3 (same for ssh)
    % 337.6 --- constant for density calc.

else

    Qgas = 0;
    dTgout = 0;

end;

% STEAM / WATER SIDE

Tbs = 0.5*(Tsin+Tsout);
Tfs = 0.5*(Tw+Tbs);
mi = load/N;
hi = 0.0279*mi^0.8/D^1.8* ...
((Cpv(Tbs)*1000)^0.4*kv(Tfs)^0.6/muvap(Tfs+273)^0.4)* ...
((Tbs+273.15)/(Tfs+273.15))^0.8;
LMTD = Tw-0.5*(Tsout+Tsin);

if (LMTD>0)
    qsc = hi*Assh*LMTD;
    dTsout= 2*(load*(Tsin-Tsout)+qsc/Cpv(Tbs)/1000)/240;
else
    qsc = 0;
    dhout = 0;
    SpEn = 0;
    dTsout= 0;
end;

```

```
dTm = (Qgas - qsc)/MC;  
  
% OUTPUTS  
  
ss = [dTgout dTsout dTm 0];
```

```

function sc=screen(u)

% Calculates heat transfer in slag screen

% INITIALIZATION

sc = zeros(3,1);

Tgin = u(1);
mwg = u(2);
Tgout = u(3);
Tsin = u(4);
P = u(5);
Tw = u(6);
x = u(7:15)';
HrF = u(16);
Hww = 0;

A = 100; % m2 (close to that in furn.m)
Ap = 32.1; % projected area, m2
Ag = 19.7; % Area available for flue gas
Kscr = 0.2; % Fuel factor
sigma = 5.6705e-8; % J/s.m2.K4
ef = 0.318; % Emissivity
D = 2.5*0.0254; % Screen tube outside diameter
Fa = 0.9; % Arrangement factor
Fd = 0.9; % Depth factor
Fs = 1; % Intertube radiation
% effectiveness factor

% FLUE GAS SIDE

LMTD = 0.5*(Tgout+Tgin)-Tw;

if (LMTD>0)

    Tbg = 0.5*(Tgin+Tgout);
    Tfg = 0.5*(Tbg+Tsat(P));
    p = 0.1; % Gas pressure MPa
    rH2O = x(9);
    rCO2 = x(8);
    r = rH2O+rCO2;
    S = 1.8/(1/4.8 +1/9.1 +1/0.1);
    kg = 10*((0.78+1.6*rH2O)/(10*p*S*r)-0.1)*...

```

```

        (1-0.37*(Tgout+273)/1000);
        k = kg*r; % ka*mua = 0 (mua = 0)
        ag = 1-exp(-k*p*S);
        hr = 5.1e-8*ag*Tbg^3*(1-((Tw+273)/(Tbg+273))^3.6)/ ...
(1-(Tw+273)/(Tbg+273)); % W/m2.K
        [muf,kf]= flueprop([Tfg x]);
        Cpf = Cpflue([Tfg x])*1000;
        ho = 0.287*(mwg/Ag)^0.61/(D^0.39)*...
(Cpf^0.33)*(kf^0.67)/(muf^0.28)*Fa*Fd;
        q = (ho+hr)*A*LMTD;
        qrtube = 0;
        qflue = q+HrF+Hww;
        qrflue = 0;
        Tgout = Tgin-q/mwg/Cpf;

    else

        qrflue= 0;
        qc    = 0;
        qrtube= 0;
        qflue = 0;
        Tgout = Tgin;

    end;

% STEAM / WATER SIDE

sc = [ qrflue Tgout qflue];

```

```

function dc=downcomer(u)

% Calculates downcomer heat transfer

% INITIALIZATION

dc = zeros(2,1);

Tgin = u(1);
mwg = u(2);
Tgout = u(3);
Tw = u(4);
x = u(5:13)';
Qdc = u(14);

A = 2291; % m2
Ag = 10; % Area available for flue gas
D = 2.5*0.0254; %
MC = 9.8e7;

% FLUE GAS SIDE

LMTD = 0.5*(Tgout+Tgin)-Tw;

if (LMTD>0)

    Tbg = 0.5*(Tgin+Tgout);
    Tfg = 0.5*(Tbg+Tw);
    [muf,kf]= flueprop([Tfg x]);
    Cpf = Cpflue([Tfg x])*1000;

    ho = 0.287*(mwg/Ag)^0.61/(D^0.39)*...
(Cpf^0.33)*(kf^0.67)/(muf^0.28);
    q = ho*A*LMTD;
    qflue = q;
    Tgout = Tgin-q/mwg/Cpf;
    dTm = (qflue-Qdc)/MC;

else

    qflue = 0;
    Tgout = Tgin;
    dTm = 0;

```

```
end;  
  
% STEAM / WATER SIDE  
  
dc = [Tgout dTm];
```



```

function att=attemp(u)

% Calculates attemperator steam exit temperature

att = zeros(2,1);

Wsp = u(1); % Spray water flow
Tsp = u(2); % Spray water temperature (Econ exit)
Wst = u(3); % Steam flow + spray water
Tpsh = u(4); % Steam temperature at PSH exit
P = u(5); % Drum pressure

% Enthalpy in kJ/kg

hps = (3.4093+0.0028*(Tpsh-500)-0.0314*(P/1000-6) ...
      +0.0193*(P/1000-6)^2-0.0005*(Tpsh-500)*(P/1000-6))*1000;

% No accumulation in attemperator --> in = out

TotalEn = (Wsp*Hl(Tsp)+(Wst-Wsp)*hps);
SpEn = TotalEn/Wst;

if SpEn < hlsat(P),
    Tout =(SpEn/1000+38.2736-1.3994*P/1000)/(4.4868-.00538*P/1000);
elseif SpEn > hvsat(P),
    Tout = (SpEn/1000-3.4093+.0314*(P/1000-6) ...
            -.0193*(P/1000-6)^2)/(.0028-.0005*(P/1000-6))+500;
else
    Tout = Tsat(P);
end

att = [Tout TotalEn];

```

```

function pd=PD(u)

% Calculates pressure and level in steam drum

% Initialization

pd = zeros(13,1);

% Steam drum dimensions

R = 72/2*0.0254; % Radius, m
L = 39*12*0.0254; % Length, m
Di = 2.5*0.0254; % Inside diameter, m
MC = 9.2e7; % J/C

qscr = u(1); % Heat transfer from flue gas to screen wall, W
qgen = u(2); % Heat transfer from flue gas to generator wall, W
Tsin = u(3); % Steam inlet temperature, C
D = u(4); % Drum level (previous time step), m
P = u(5); % Drum pressure (previous time step), kPa
Ws = u(6); % Steam load, kg/s
Wf = u(7); % Feed water rate, kg/s
Tgen = u(8); % Generator wall temperature, C
Tscr = u(9); % Screen wall temperature, C
Qsgen = u(10); % Heat transfer to steam in genbank
Hww = u(11); % Heat transfer to waterwalls
wdmwr = u(12); % -d/dt(Total mass in CV2)
dgen = u(13); % A * d/dt(Total energy in CV2)
homhdc = u(14);
Wd = u(15);

if D == 0,
D = 0.01;
end

Vl = (R^2*acos((R-D)/R)-(R-D)*sqrt(2*R*D-D^2))*L;

if Vl == 0,
Vl = 0.1;
end

Vv = 3.14159*R^2*L - Vl ... % Assumed accumulation in PSH and SSH
+ 12.4; % are important. Assume volume of
% PSH and SSH is 50 m3.

```

```

if Vv == 0,
Vv = 0.1;
end

hl = hlsat(P)*1000; % J/kg
hv = hvsat(P)*1000; % J/kg
hf = Hl(Tsin)*1000; % J/kg
rl = rholsat(P); % kg/m3
rv = rhovsat(P); % kg/m3
dhl = dhlsat(P)*1000; % J/kg/kPa
dhv = dhvsat(P)*1000; % J/kg/kPa
drl = drholsat(P); % kg/m3/kPa
drv = drhovsat(P); % kg/m3/kPa
ml = 97e-6; % N.s/m2 = kg/m.s
mv = 18.6e-6; % N.s/m2 = kg/m.s
Atube = 3.14159/4*Di^2;

A0 = 2*L*sqrt(2*D*R-D^2); % m2
A1 = rl-rv; % kg/m3
A2 = Vl*drl + Vv*drv; % kg/kPa
A3 = rl*hl - rv*hv; % J/m3
A4 = dhl*rl*Vl + drl*hl*Vl + dhv*rv*Vv + drv*hv*Vv; % J/kPa

Wcirc = 0; % Not used;

% GENERATOR + SCREEN

Tw = Tgen;

Qsww = Qsgen+Hww+qscr; % includes generator and waterwalls
                % (for Energy balance only)
Qswwd = Qsww - dgen*1000;

% dD/dt and dP/dt

dD = (Ws*(A4/A2-hv)-Wf*(A4/A2-hf)+wdmwr*A4/A2+Qswwd)/ ...
(A3*A0-A1*A4*A0/A2);

dP = (Ws*(A3/A1-hv)-Wf*(A3/A1-hf)+wdmwr*A3/A1+Qswwd)/ ...
(A4-A3*A2/A1);

dTmgen = (qgen-Qsgen)/MC; % Only gen bank heat transfer important
dTmscr = dTmgen;

```

```
x = 0; % CALCULATED ELSEWHERE
```

```
pd = [dD dP x dTngen dTmscr Wcirc V1 Vv Qsw A1 A2 A3 A4];
```

```

function ge=gen(u)

% Calculates heat transfer in gen bank

% INITIALIZATION

ge = zeros(2,1);

Tgin = u(1);
mwg = u(2);
Tgout = u(3);
Tsin = u(4);
P = u(5);
Tw = u(6);
x = u(7:15)';
flag = u(16);

A = 4450.06/2; % m2
Ag = 10; % Area available for flue gas
Kscr = 0.4; % Fuel factor
D = 2.5*0.0254; % Screen tube outside diameter
Fa = 1.01; % Arrangement factor
Fd = 0.9; % Depth factor
Fs = 1; % Intertube radiation
% effectiveness factor

% FLUE GAS SIDE

if flag == 0
    while (count<1)|((count < 500)&(eps > 1e-6))

        temp = Tgout;
        LMTD = 0.5*(Tgout+Tgin)-Tw;
        Tbg = 0.5*(Tgin+Tgout);
        Tfg = 0.5*(Tbg+Tw);
        [muf,kf]= flueprop([Tfg x]);
        Cpf = Cpflue([Tfg x])*1000;
        ho = 0.287*(mwg/Ag)^0.61/(D^0.39)*...
        (Cpf^0.33)*(kf^0.67)/(muf^0.28)*Fa*Fd;
        qc = ho*A*LMTD;
        qrtube= hrprime(LMTD,Tw)*Kscr*Fs*A*LMTD;
        qflue = qc+qrtube;
        dTgout = 1/232/337.6/Cpf*(Tgout+273.15)*...
            (mwg*Cpf*(Tgin-Tgout)-qflue);
    end
end

```

```

% volume on gas side = 232 m3
% 337.6 --- constant for density calc.

    eps = abs((Tgout-temp)/temp);
    count = count + 1;
    end;

else

    LMTD = 0.5*(Tgout+Tgin)-Tw;

    if (LMTD>0)

        Tbg = 0.5*(Tgin+Tgout);
        Tfg = 0.5*(Tbg+Tw);
        [muf,kf]= flueprop([Tfg x]);
        Cpf = Cpflue([Tfg x])*1000;

        ho = 0.287*(mwg/Ag)^0.61/(D^0.39)*...
        (Cpf^0.33)*(kf^0.67)/(muf^0.28)*Fa*Fd;
        qc = ho*A*LMTD;
        qrtube = hrprime(LMTD,Tw)*Kscr*Fs*A*LMTD;
        qflue = qc+qrtube;
        dTgout = 1/232/337.6/Cpf*(Tgout+273.15)*...
        (mwg*Cpf*(Tgin-Tgout)-qflue);
% volume on gas side = 232 m3
% 337.6 --- constant for density calc.

    else

        qc = 0;
        qrtube= 0;
        qflue = 0;
        dTgout= 0;

    end;
end;

% STEAM / WATER SIDE

ge = [ dTgout qflue ];

```

```

function head=head900(u)

% This function calculates dT/dt and dP/dt of the 900# header

miu = u(1); % Flow into 900# header, kg/s
mico = u(2);
mo = u(3); % Flow out of 900# header, kg/s
Tiu = u(4); % Temp of steam into header, C
Tico = u(5);
mo8 = u(6); % steam flow to plant 8, kg/s
To = u(7); % Temp of steam out of header, C
P = u(8); % 900# header pressure, kPa

V = 142.38; % Volume of 900# header, m3

mo = mo+mo8; % steam out = total steam demand

head = zeros(2,1);

drho = (miu+mico-mo)/V;
dT = (miu*Tiu+mico*Tico-mo*To-V*To*drho)/V*vv(To);
dP = (drho+P/8.314*18.02*dT/(To+273.15)^2)*8.314/18.02*(To+273.15);

head = [dT dP];

```

```

function w=stmflow(u)

% This function calculates the steam flow from the superheaters to
% the 900# header, i.e. outlet of SSH and inlet of 900# header.

P900 = u(1); % 900# header in kPa
Pd = u(2); % Drum and Superheater Pressure
% in kPa

if (Pd-P900) >= 0
w = 4.15*sqrt(Pd-P900);
else
w = 1;
end;

```


Appendix D

Physical Properties Correlations

This appendix provides all the physical properties correlations used in the dynamic model of the Syncrude boiler system.

```

function y=Cpflue(u)

% Calculates flue gas specific heat capacity

% u(1) T Temperature in Deg C
% u(2):u(10) x Mole fractions
%
% Cp's are given in kJ/kmol.K
% Returns Cp in kJ/kg.K

T = u(1);
x = [ u(2:10) ];
if T > 1500
    T = 1500;
end;

C = [ 29.1    1.158e-2  -0.6076e-5   1.311e-9; % O2
      29      0.2199e-2  0.5723e-5  -2.871e-9; % N2
      28.84   0.765e-4   0.3288e-5  -0.8698e-9; % H2
      68.032  22.59e-2  -13.11e-5   31.71e-9; % C3H8
      34.31   5.469e-2   0.3661e-5  -11e-9; % CH4
      40.75   11.47e-2  -6.891e-5   17.66e-9; % C2H4
      49.37   13.92e-2  -5.816e-5   7.28e-9; % C2H6
      36.11   4.233e-2  -2.887e-5   7.464e-9; % CO2
      33.46   0.688e-2   0.7604e-5  -3.593e-9]; % H2O(g)

MW = [ 32 28 2 44 16 28 30 44 18 ]';

Cp = C * [ 1 T T^2 T^3 ]'./MW;

y = sum(x*Cp);

```

```
function y=Cpl(T)
```

```
% Specific heat (kJ/kg.K) of liquid water at  
% temperature T (C) at 6 MPa
```

```
y=[6e-8 -2.3729e-6 6.5965e-4 4.1458]*[T^3;T^2;T;1];
```

```

function y=Cpv(T)

% Specific heat (kJ/kg.K) of steam at
% temperature T (C) at 6MPa

y=[-1.6127e-12 4.7084e-09 -5.4182e-06 3.0756e-03 -8.6317e-01 .../
    9.8553e+01]*[T^5;T^4;T^3;T^2;T;1];

```

```

function hl=Hl(T)

% Enthalpy (kJ/kg) of subcooled liquid at
% temperature T (C) at 6 MPa

hl=[1.5e-8 -2.3729e-6 3.2983e-4 4.1458]*[T^4;T^3;T^2;T];

```

```
function hv=Hv(T)
```

```
% Enthalpy (kJ/kg) of superheated steam at  
% temperature T (C) at 6 MPa
```

```
hv=[1.97182 2082.22]*[T;1];
```

```

function hsat=hsat(P,x)

% Liquid water enthalpy (kJ/kg) at saturation
% pressure P (kPa)
% Water vapour enthalpy (kJ/kg) at saturation
% pressure P (kPa)

if x >= 1,
    x=1;
elseif x <= 0,
    x=0;
end

hsat = x*hvsat(P) + (1-x)*hlsat(P);

```

```

function y=hvsup(T,P)

% This function calculates the specific enthalpy of superheated
% steam (in the range of T = 450 - 550 Deg C, P = 5 - 7 MPa)
% in kJ/kg
% Input T in Deg C, P in MPa

y = (3.4093+.0028*(T-500)-.0314*(P-6)+.0193*(P-6)^2 ...
    -.0005*(T-500)*(P-6))*1000;

```



```

function kflue=kflue(u)

% Calculates the thermal conductivity of flue gas
% in W/m.K given temperature in C

T = u(1);
x = [ u(9) u(2) u(10) u(3) ];
%   CO2   O2   H2O   N2

% UNIT CONVERSION OF TEMPERATURE FROM C to K

T = T + 273.15;

% COMPOSITION OF FLUE GAS (MOLE FRACTION)
% Table 2(b), Rackette

%x =      [ 0.0913 % CO2
% 0.0204 % O2
% 0.1622 % H2O
% 0.7261 ]'; % N2

% THERMAL CONDUCTIVITIES AS A FUNCTION OF TEMPERATURE

k =      [ 0          7.83282e-5 -6.8542e-3
-9.9581e-9 7.62088e-5  4.60646e-3
0          8.3154e-5  -7.4556e-3
-5.7625e-9 6.28992e-5  8.34966e-3];

k = k * [ T^-2 T 1 ]';

kflue = sum(x*k);

```

```

function [muflue,kflue]=flueprop(u)

% Calculates the viscosity of flue gas
% in kg/m.s given temperature in C

T = u(1);
x = [ u(9) u(2) u(10) u(3) ];
%   CO2   O2   H2O   N2

% UNIT CONVERSION OF TEMPERATURE FROM C to K

T = T + 273.15;

% COMPOSITION OF FLUE GAS (MOLE FRACTION)
% Table 2(b), Rackette

%x =      [ 0.0913 % CO2
% 0.0204 % O2
% 0.1622 % H2O
% 0.7261 ]'; % N2

% VISCOSITIES AS FUNCTIONS OF TEMPERATURE

C =      [ 0          0.38508e-7  35.0096e-7
-8.1585e-12  4.88265e-8  7.55213e-6
0          3.6078e-8  -9.93254e-7
-1.09153e-11 4.5665e-8  5.45285e-6 ];

C = C * [ T^2 T 1 ]';

% THERMAL CONDUCTIVITIES AS FUNCTIONS OF TEMPERATURE

B =      [ 0          7.83282e-5 -6.8542e-3
-9.9581e-9 7.62088e-5  4.60646e-3
0          8.3154e-5  -7.4556e-3
-5.7625e-9 6.28992e-5  8.34966e-3];

```

```

B = B * [ T^2 T 1 ]';

M = [44 32 18 28];

phi = ones(4,4);
for i = 1:3
    for j = i+1:4
        phi(i,j) = (1 + sqrt(C(i)/C(j))*((M(j)/M(i))^0.25))^2 ...
        / sqrt(8*(1+M(i)/M(j)));
        phi(j,i) = (C(j)/C(i))*(M(i)/M(j))*phi(i,j);
    end;
end;

A = phi;

num = x' .* C;
numk = x' .* B;

for i = 1:4
    den = sum(x.*phi(i,:));
    mu(i) = num(i)/den;
    denk = sum(x.*A(i,:));
    k(i) = numk(i)/denk;
end;

muflue = sum(mu);
kflue = sum(k);

```

```
function kl=kl(T)

% Thermal conductivity (W/m.K) of liquid water at
% 60 bar at temperature T (C)

kl=[-.000176 .69973]*[T;1];
```

```

function kv=kv(T)

% Thermal conductivity (W/m.K) of superheated
% steam at 60 bar at
% temperature T (C)

kv=[.0000001175 .00000004025 .043419]*[T*T;T;1];

```

```

%
% This function to evaluate the liquid viscosity for Tr > 0.75
%
% T - temperature, K.
%

function muliq = muliq(T)

Tc = 647.3; % K
Pc = 218.01; % atm
Tr = T / Tc;
M = 18.01; % kg/kg-mole
w = 0.0;

A = 0.015174 - 0.02135 * Tr + 0.0075 * Tr^2;
B = 0.042552 - 0.07674 * Tr + 0.0340 * Tr^2;
C = Tc^(1/6) * M^(-1/2) * Pc^(-2/3);

muliq = ((A + B * w) / C) * 0.001; % Pa s or kg/m s

```

```

%
% This function is to evaluate the vapor viscosity for Tr < 2.0.
%
% T - temperature, K.
%

function muvap = muvap(T)

Tc = 647.3; % K
Pc = 218.01; % atm
Tr = T / Tc;
M = 18.01; % kg/kg-mole
R = 8.314; % kPa m3/kmol K

Zc = Pc * 101.325 * 0.0568 / 8.314 / 647.3;
C = Tc^(1/6) * M^(-1/2) * Pc^(-2/3);

muvap = ((0.755*Tr-0.055) * Zc^(-5/4)/C) * 1e-7; % Pa s or kg/m s

```

```
function rsat=rholsat(P)

% Liquid water density (kg/m3) at saturation
% pressure P (kPa)

rsat=[4.7954e-7 -2.4793e-2 8.8989e2]*[P*P;P;1];
```



```

function rvs=rhovsat(P)

% Water vapour density (kg/m3) at saturation
% pressure P (kPa)

rvs= [ 1.2808e-7  4.0718e-3  1.7737  ]*[P*P;P;1];

```

```

function vl=vl(T)

% Specific volume (m3/kg) of subcooled liquid at
% at 5 MPa at temperature T (C)

vl=[.0000000046032 -.00000021246 .0010142]*[T^2;T;1];

```

```
function vv=vv(T)

% Specific volume (m3/kg) of superheated vapour at
% at 6 MPa at temperature T (C)

vv=[.0000958 .00843857]*[T;1];
```